In-situ synchrotron X-ray diffraction studies of ion exchange in zeolites

H. A. Parish[1], G. Cutts[2] and J. A. Hriljac[3]

[1, 3] School of Chemistry, University of Birmingham, Edgbaston, B15 2TT
[2, 3] Diamond Light Source, Didcot, OX11 0DE
[1] hap431@student.bham.ac.uk
[2] geoff.cutts@diamond.ac.uk
[3] joseph.hriljac@diamond.ac.uk

Introduction

Zeolites and related inorganic materials with open framework structures are often used in the clean up of radionuclides from nuclear waste streams. These materials have high stability towards heat and radiation and can also be highly selective towards radioactive cations, even in the presence of other competing ions. ^{137}Cs is a common and particularly problematic radionuclide; it is water soluble and harmful to humans. This work will focus on the analysis of zeolite structures in order to determine their ability to act as efficient ion exchangers for radioactive Cs.

The Pair Distribution Function

The pair distribution function (PDF) gives the probability of finding one atom at a certain distance from another in a unit cell. Unlike XRD, which uses Bragg scattering to determine average long-range structures of crystalline solids, PDF uses both Bragg and diffuse scattering to probe a material's structure. This means that information about local order can be acquired. In this work, PDF data will be obtained from beamline I15-1 (XPDF)[1] at Diamond Light Source.
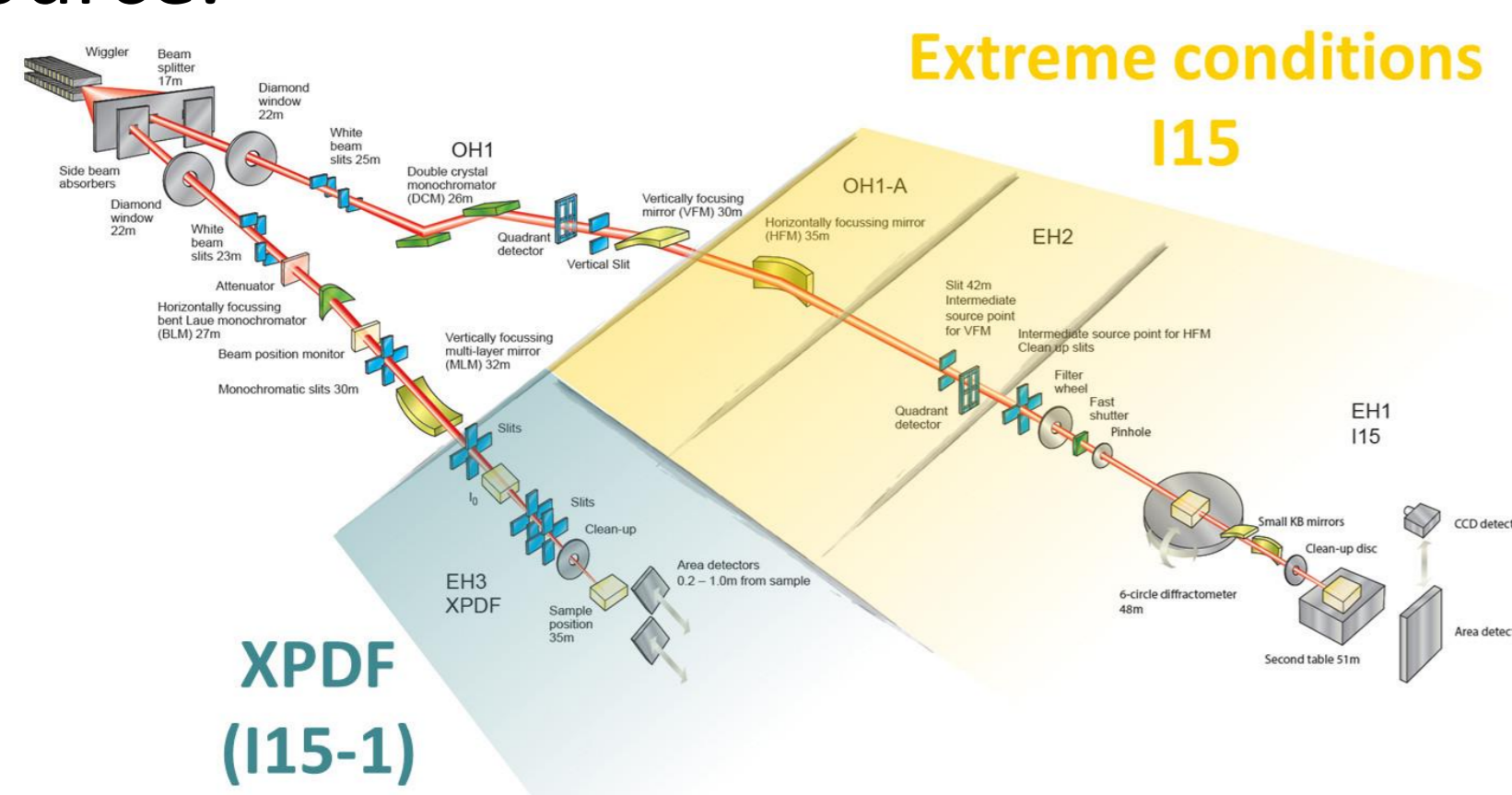
Structure and Properties of Zeolites

Zeolites are a class of porous aluminosilicates with the general formula $M_{x/n}[Al_xSi_yO_{2(x+y)}].pH_2O$, where M is a cation such as Na, K or Ca and n is the charge on the cation. Their structures are made up of SiO_4 and AlO_4 tetrahedra (primary building units) that are linked by corner sharing of oxygen atoms to form a 3D network of rings and cages (secondary building units). The tetrahedra give the structure an excess negative charge, which is accounted for by cations occupying the pores. Pores in the framework also contain water molecules. Zeolites are known for their remarkable selectivity towards certain cations as well as their unusual tendency to contract rather than expand upon heating, a phenomenon known as negative thermal expansion (NTE).
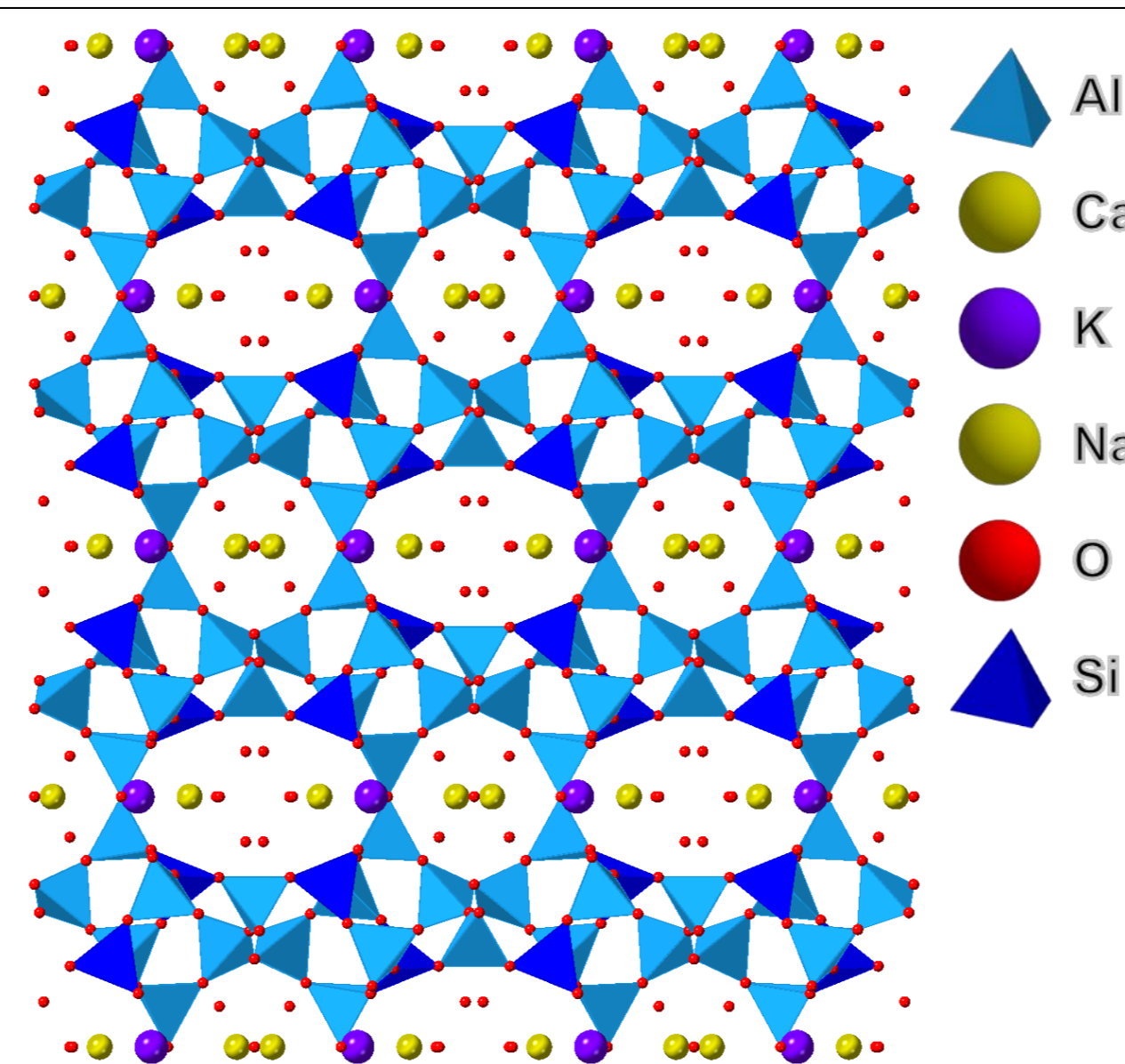

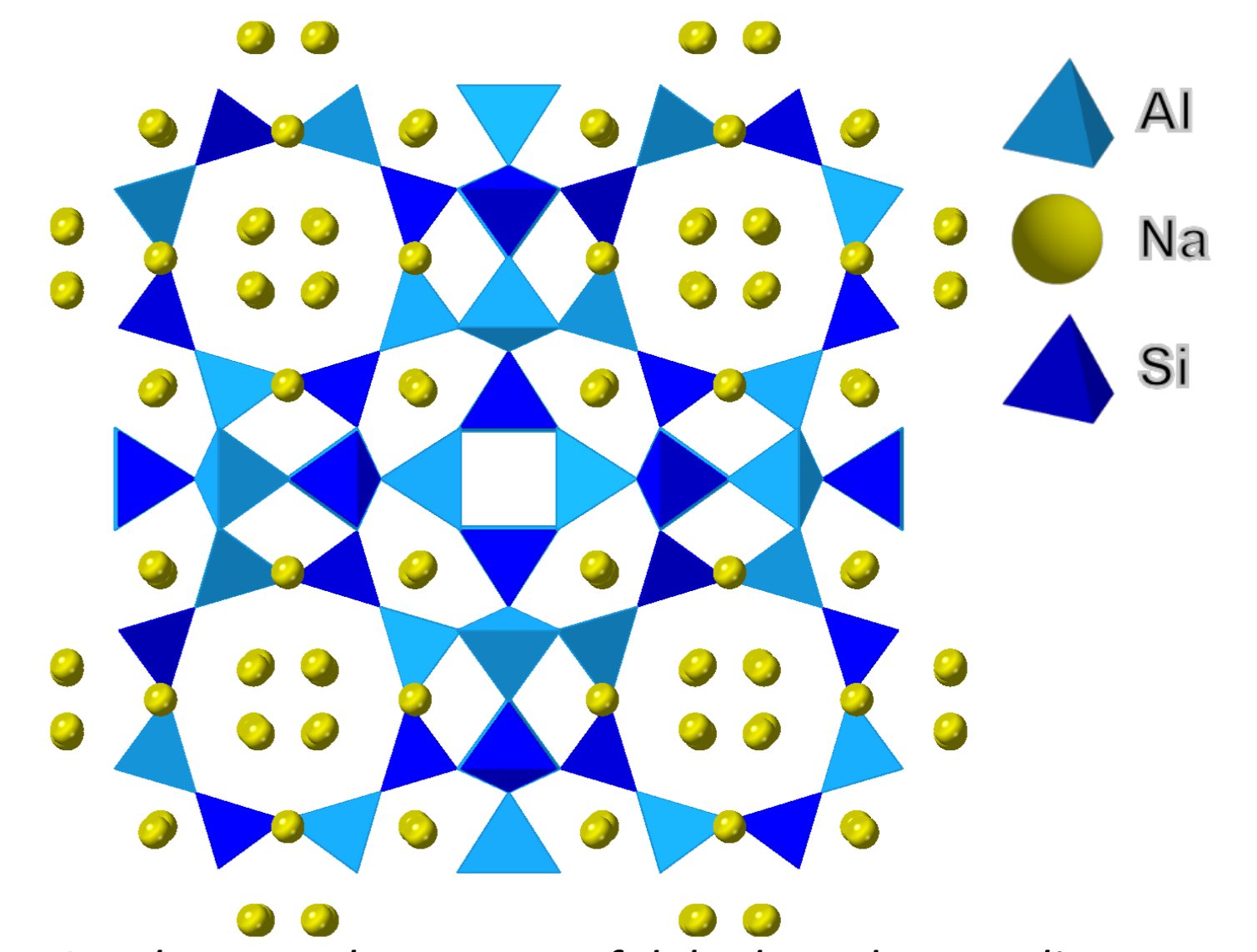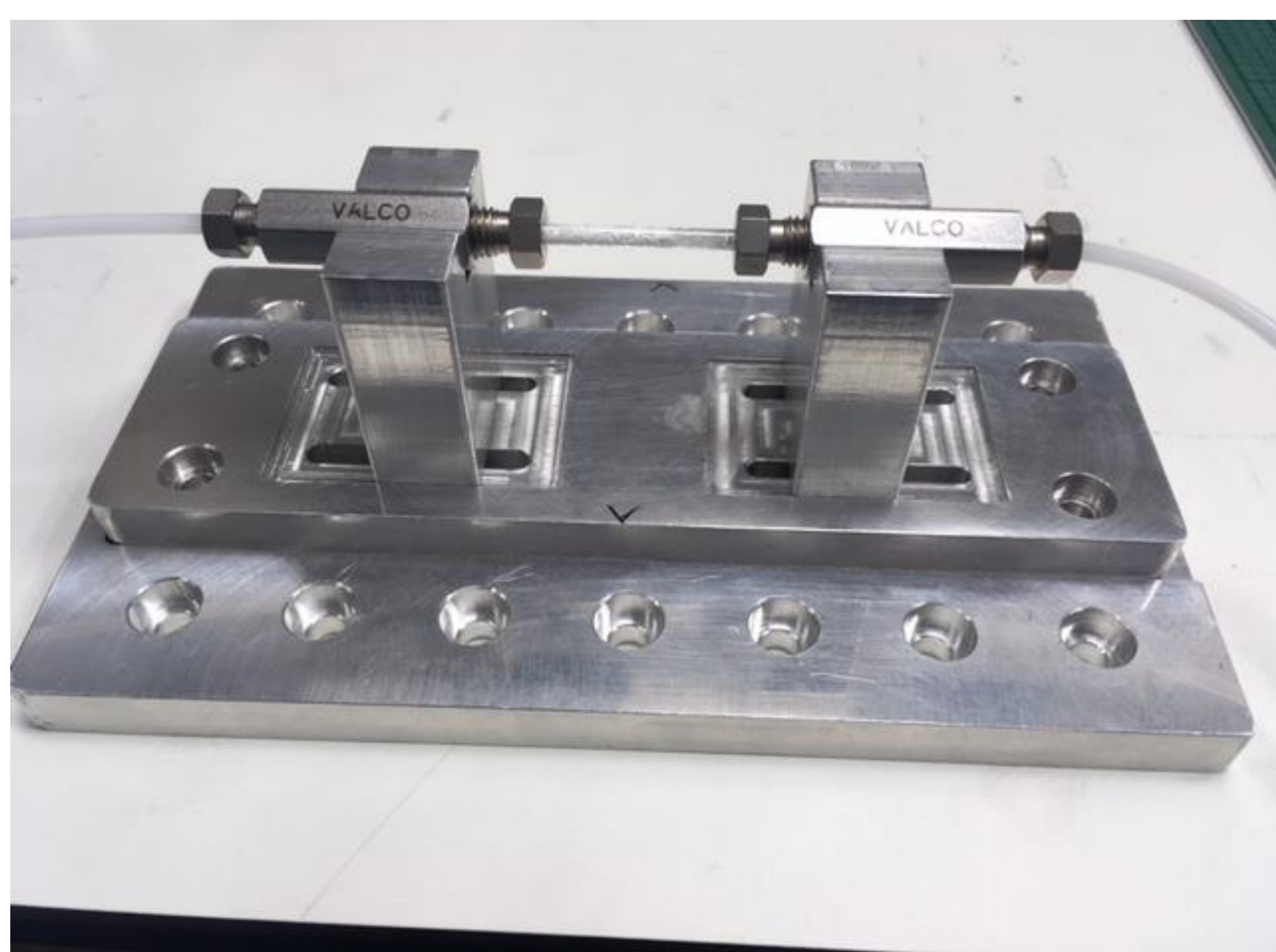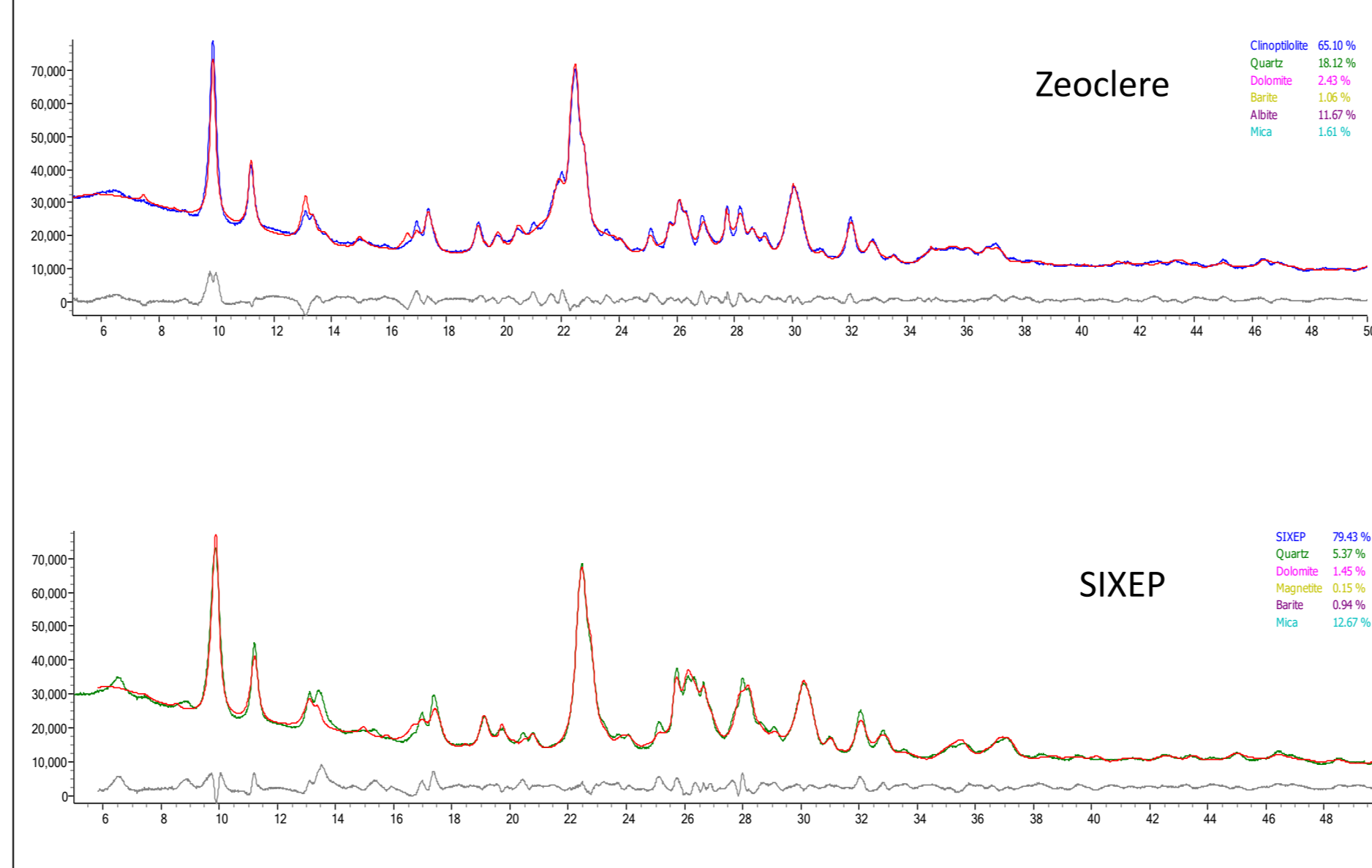Figure 1 – the crystal structure of clinoptilolite along the c-axis[2]

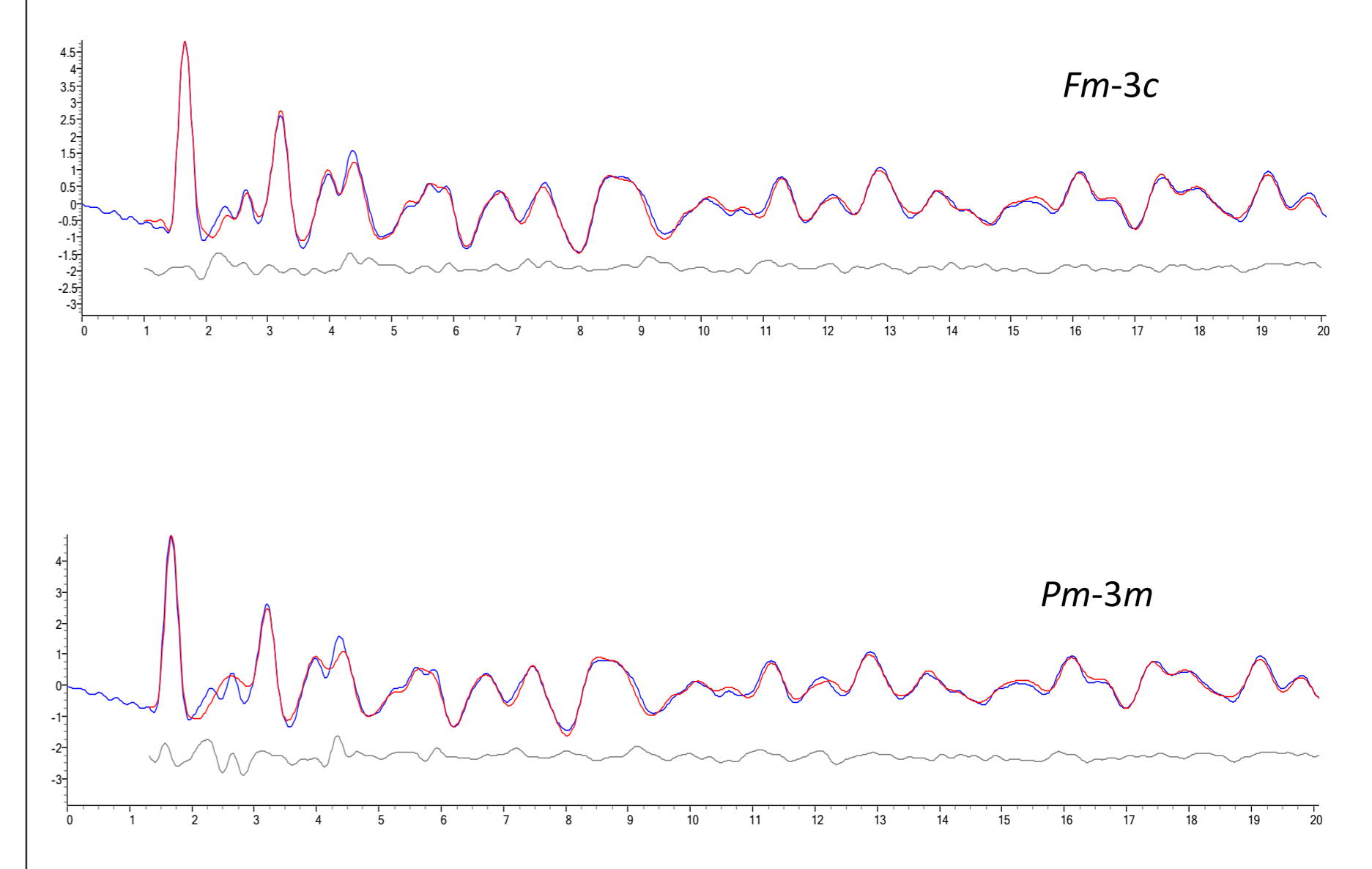Figure 2 – the crystal structure of dehydrated Na zeolite A along the c-axis

In-Situ Diffraction Cell

The in-situ flow cell that will be used for ion exchange experiments was designed by Geoff Cutts at Diamond Light Source. Experiments will be undertaken on beamline I11 (high resolution powder diffraction) to compare the Cs and Sr exchange abilities and rates of two different types of clinoptilolite, including a sample from SIXEP. Rietveld analysis of lab data using TOPAS[3] has resulted in a good model of the long-range structure of the samples.

Rietveld Analysis of Clinoptilolite

PDF Analysis of Dehydrated Sodium Zeolite A

PDF data for exchanged zeolite A samples were obtained from beamline I15-1. Analysing dehydrated Na-A resulted in a good overall fit, but fitting the Na-O peak has proven difficult, suggesting that the crystallographic model is probably wrong.

References

[1] P. A. Chater, D. S. Keeble, M. G. Tucker, J. P. Sutter, M. Hillman and H. Wilhelm, poster presented at the Debye Scattering Equation conference, Trento, Italy, 14 – 18th June 2015
[2] J. R. Smyth, A. T. Spaid, D. L. Bish, Am. Mineral, 1990, 75, 522 – 528
[3] A. A. Coelho, J. Appl. Cryst., 2018, 51, 210 - 218

Transformative Science and Engineering for Nuclear Decommissioning

transcendconsortium.org

Energy For a Low Carbon Future

TRANSCEND

Particle-laden flow characterisation and prediction

L. F. Mortimer & M. Fairweather

School of Chemical and Process Engineering, University of Leeds, Leeds, LS2 9JT

l.f.mortimer@leeds.ac.uk, m.fairweather@leeds.ac.uk

1. Introduction

- **Particle-laden turbulent flows** occur commonly in both natural and industrial environments.
- Decontamination of legacy ponds and silos is of great importance and stands as a matter of increasing urgency throughout the nuclear industry. In facilities around the UK, waste suspension flows transport legacy material from historic ponds to other interim locations where they are safely stored.
- The work presented here uses an **immersed boundary method**, coupled to a spectral element method based **direct numerical simulation** solver to resolve the flow around interacting dynamic particle meshes to elucidate the aggregation dynamics of waste-suspension flows.
- The aim is to develop **behavioural modification techniques** by studying **particle-particle interactions** on a **fundamental scale**.

2. Direct numerical simulation

- **DNS** fully resolves all relevant space and time-scales associated with the flow.
- This means we are able to take into account the effect that **eddies** of all sizes have on the particulate phase.
- This is important since **collisions** tend to occur more frequently in regions of high turbulence.
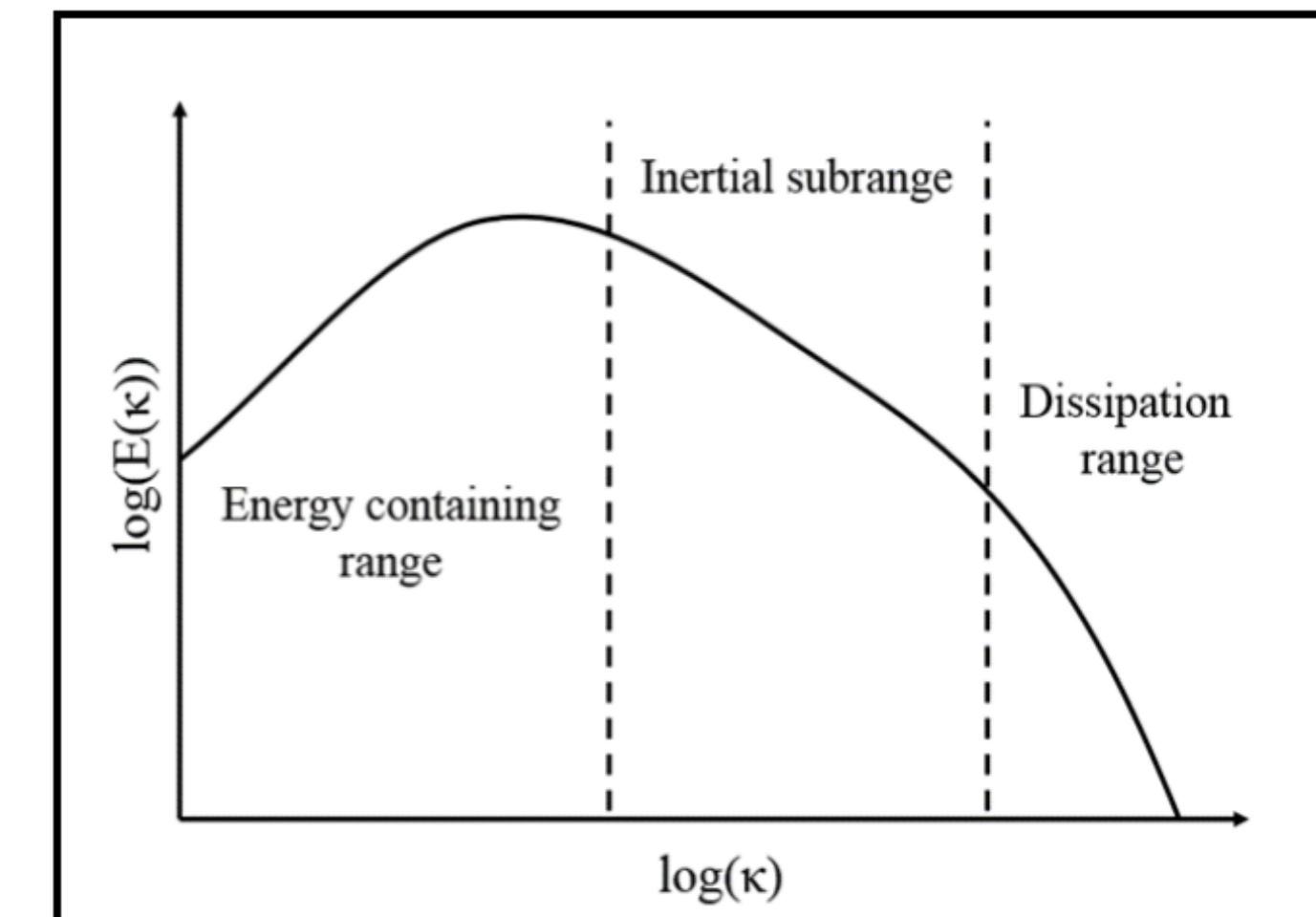

3. Forced homogeneous isotropic turbulence

- NEK5000 solves the Navier-Stokes equations directly using a high-order (N=8) spectral element method.
- We use the linear forcing method to produce statistically stationary periodic boxes of isotropic turbulence using 48^3 elements.
- Fluid Taylor microscales are representative of the bulk flow region and the viscous sublayer from $Re\tau$ = 180 channel flow.
- **Right:** Contour plot of velocity magnitude (ms^{-1}) sampled from steady state (slice through z=0).
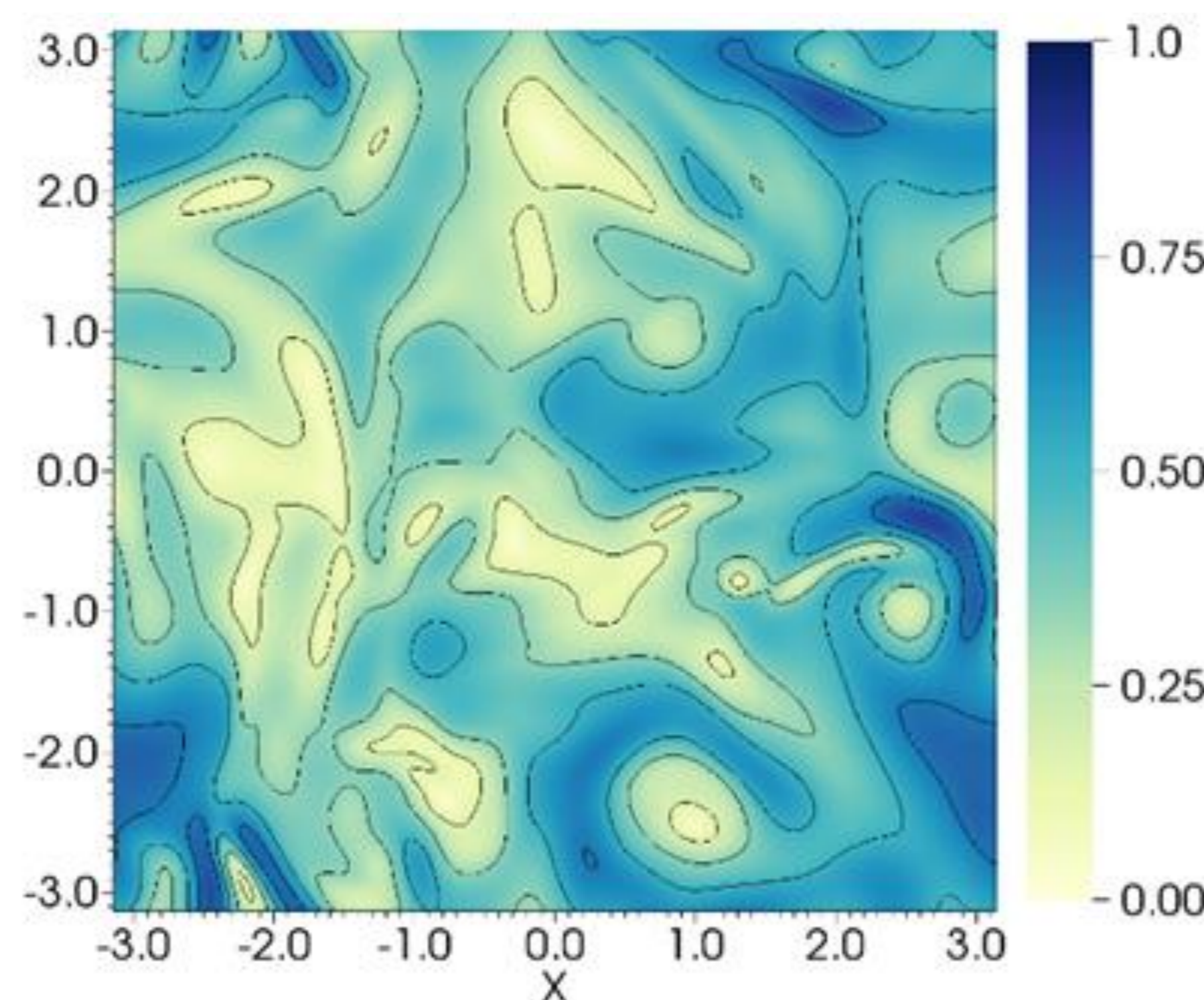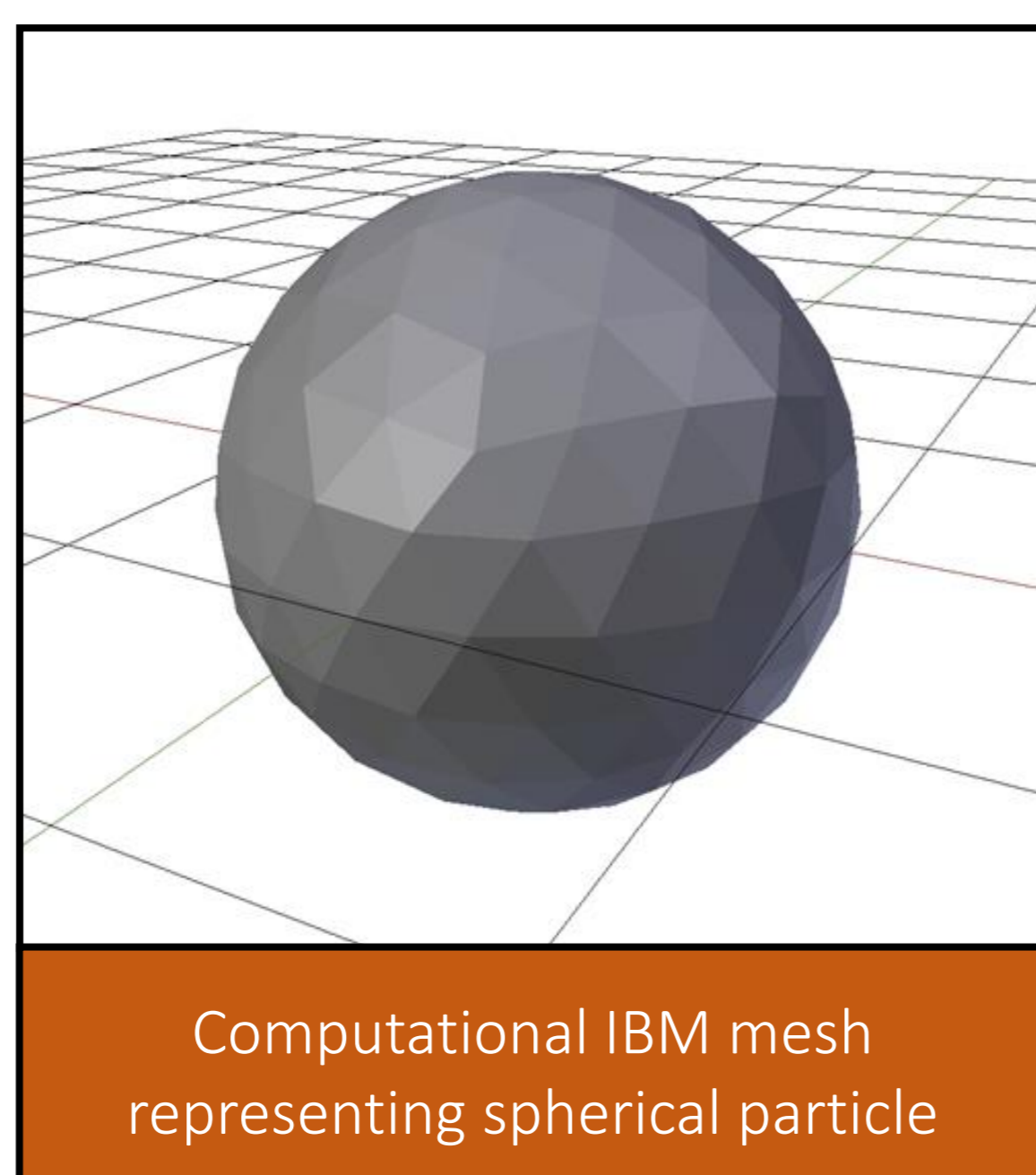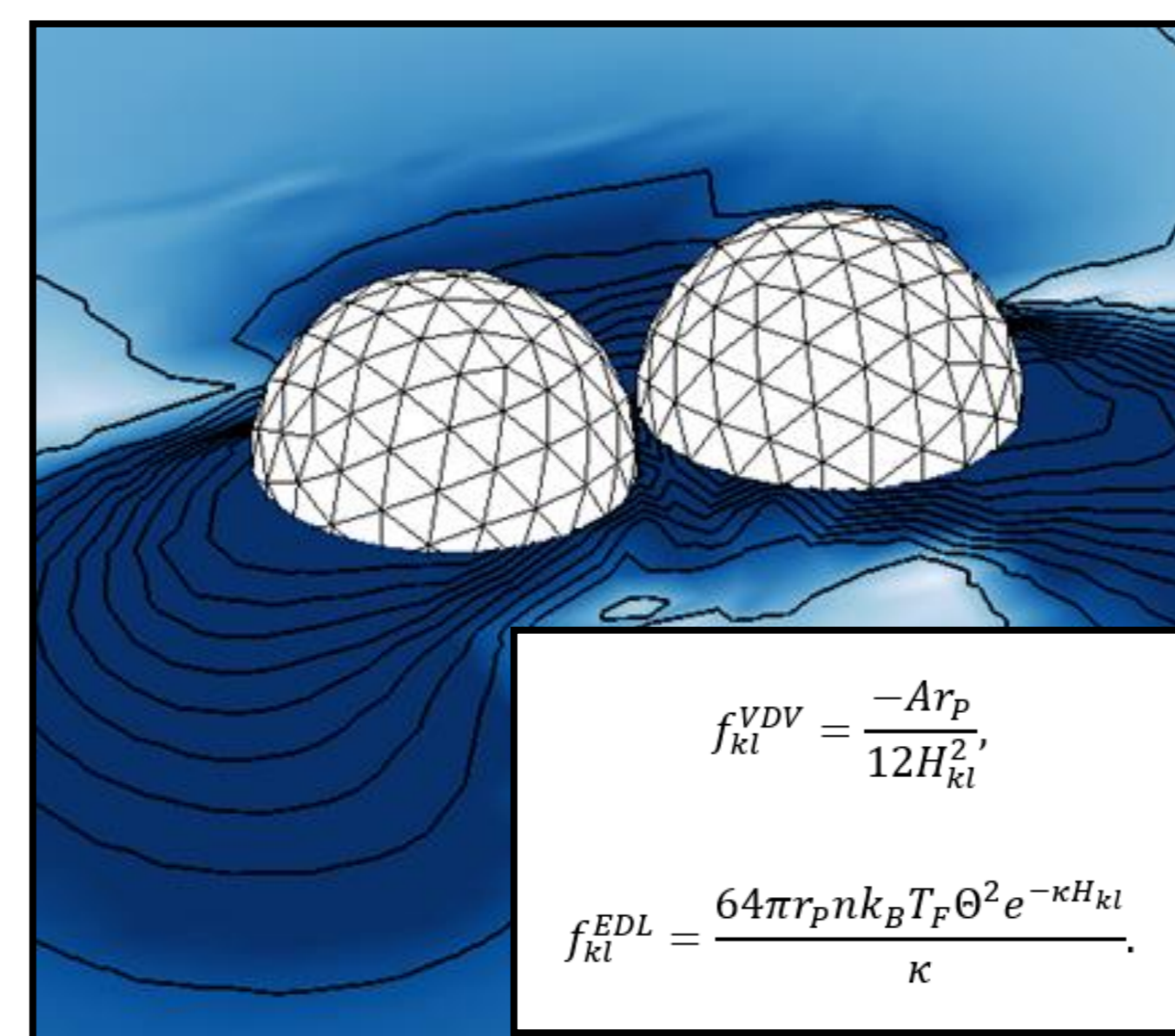

Re_λ=29 (Bulk flow)
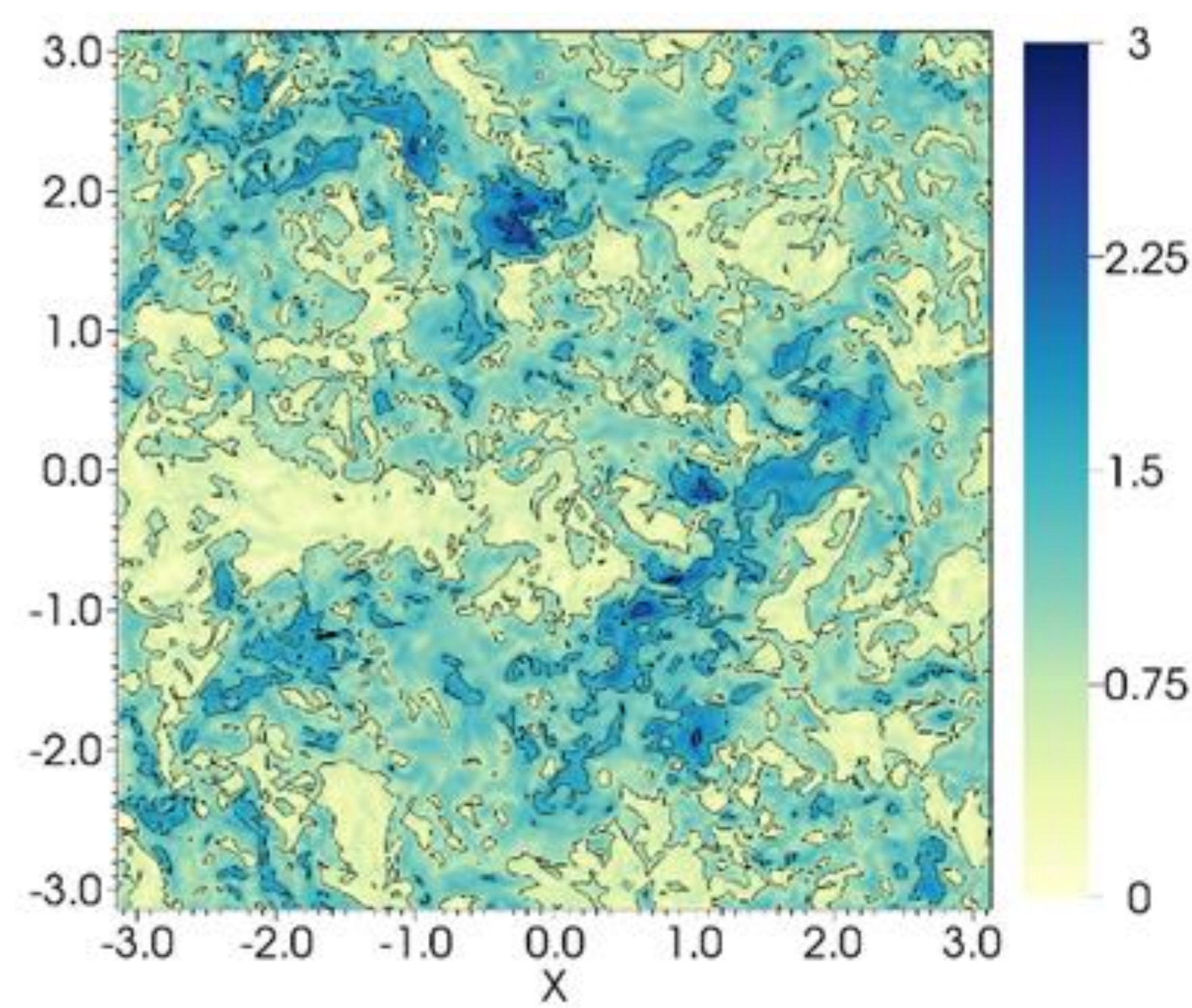
Re_λ=197 (Viscous sublayer)

4. Immersed boundary method

- Particles are represented by **icospheres** (right) on a secondary computational mesh consisting of 320 faces.
- The **immersed boundary condition** is a Dirichlet condition such that the fluid velocity on the surface of the boundary is precisely the velocity of the surface at that point.

Computational IBM mesh representing spherical particle

- This is achieved via the **ghost-cell method** wherein each cell in the domain is identified as external fluid, an internal ghost-cell or internal fictitious fluid. (See below)
- Particles are advected using **surface forces** (pressure and viscous) to predict translation and rotational motion.
- Orientation is tracked using the **quaternion formulation**.

Ghost-cell approach

Rotational dynamics

$$F_j = \sum_{f=1}^{N_f} \left(\underbrace{-P^f \delta_{ij}}_{Pressure} + \underbrace{\tau_{ij}^f}_{Viscous} \right) n_j^f dS^f$$

Hydrodynamic forces

5. DLVO interaction and behavioural modification

$$f_{kl}^{VDV} = \frac{-Ar_P}{12H_{kl}^2},$$

$$f_{kl}^{EDL} = \frac{64\pi r_P n k_B T_F \Theta^2 e^{-\kappa H_{kl}}}{\kappa}.$$

- Attractive (van der Waals) and repulsive (electric double layer) forces are used to predict interaction dynamics.
- Greatest response in collision dynamics is shown to coefficient of restitution, with Hamaker constant affecting collision velocities.
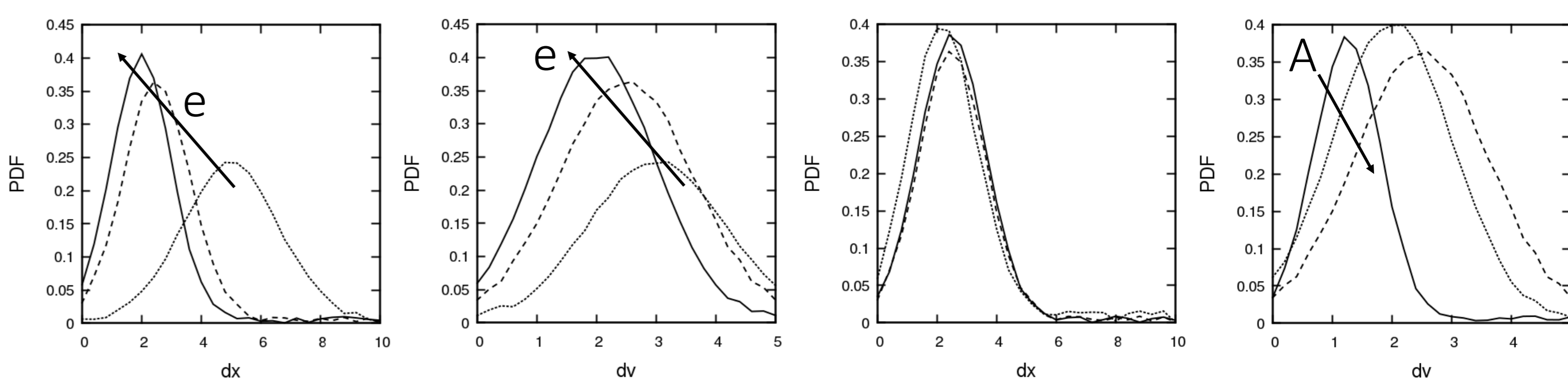
PDFs of relative displacement (dx) and relative velocity (dv) for restitution coefficient (left) and Hamaker constant (right).
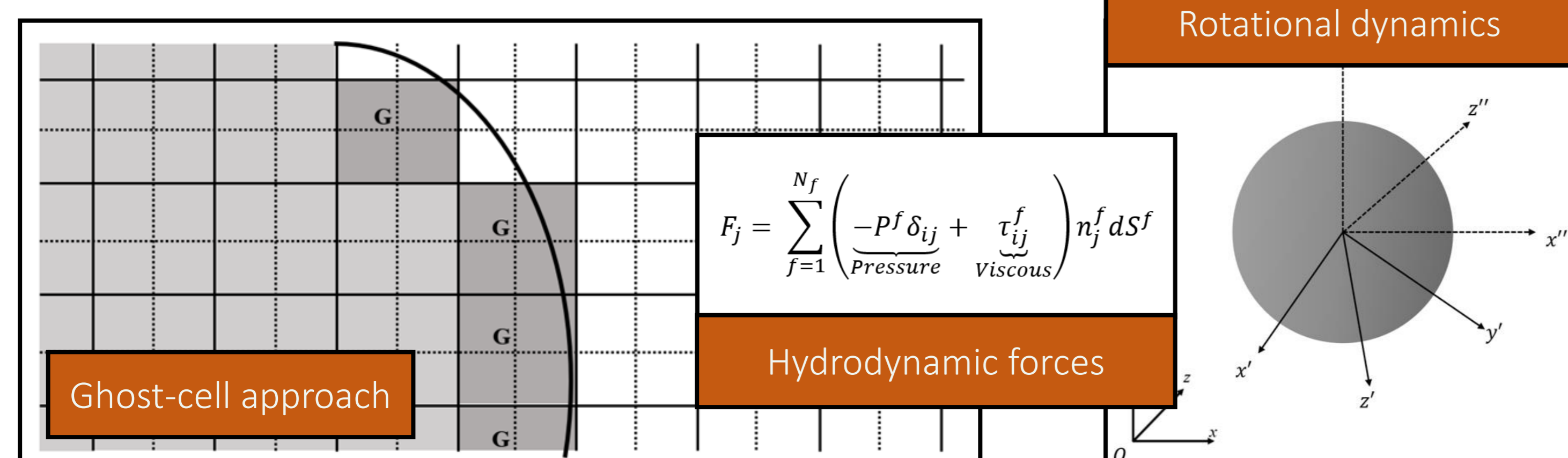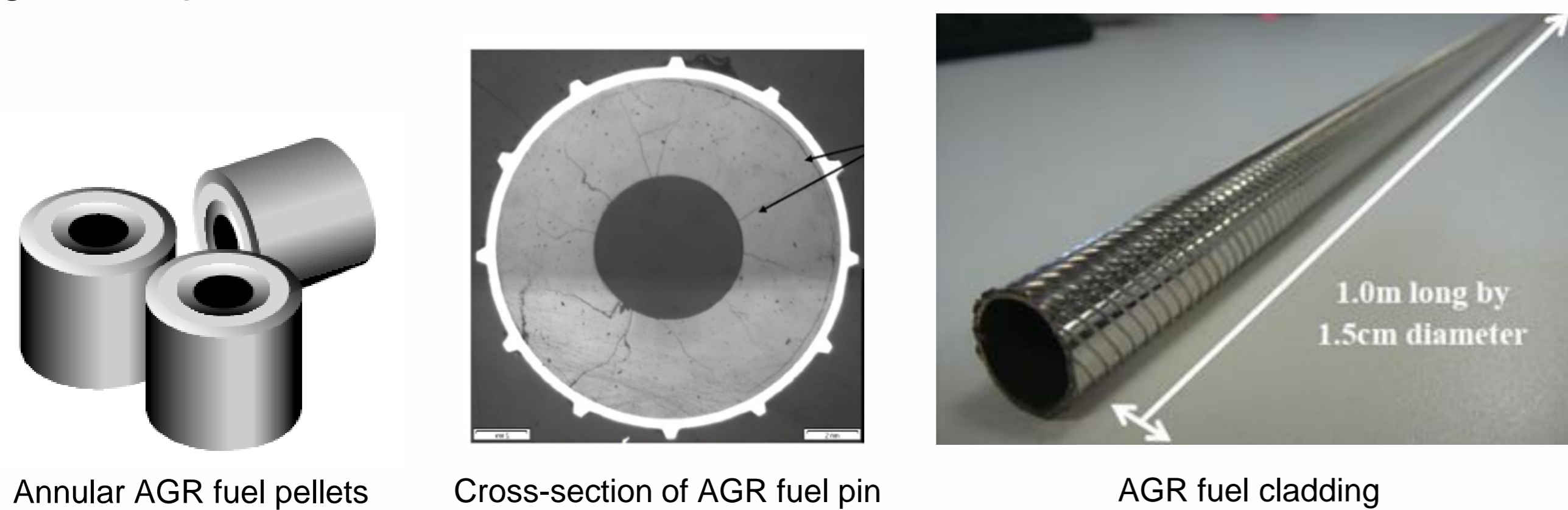
6. Conclusions & further work

- DNS-IBM used to study particle-particle interaction on fundamental level to investigate behavioural modification by controlling important flow parameters.
- In the future, properties such as temperature, pH and polymer additive concentration will be studied.

Transformative Science and Engineering for Nuclear Decommissioning

Oxidation of Uranium Oxide (UO₂) at Low Temperatures

YiFeng Huang (Nigel)[1]*, Prof Colin Boxall[1], David I. Hambley[2]

[1] Department of Engineering, Lancaster University, Lancaster, LA1 4YR

[2] Spent Fuel Management and Disposal, UK National Nuclear Laboratory (NNL), Central Laboratory, Sellafield CA20 1PG

* y.f.Huang@Lancaster.ac.uk

Introduction

UO₂ is the fuel source for the UK's fleet of **Advanced Gas Cooled Reactors (AGR)**, existing in the form of annular UO₂ ceramic pellets, at approximately ~3-4% U235 enrichment, sealed inside 20/25/Nb stainless steel cladding to give fuel pins.

Annular AGR fuel pellets · Cross-section of AGR fuel pin · AGR fuel cladding

1.0m long by 1.5cm diameter

AGR spent nuclear fuel (SNF) reprocessing has historically taken place at THORP, however, since November 2018, THORP is no longer in operation. The **fate of reprocessing** has led to a change in the future management of AGR SNF, moving the UK towards an open fuel cycle likely to involve long term fuel storage followed by final disposal in a geological repository.

Up to 1000m · 4400m · 2600m
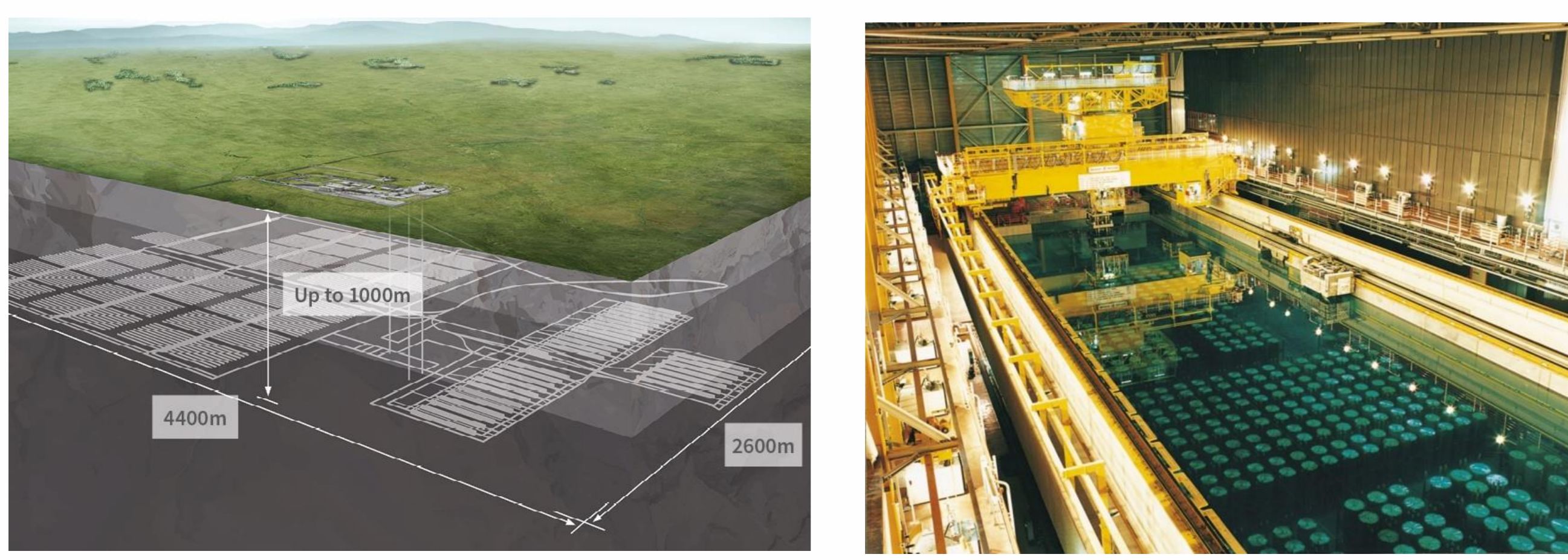
GDF: Artist's interpretation · THORP storage ponds

Based on the expected operational lifetime of the current AGR's, it is estimated that **~6600 tonnes of AGR SNF** will be generated. This leaves many questions about the UK's future strategy on dealing with the AGR SNF prior to its final disposal in a **Geological Disposal Facility (GDF)**.

Research Motivation

- To underpin the options for **pre-disposal storage** of SNF and prediction of the behaviour during **final disposal**.
- Must **satisfy safety case requirements** for the UK's Geological Disposal Facility and for interim storage options prior to final disposal.
- Concerned with the management of in-reactor or in-pond failed fuels. The **loss of fuel pellet integrity** can lead to potential release of fission products and radionuclides.
- Much of the existing research on simulant fuels (SIMFuels) are based on the study of Light Water Reactor and CANDU Pressurised Heavy Water Reactor SIMFuels. There is a need for **UK specific AGR spent fuel research**.

References

Elorrieta, J. M. et al. (2016). "A detailed Raman and X-ray study of UO₂₊ₓ oxides and related structure transitions". In: Physical Chemistry Chemical Physics 18.40, pp. 28209–28216.

Seibert, A. et al. (Dec.2011). "The use of the electrochemical quartz crystal microbalance (EQCM) in corrosion studies of UO₂ thin film models". In: Journal of Nuclear Materials 419.1-3, pp. 112–121.

Wilbraham, Richard J et al. (2018). "Raman studies of advanced gas-cooled reactor simulated spent nuclear fuels". In: Progress in Nuclear Science and Technology 5, p. 4.

Methods in Literature

μ-Raman Spectroscopy

The use of μ-Raman spectroscopy for **surface and structural study of UO₂** has been an increasing method of choice. Enabling analysis of the surface structure in relation to oxidative and reductive activity, the effects of dopants and hyperstoichiometry on its lattice structure.
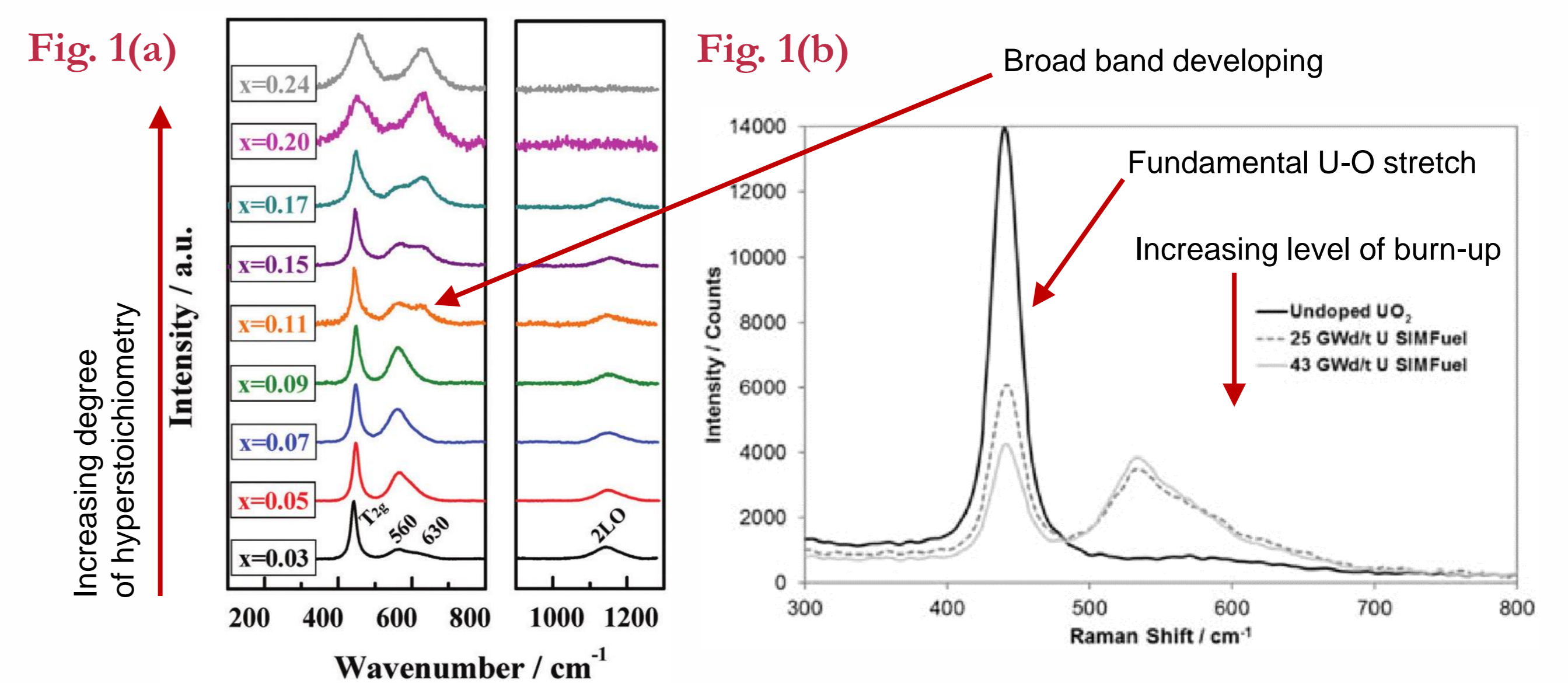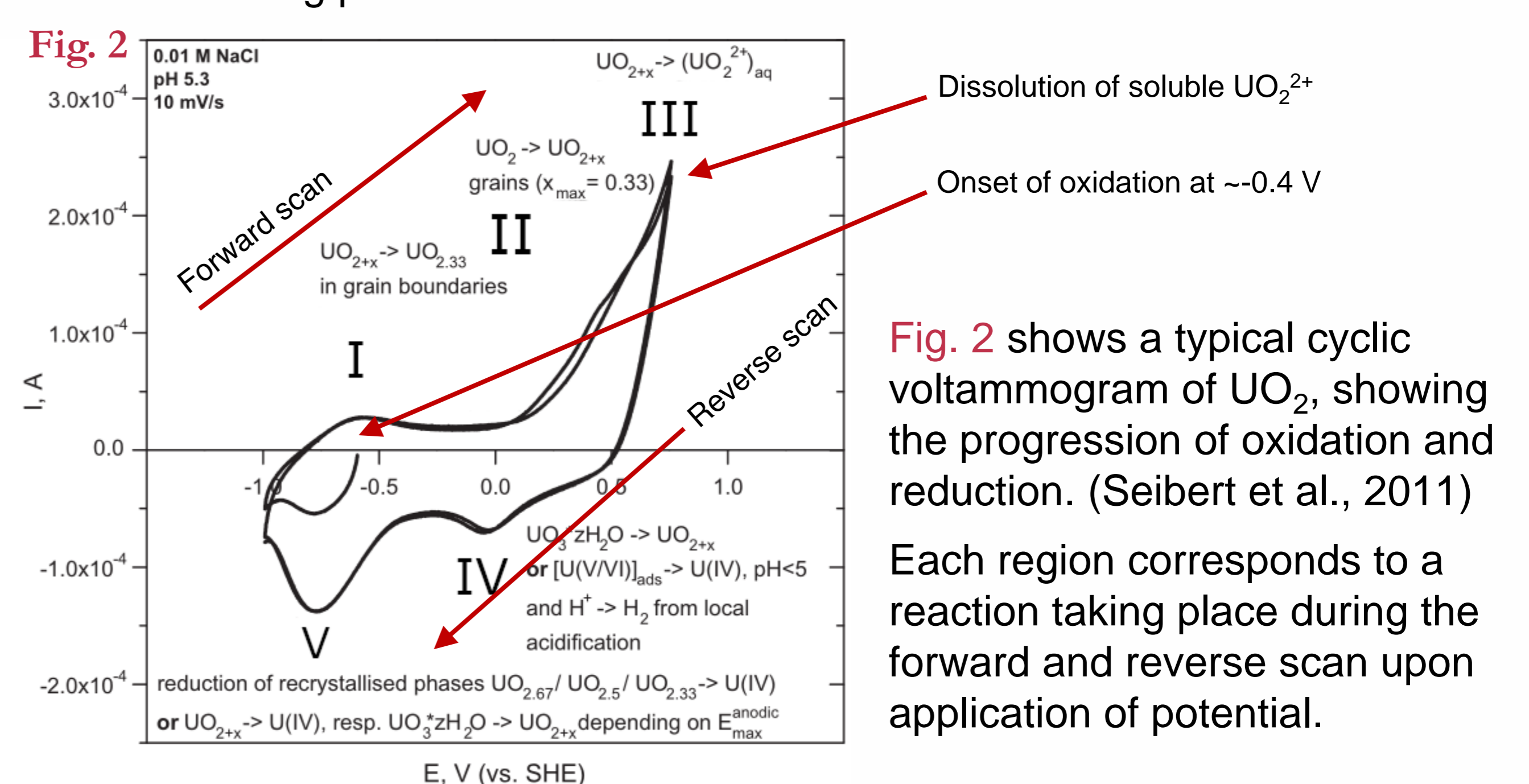

Fig. 1(a) · Fig. 1(b)

Broad band developing · Fundamental U-O stretch · Increasing level of burn-up

Undoped UO₂ · 25 GWdt U SIMFuel · 43 GWdt U SIMFuel

Fig. 1 shows how the Raman spectra of UO₂ changes depending on its degree of hyperstoichiometry (UO₂₊ₓ), (Fig.1a) (Elorrieta et al., 2016) and degree of simulated burn-up (level of doping) (Fig.1b) (Wilbraham et al., 2018).

As hyperstoichiometry and doping increases the presence of a new broad band appears, indicating lattice damage and formation of defect structures. This is said to enhance the galvanic coupling at anodic and cathodic sites, promoting corrosion (Fig.1a/b). Coupled with the decrease in intensity of the fundamental U-O stretch, suggesting transition away from a perfect cubic fluorite lattice structure.

Electrochemistry

Various factors can affect fuel corrosion/dissolution such as pH, temperature, groundwater chemistry, fuel matrix dopants and the influence of products derived from water radiolysis. Electrochemistry can be used to study the anodic and cathodic activity of the fuel surface with respect to these factors. Giving information about corrosion potentials and the oxidation/reduction reactions taking place.

Fig. 2 — 0.01 M NaCl, pH 5.3, 10 mV/s

Dissolution of soluble UO₂²⁺ · Onset of oxidation at ~-0.4 V

Fig. 2 shows a typical cyclic voltammogram of UO₂, showing the progression of oxidation and reduction. (Seibert et al., 2011)

Each region corresponds to a reaction taking place during the forward and reverse scan upon application of potential.

Aims & Objectives

Using **AGR SIMFuels** to understand the oxidation behaviour of the UO₂ matrix in failed AGR spent fuel, at low temperatures and under conditions relevant to UK interim storage and the drying of wet stored SNF.

- Study UO₂ and AGR SIMFUEL oxidation as a function of **simulated burn-up** and **temperatures of < 200°C**, in:
  - simulated interim storage pond-waters and repository ground-waters
  - **dry air** as a function of oxygen partial pressure (P$_{O2}$)
  - **damp air** as a function of relative humidity (RH) and P$_{O2}$
- Hence determine thresholds for the onset of UO₂ oxidation in AGR SIMFUELS and pure UO₂.

Transformative Science and Engineering for Nuclear Decommissioning

EPSRC — Engineering and Physical Sciences Research Council · UK Research and Innovation

transcendconsortium.org

Energy for a Low Carbon Future

Characterisation of Uranium Mineral Phases by Time-Resolved Laser Fluorescence and Raman Spectroscopy

Victoria L. Frankland[1]*, Antoni Milodowski[1] and David Read[1,2]

[1] Department of Chemistry, University of Surrey, Guildford, GU2 7XH, UK;
[2] National Physical Laboratory, Teddington, TW11 0LW, UK

* v.frankland@surrey.ac.uk

Introduction

Corrosion of spent nuclear fuels (SNF) typically proceeds from the development of ultra-thin films on the fuel's altered surface, through colloidal particulates to aqueous solution. The physical persistence and chemical composition of these species is largely dependent on the surrounding solution resulting in the potential formation of a large number of mineral species. Monitoring of stored SNF and their corrosion products can be achieved using remote techniques including laser-based methods such as Raman and time-resolved laser fluorescence spectroscopy (TRLFS). Characterisation of natural uranium minerals, representing potential corrosion products, provides essential reference spectra for validation purposes and to help guide in situ, real-time experimental simulation of the corrosion process.

Raman Spectroscopy

Figure 1: Raman apparatus

Raman spectroscopy is used to observe vibrational, rotational and other low frequency modes in a sample. The apparatus (Figure 1) has four lasers (457, 532, 633 and 785 nm) enabling a greater range of Raman modes to be observed. An advantage of using Raman over IR spectroscopy is the position of the H_2O features (~1650 and 3200 – 3800 cm^{-1}) [1-4] do not mask other transitions. This enables aqueous solutions and colloidal particulates to be characterised in addition to solid phases.

Time-Resolved Laser Fluorescence Spectroscopy (TRLFS)

This technique explores the fluorescence behaviour of fine powder (amorphous or crystalline), colloidal or solution samples. Fluorescence excitation and emission spectra are obtained using a xenon lamp and steady state detector whereas fluorescence decay half-life, τ, measurements are performed using either a supercontinuum or picosecond laser with lifetime detector (Figure 2).
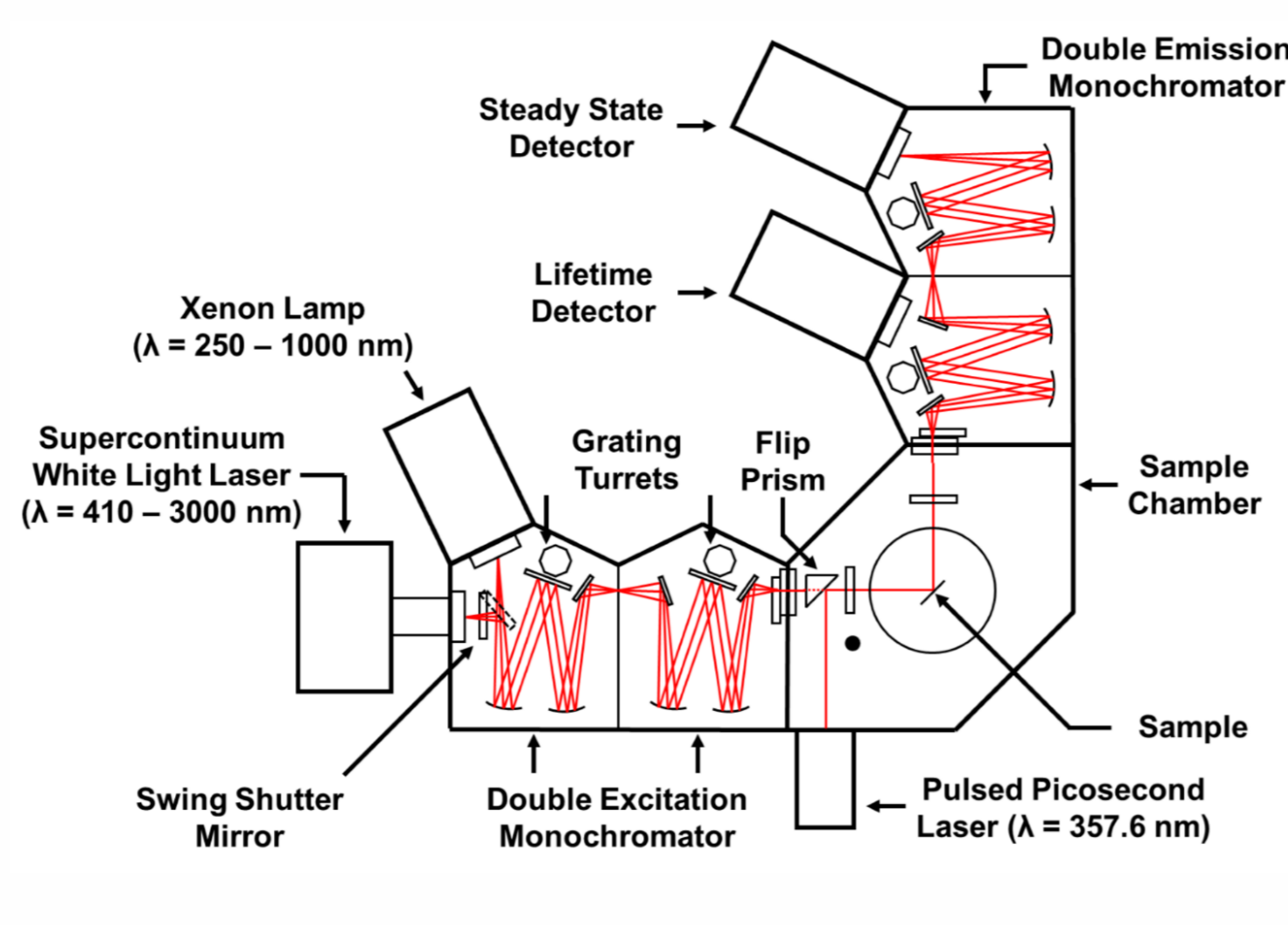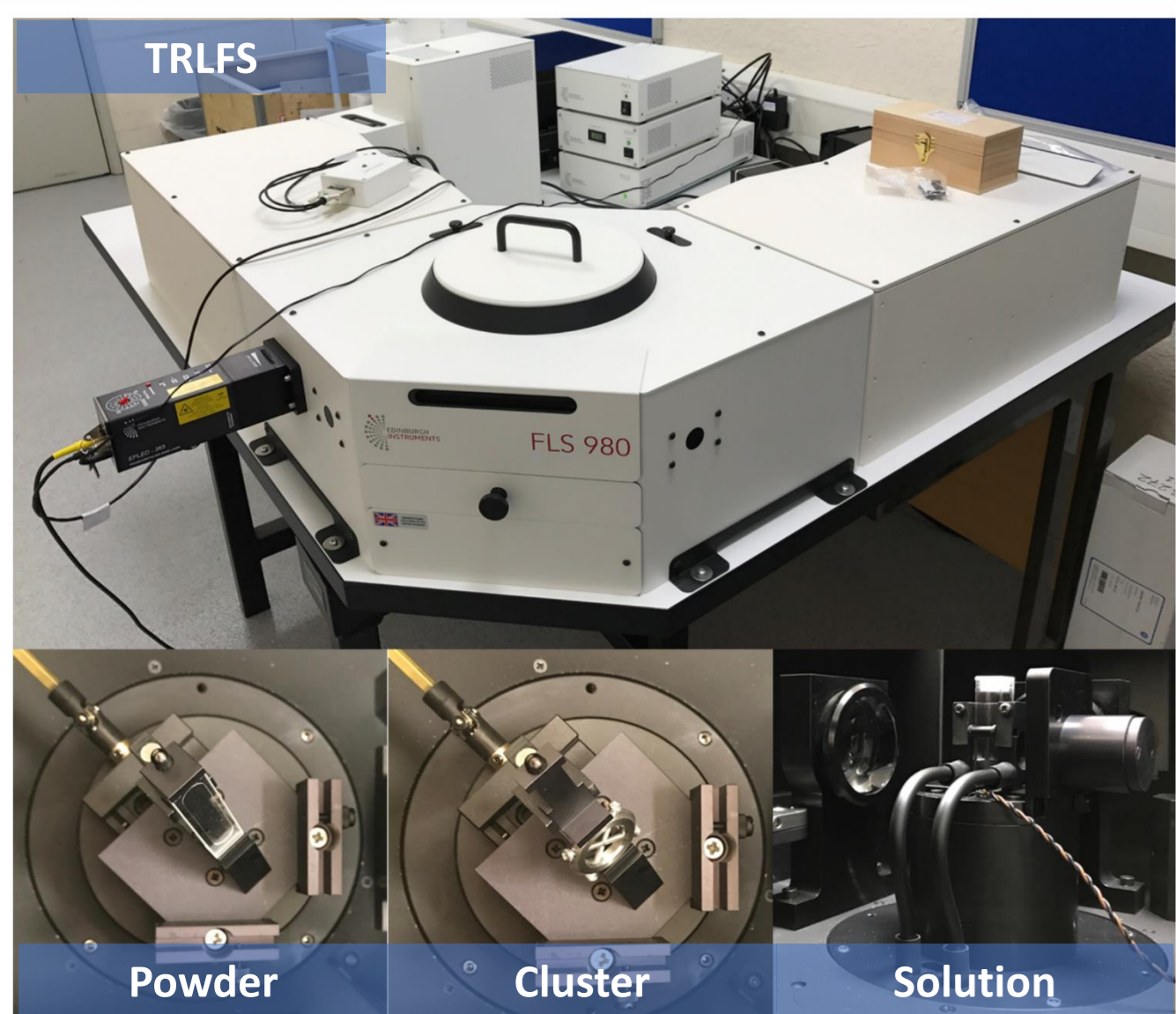

Figure 2: TRLFS apparatus (left) and schematic (above)

Samples

The mineral samples included here (Figure 3) were loaned by the British Geological Survey (BGS). Chemical composition was confirmed using scanning electron microscopy with energy dispersive X-ray spectroscopy (SEM-EDX) and X-ray diffraction (XRD)

Figure 3: From left: meta-autunite (Ca(UO$_2$)$_2$(PO$_4$)$_2$·6-8(H$_2$O)); meta-torbernite (Cu(UO$_2$)$_2$(PO$_4$)$_2$·8(H$_2$O)); vandenbrandeite (CuUO$_2$(OH)$_4$); and vandendriesscheite (Pb$_{1.5}$(UO$_2$)$_{10}$O$_6$(OH)$_{11}$·11(H$_2$O)).

Data Interpretation

Fluorescence effects during Raman analysis were observed for all samples with all four lasers but to a lesser extent at 785 nm, corresponding to the lack of fluorescence observed above 650 nm in the TRLFS emission spectra. All the spectral data could be resolved into individual peaks (Figures 4 and 5). The most intense feature observed in the Raman spectra was the uranyl symmetric stretch vibration, $v_1(UO_2)^{2+}$ (Figure 4), from which the bond length, d_{U-O}, force constant, k_{U-O}, and uranyl symmetric bending vibration, $v_3(UO_2)^{2+}$, were calculated using the following equations [5-7]:

$$d_{U-O} \text{ (Å)} = 106.5 \times v_1(UO_2)^{2+} + 0.575 \qquad (1)$$
$$k_{U-O} \text{ (millidynes Å}^{-1}) = [1.08 / (d_{U-O} - 1.17)]^3 \qquad (2)$$
$$v_3(UO_2)^{2+} \text{ (cm}^{-1}) = [91.41 / (d_{U-O} - 0.804)]^{3/2} \qquad (3)$$

Values for τ were extracted using multiple exponential fits.

References:
1) Zotov, et al., Am. Mineral., 1998, 83, 823
2) Bell, et al., J. Am. Chem. Soc., 1997, 119, 6006
3) Kolesov, et al., Am. Mineral., 2002, 87, 1426
4) Pershin, et al., Opt. Spectrosc., 2005, 98, 543
5) Bartlett & Coone, J. Mol. Struct., 1989, 193, 295
6) Badger, Phys. Rev., 1935, 3, 284
7) Jones, Spectrochim. Acta, 1959, 15, 409
8) Baumann, et al., Environ. Sci. Technol., 2008, 42, 8266
9) Frost and Weier, Spectrochim. Acta A, 2004, 60, 2399
10) Faulques, et al., RSC Adv., 2015, , 71219
11) Massuyeau, et al., RSC Adv., 2017, 7, 919
12) Botto, et al., J. Mater.Sci., 2002, 37, 177
13) Frost and Cejka, J. Raman Spectrosc., 2007, 38, 460

Characterisation of Uranium Phases

Good agreement with existing Raman and fluorescence emission data was obtained for meta-autunite, meta-torbernite, vandenbrandeite and vandendriesscheite (Figures 4 and 5) [8-13]. Calculations of d_{U-O} and k_{U-O} varied between 1.78 – 1.87 Å and 3.68 – 5.69 millidynes Å^{-1}. The presence of the weak intensity $v_3(UO_2)^{2+}$ Raman mode in most of these samples indicates a deviation from the linear uranyl ion structure resulting in a lower symmetry for this ion.

Fluorescence emission spectra for meta-autunite and vandendriesscheite (Figure 5) were resolved into 7 peaks. Triple exponential fits were applied to obtain τ. The longest half-life was assigned to the fluorescence decay whereas the shorter two are attributed to light scattering on the sample surface.

Negligible fluorescence was detected for the vandenbrandeite sample. This could be due to either chemical or colour quenching effects or both.
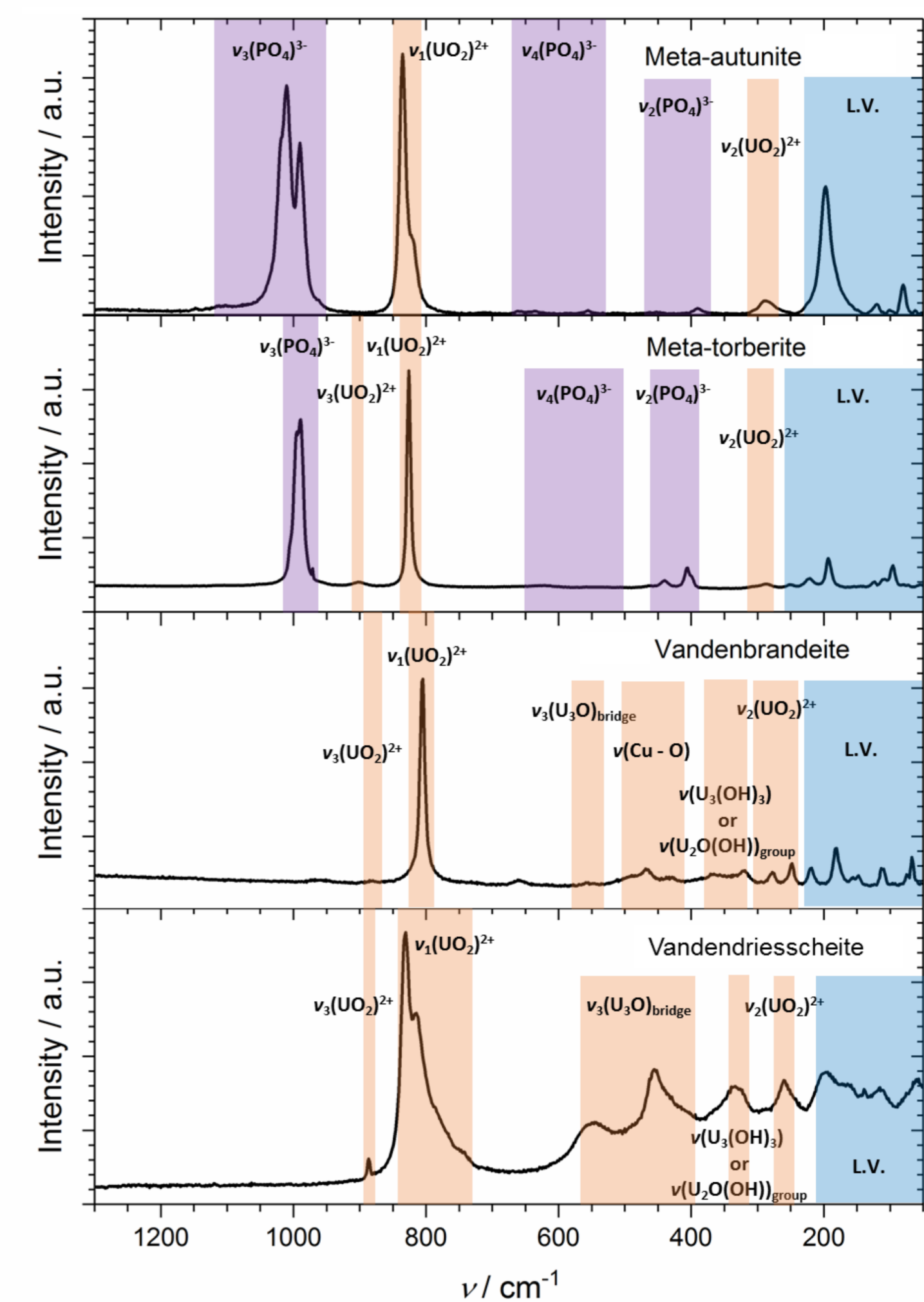

Figure 4: Assigned Raman spectra of U minerals with highlighted regions showing literature comparisons
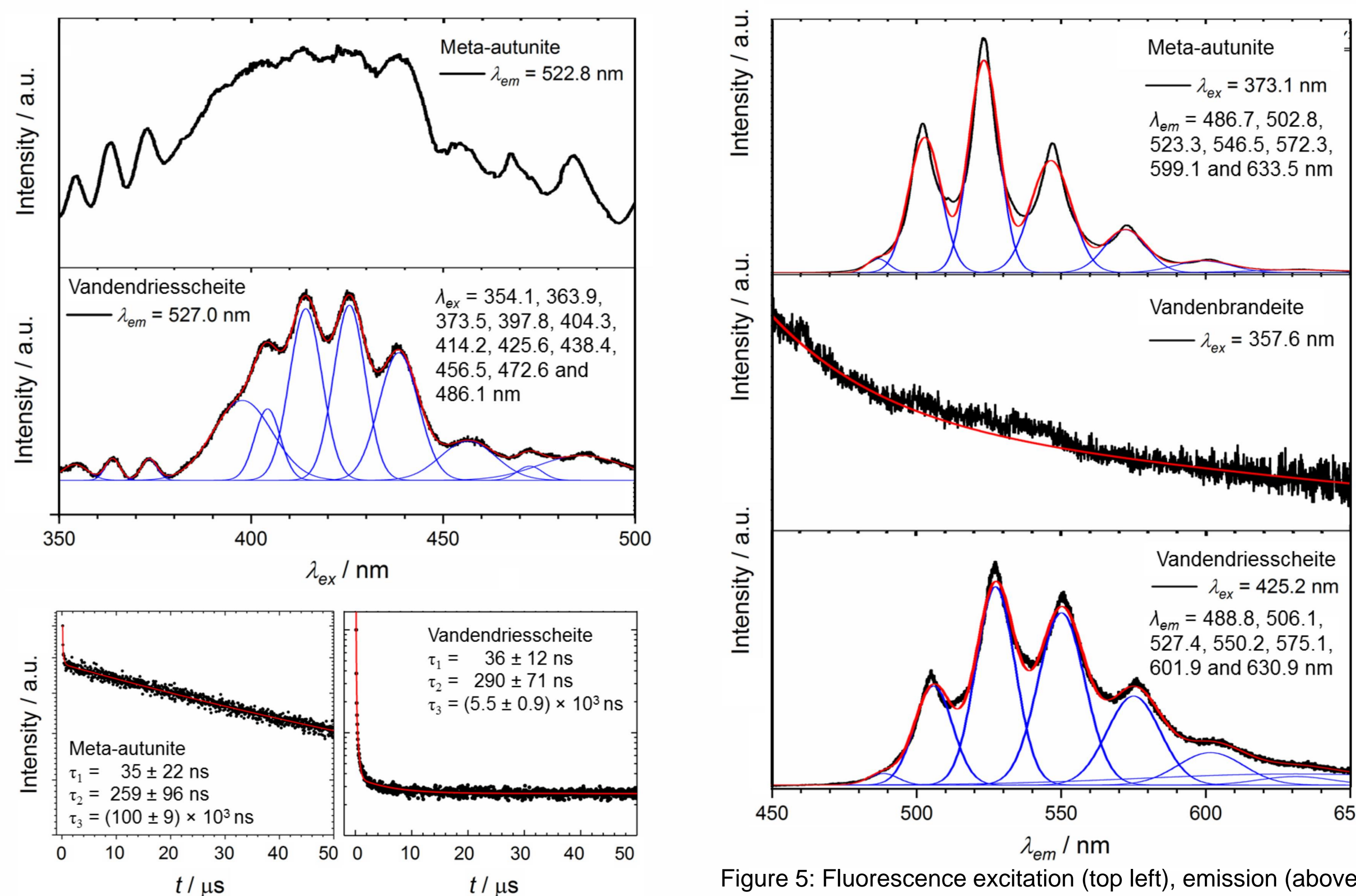

Figure 5: Fluorescence excitation (top left), emission (above) and decay (bottom left)

Future Work

Characterisation of uranium mineral and solution samples by TRLFS and Raman spectroscopy will continue. Reference spectra will be compiled into a database as a resource for project partners and the wider community. During the next phase the aim is to run simulation SNF corrosion experiments on thin U phase films with real-time characterisation of the evolving secondary phases.

Acknowledgement

Transformative Science and Engineering for Nuclear Decommissioning

transcendconsortium.org

Haris Paraskevoulakos, Tom Scott

HH Wills Physics Laboratory, Bristol, BS8 1TL

cp13846@bristol.ac.uk, t.b.scott @bristol.ac.uk

Introduction

Magnox nuclear reactors, using metallic uranium as fuel operated in the UK from the 1960's until just a few years ago. The metallic fuel was encased in a Magnesium alloy 'Magnox' cladding, which along with the U metal, is susceptible to corrosion by water. Until 1992, a significant volume of Magnox waste materials, including spent fuel assemblies, had been accumulated in the storage ponds at Sellafield in Cumbria [1]. These ponds were maintained at a high pH (above 10.5) to minimise corrosion [2]. However, considerable corrosion has still occurred over extended periods, raising concerns about the safe decommissioning of the facilities [3]. Corroded Magnox Sludge (CMS) arising from long-term corrosion of the cladding material is a prevalent residual material amongst others (e.g. fuel fragments and wind-blown debris) [4]. Corrosion of Magnox forms brucite (Mg(OH)$_2$) and liberates hydrogen. Embedded uranium metal fuel is also expected to have been exposed to water throughout the storage period. Uranium reacts with water to form uranium hydride (UH$_3$), uranium dioxide (UO$_2$) and hydrogen, presenting potential uncontrolled thermal hazards during decommissioning.
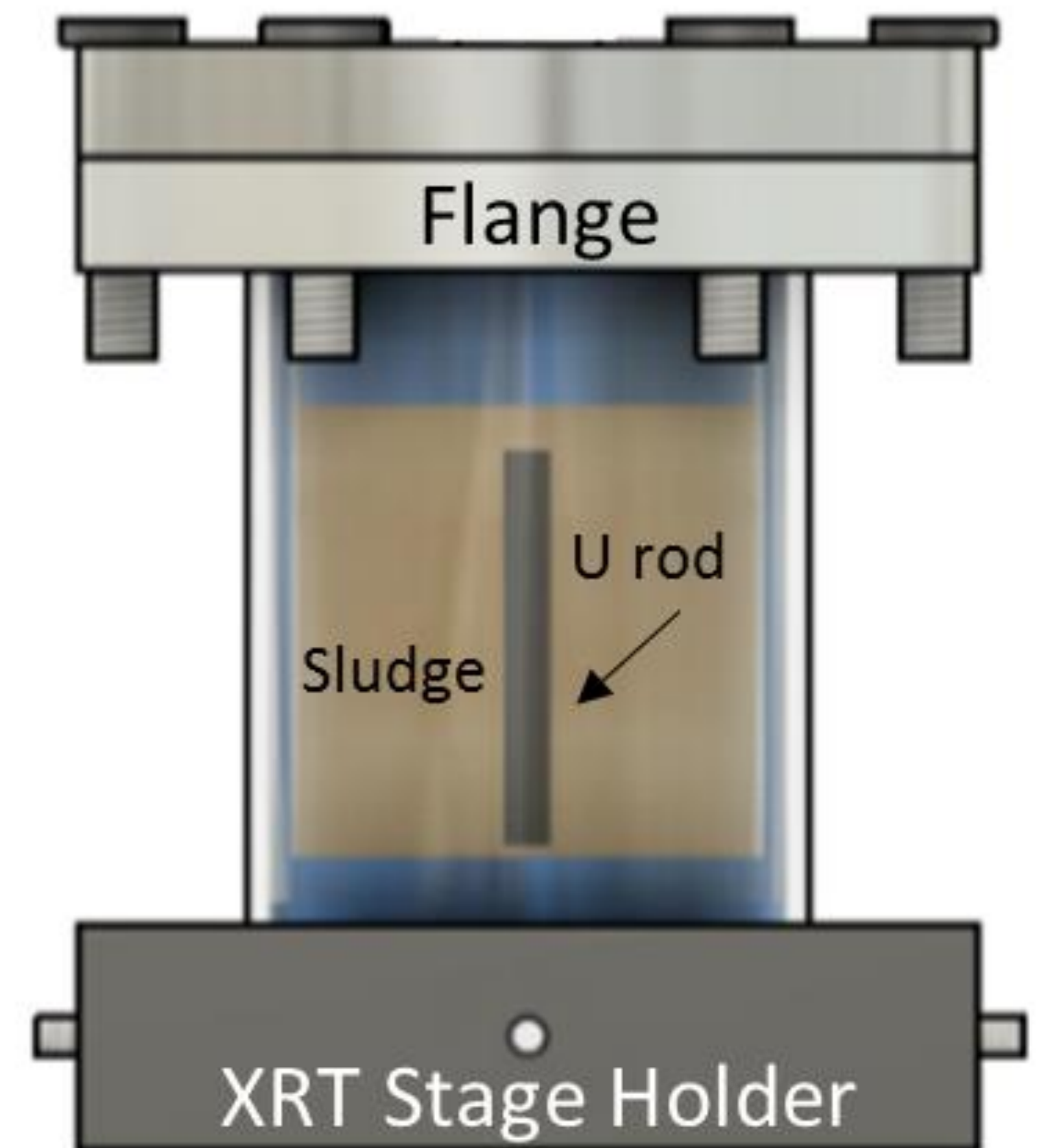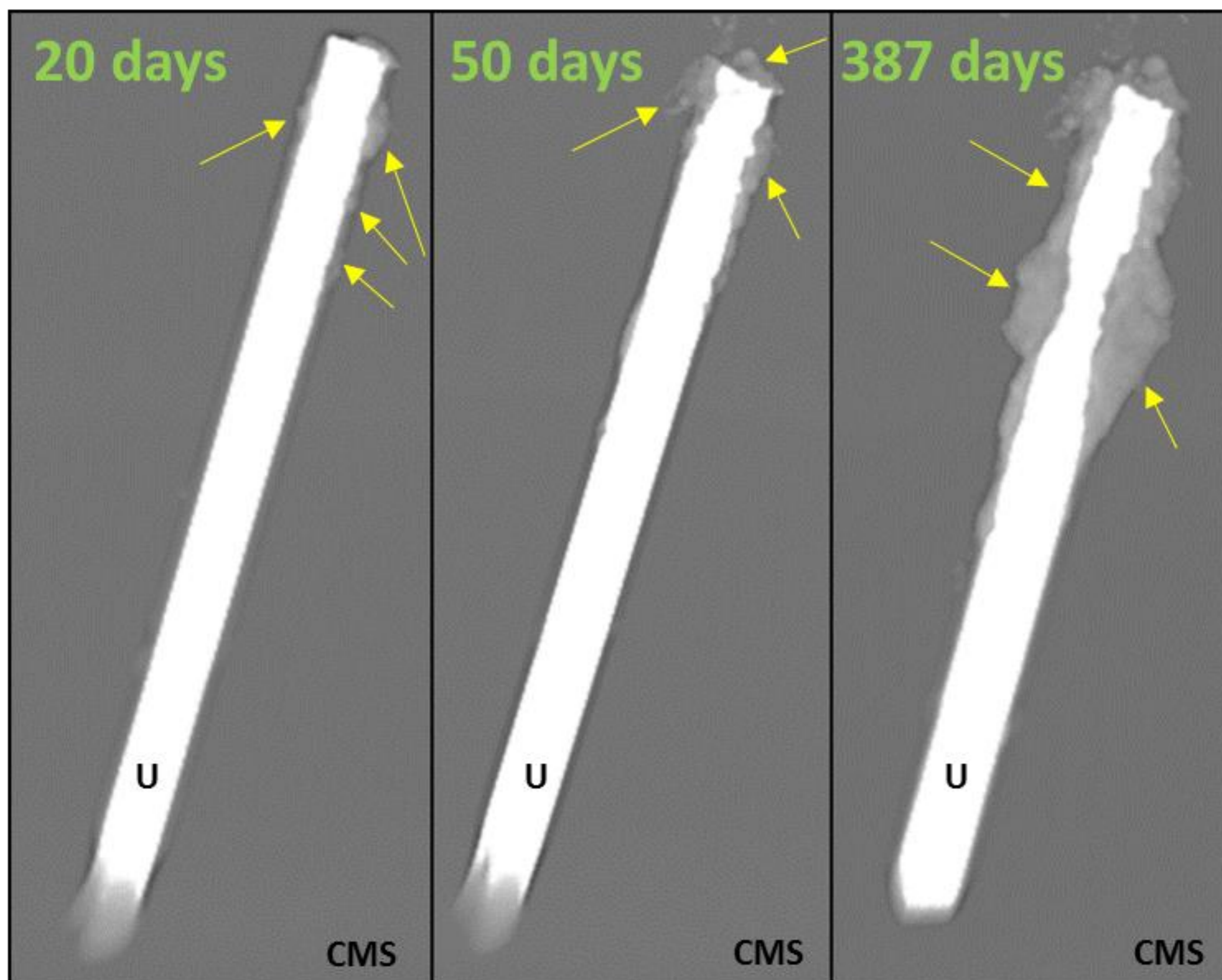
Figure 1: Experimental Analogue

Figure 2: XCT scans exhibiting uranium corrosion evolution within a CMS environment. The "age" of the sample at each different scan is shown in green letters.

Experimental Approach

A miniature analogue of storage pond conditions was experimentally replicated to investigate the behaviour of uranium while embedded in CMS (**Figure 1**). Powderised CMS–simulant was diluted in water to produce a thick slurry, resembling pond conditions. The sludge was poured into a cylindrical stainless steel cell. A single uranium specimen (1 mm x 1 mm x 20 mm) was then encapsulated in the CMS and the system was allowed to dry in air for 3 days before being sealed. At distinct time intervals, X-Ray Computed Tomography (XCT) was used to probe the evolving interior state of the sample and investigate the corrosion behaviour. Primary results are shown in **figure 2**. It can be observed that there is a notable change in the morphology around the embedded uranium specimen, attributed to progressive corrosion. The morphology of the developing corrosion layer at the uranium–CMS interface suggests the formation of UH$_3$ based on a morphology very similar to experiments performed in uranium–grout systems [5]. The progress of uranium corrosion can also be observed in **figure 3** where the residual metal has been segmented from the rest of the materials.

Summary–Future Plans

Feasibility trials have proven that XCT is a powerful non destructive method for investigating complex corrosion systems. Corrosion of the uranium, based on morphology change, has been observed to progress over more than a year since sample preparation. Using relevant software, a quantification of the corrosion percentage over time is now possible. Confirming the phase of the corrosion product (UH$_3$ versus UO$_2$) is now of **significant importance** for the project. Synchrotron X-ray Diffraction may provide a method to characterise the interacting materials without breaking the sealed containment. Thus, potential formation and persistence of the pyrophoric UH$_3$ could be validated.

Figure 3: 3D views of the uranium specimen. Threshold segmentation allowed separation of the non–corroded metal.

References:
[1] S.F Jackson, S.D Monk, Z Riaz, Appl. Radiat. Isot. 94 (2014)
[2] N.C Colier, N.B Milstone, Cem. Concr. Res. 40 (2010)
[3] https://www.nda.gov.uk/documents/upload/Annual-Report-and-Accounts-2012-2013.pdf).
[4] Sellafield Ltd., Sellafield Plan Issue1 August 2011
[5] C. Paraskevoulakos, University of Bristol, PhD Thesis, 2017

Transformative Science and Engineering for Nuclear Decommissioning

transcendconsortium.org

TRANSCEND

Building the Foundations of a Predictive Tool for Spent Fuel Behaviour

A. Siberry[*1], R. Burrows[2], D. I. Hambley[2], A. M. Adamska[3], R. Springell[1]

[1] University of Bristol, BS8 1TL, UK *e-mail: as14659@my.bristol.ac.uk
[2] National Nuclear Laboratory, Gloucestershire, GL10 3UT, UK
[3] Sellafield Ltd, Cumbria, CA20 1PG, UK

Spent Fuel in the UK

As UO_2 comprises the majority of high level nuclear waste generated by modern society, it is crucial that we develop a safe and efficient storage strategy for this material. While many advances have been made to improve nuclear storage facilities, eventual failure of these systems will expose the surface of UO_2 to ground water, resulting in the release of radionuclides [2].

Figure 1: Spent fuel storage pond at Sellafield. Taken from [1].

Examination of a safety case that covers operation and post-closure safety must be included in the licensing process for such a facility [3]. The sheer timescales at which the waste remains hazardous gives rise to high levels of uncertainty that must be mitigated. By building predictive models for the likely corrosion behaviour of spent fuel exposed to pond or groundwater this can be achieved.
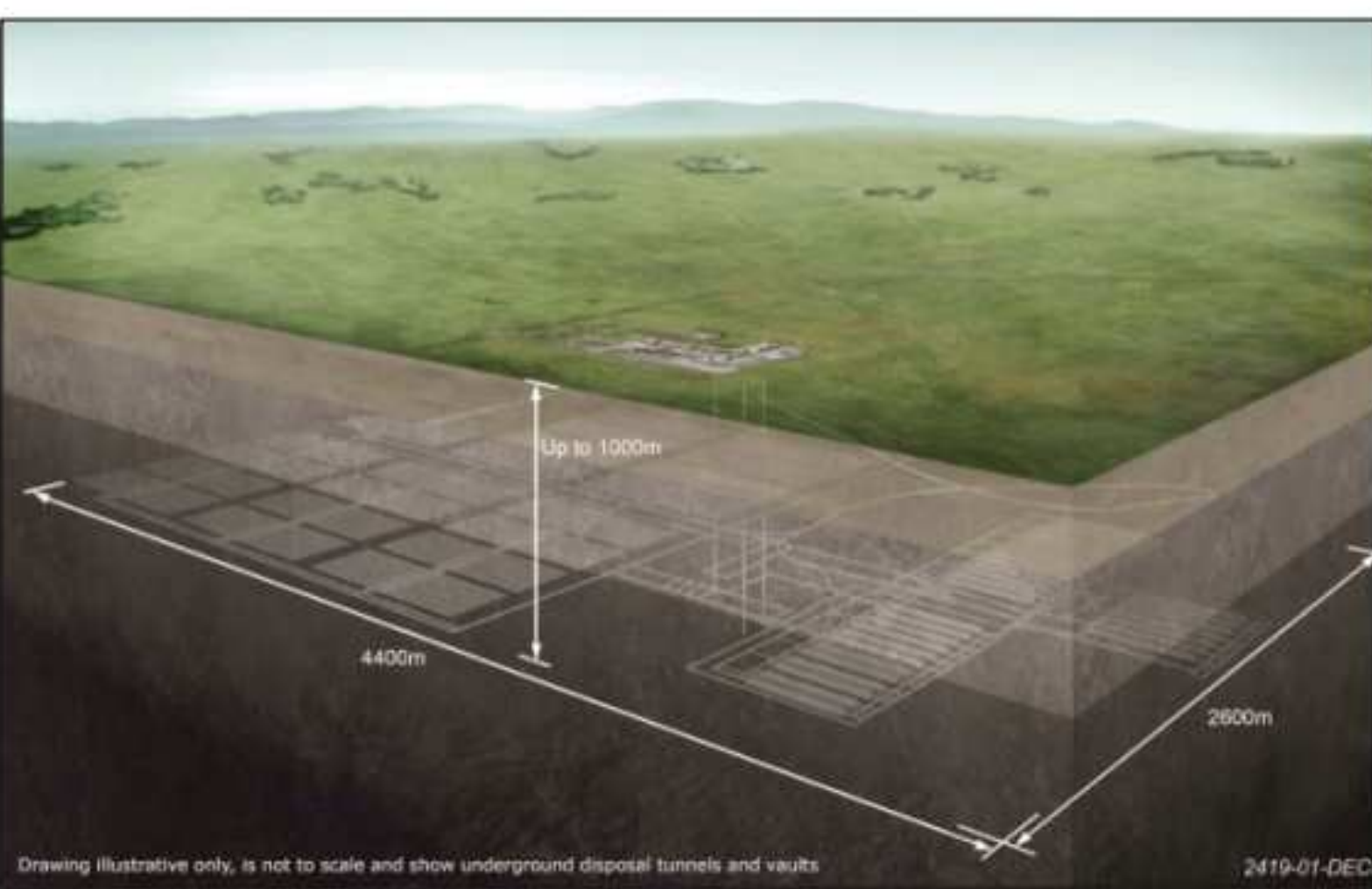
Figure 2: Artists impression of a Geological Disposal Facility (GDF). Taken from [1].

Thin Film Approach

Single crystal, thin films of UOx can be grown via reactive magnetron sputtering have been used to investigate the dissolution process. Yttria stabilised zirconia (YSZ) is used as a crystal substrate, giving a lattice strain of 6% (Fig 4) [4].

UO_2 (001) / YSZ (001) UO_2 (110) / YSZ (110) UO_2 (111) / YSZ (111)

Figure 4: YSZ crystal lattice match with [001], [110] and [111] oriented UO_2 [4].

Exposure to an Intense X-ray beam at a synchrotron source in the presence of water, radiolysis was induced to a 40 Å [001]-UO_2 thin film. Modelling the electron density, surface roughness and change in oxide composition a dissolution rate was achieved at the Ångström level [4].

Figure 3: Reactive DC magnetron sputter deposition mechanism of UO_2.

Figure 5: (Top) Panel (a) shows X-ray reflectivity data and (b) shows the high angle diffraction data of nominal 40 Å [001]-UO_2 thin film, grown on YSZ. The dashed black arrows indicate an increase in fringe, which suggests a concomitant loss of material. (Bottom) Pictorial representation of the increase in roughness and UO_x thickness, and the amount of dissolution as the surface undergoes corrosion [4].

Spent Fuel Dissolution

Well mixed bulk
Diffusion layer
Precipitate

Radiolysis (more possible oxidative products)

OH^*

H_2O_2 O_2

H_2O

α, β, γ

U(IV) chemical dissolution (Slow)

U(VI) chemical dissolution (Fast)

Precipitation attenuating radiation (Reducing radiolysis effects)

Precipitates limiting dissolution sites (Reducing the area available)

β, γ

α, β, γ

Precipitation retarding diffusion (Too and from fuel surface)

Small noble metal particles (NMP or ε) (Supply or consume e- at rapid rates)

U(IV) oxidation

Galvanic corrosion of metal/ceramic coupling

Formed during fission

Potential Hydrogen generation (from corrosion of steel surfaces)

Modelling Tools

MOOSE Framework (MARMOT)
Open source, parallel finite element framework for developing Multiphysics solvers.

Use – with the inclusion of mesoscale simulation environment MARMOT modelling of microstructure and material properties under stress, temperature and irradiation damage.
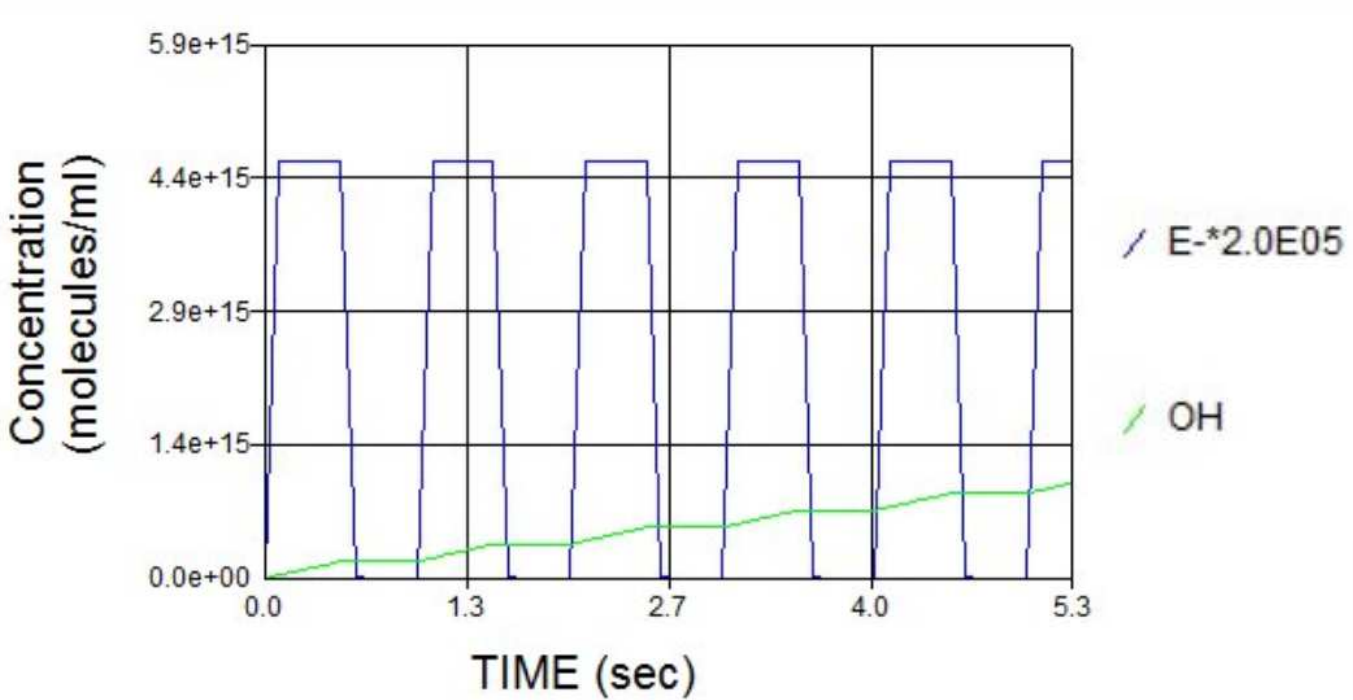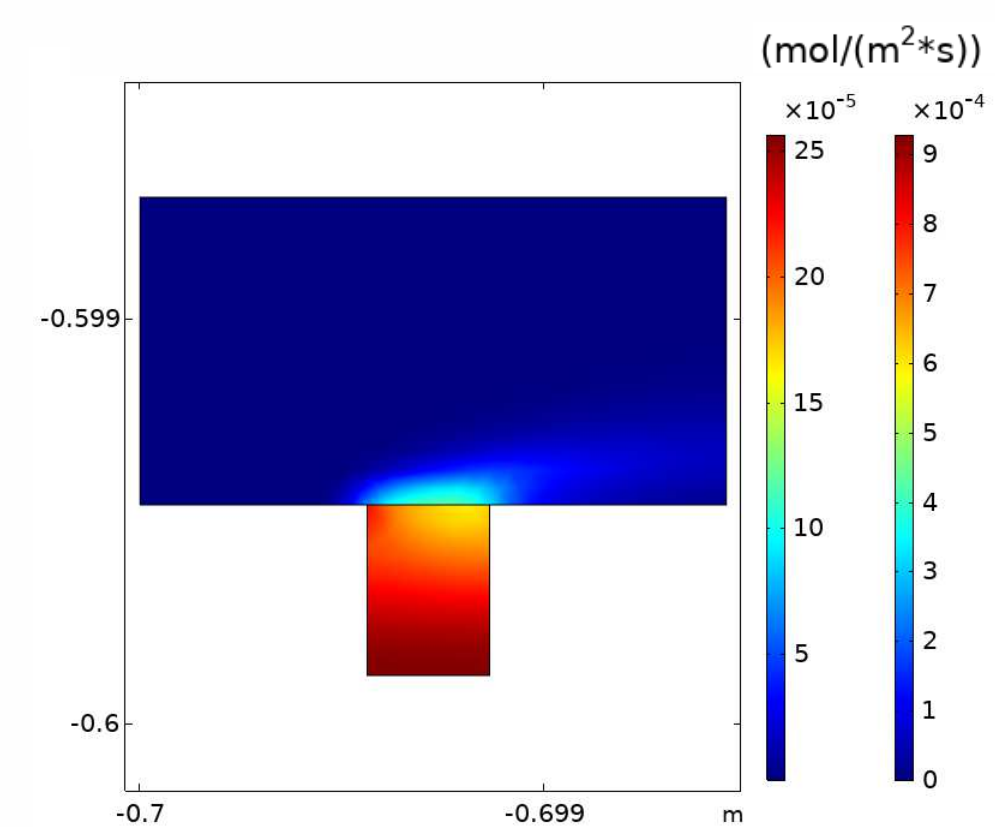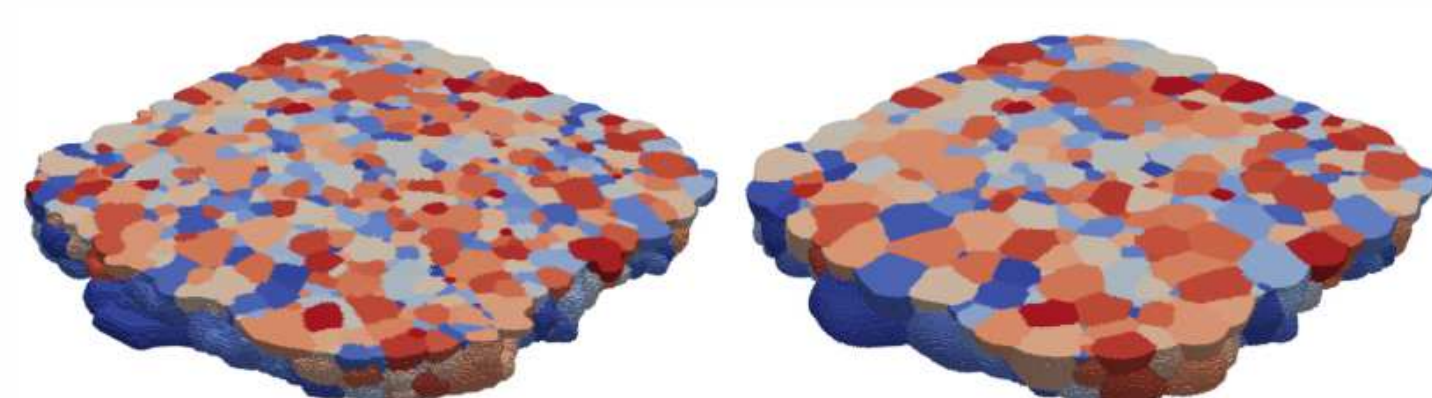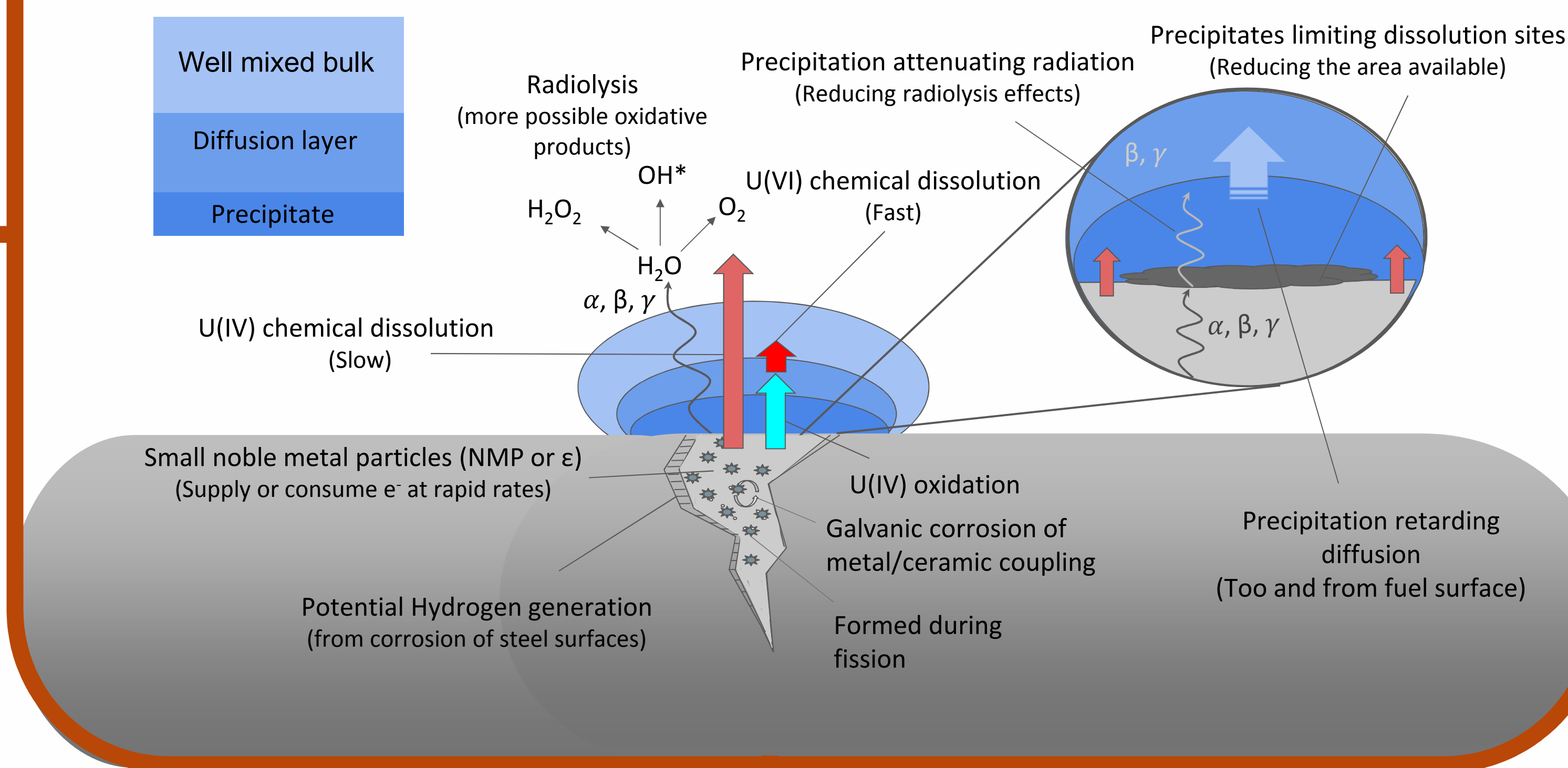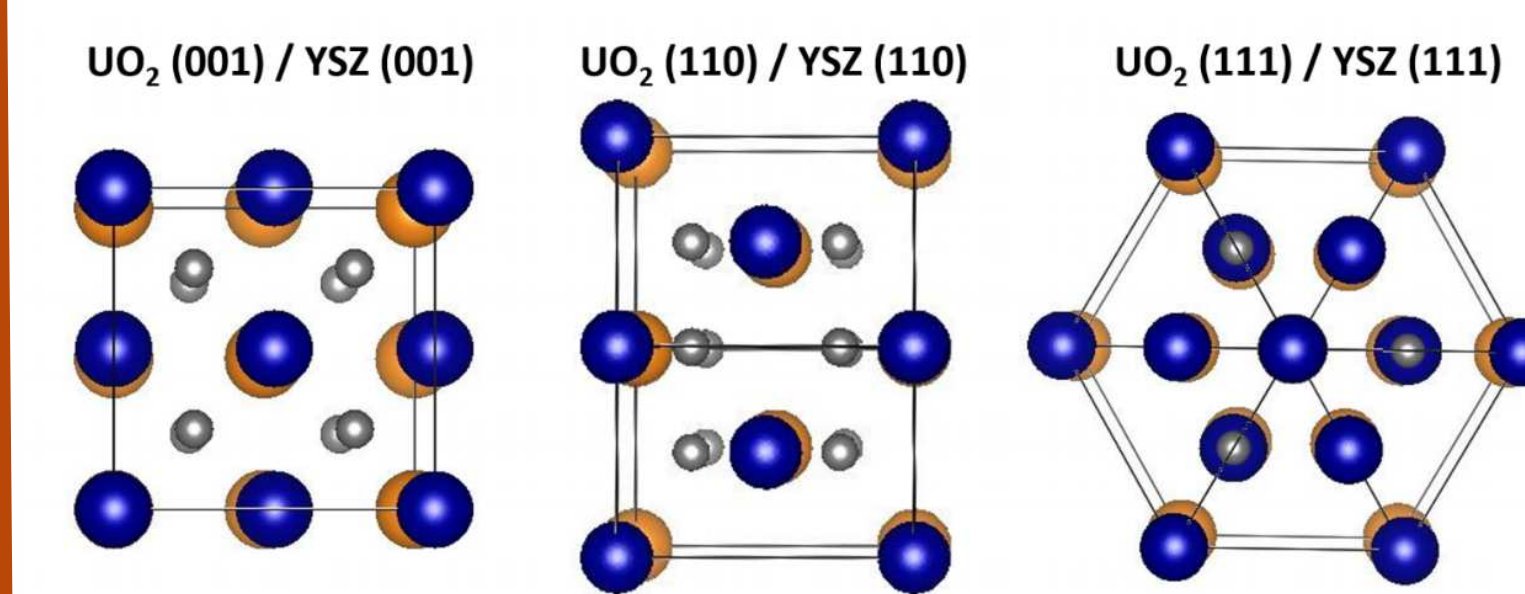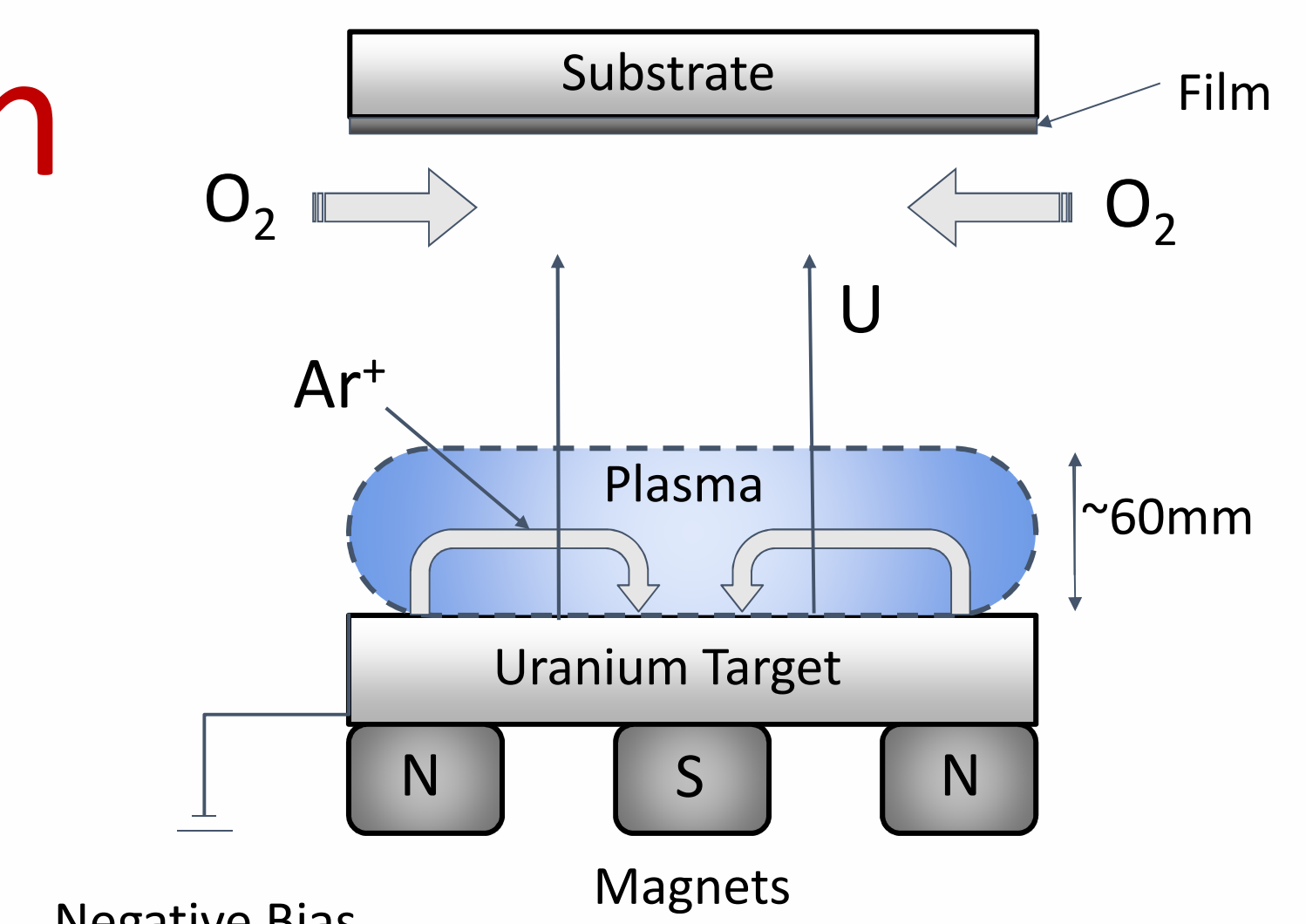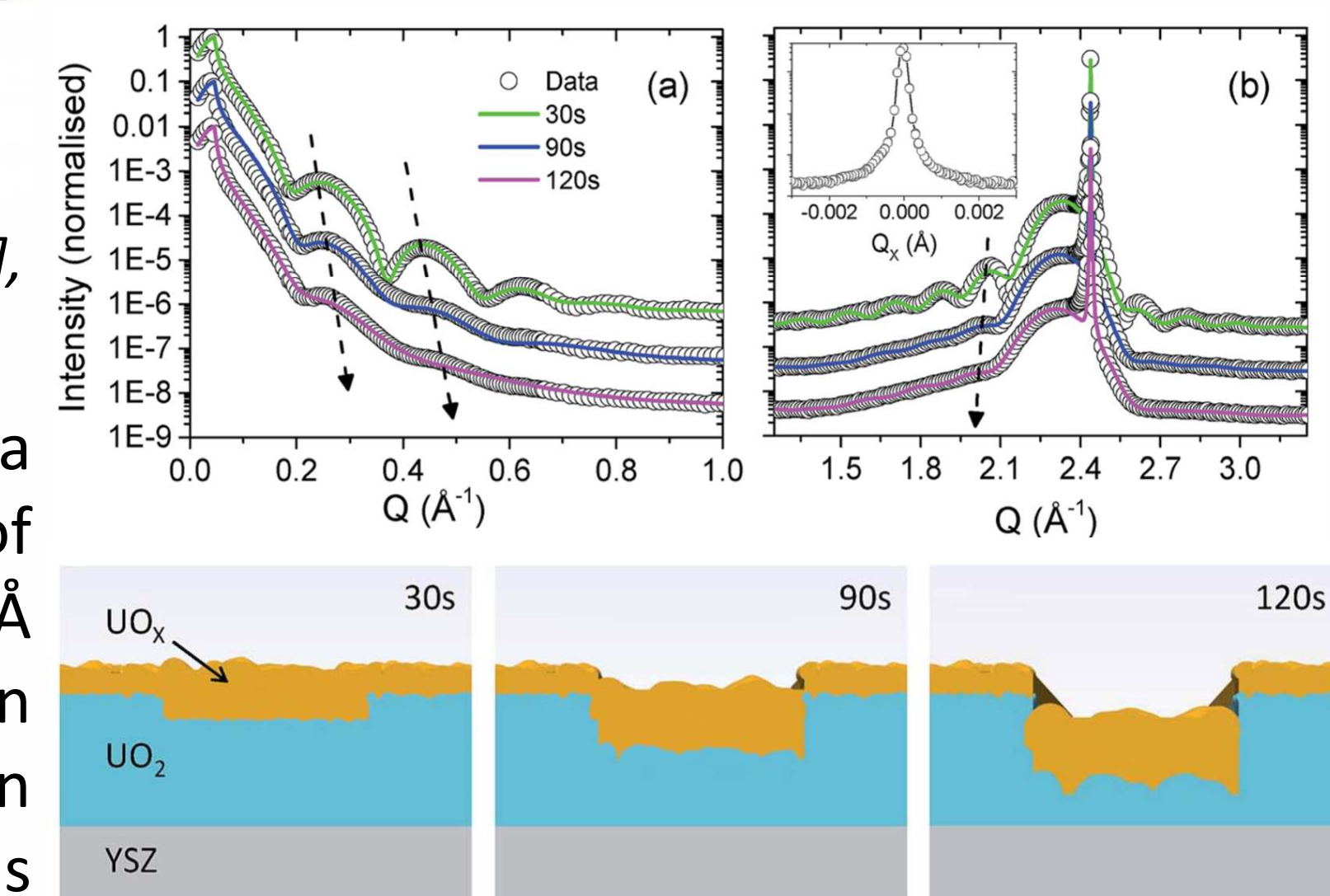
Figure 6: MARMOT grain growth simulation of UO_2. Left: reconstructed experimental microstructure, right: sample with observable grain growth after simulated annealing [5].

Figure 7: Model results of OH production in H_2O under a pulsed radiation source. Data taken from FACSIMILE code [6].

FACSIMILE
Modelling tool to solve differential equations, specifically for chemical kinetics.

Use – Radiolysis and chemical kinetics of dissolution process.

COMSOL
Multiphysics general-purpose simulation software.

Use – Multi scale simulation incorporating FACSIMILE and MOOSE.

Figure 8: Snapshot of Convective flux above a pit and Diffusive flux inside a pit modelled of a given chemical species in COMSOL.

Case study: Add complexity to single crystal model using data collected of grain size and boundary effects on dissolution rate of UO_2 poly-epitaxial thin films
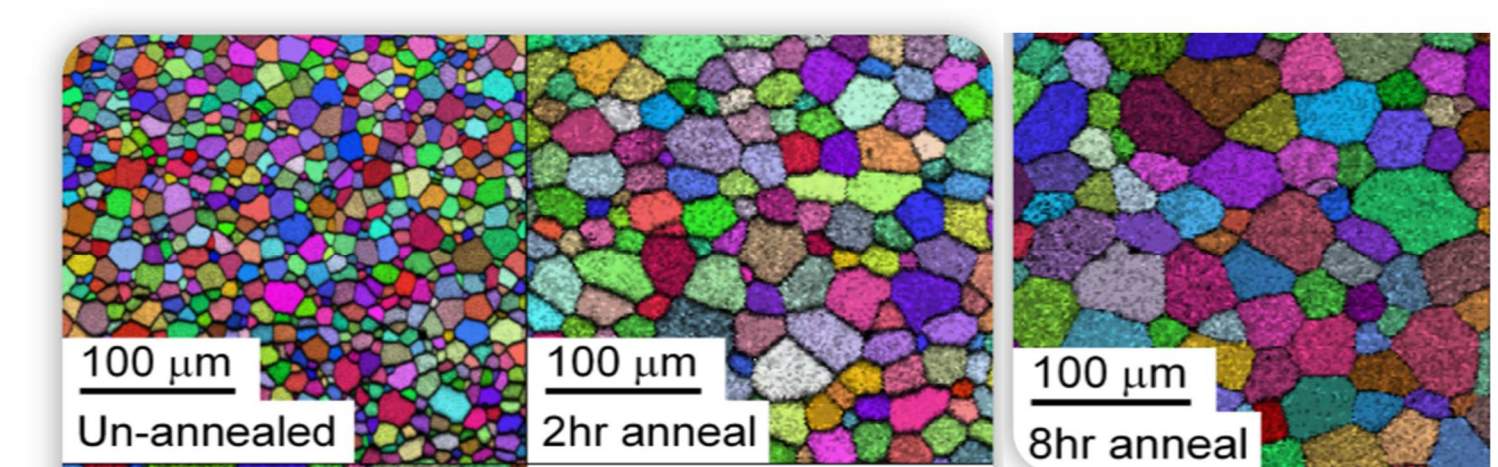
Figure 9: Average fuel grain size is tens of microns that can be achieved through annealing. EBSD patterns of controlled poly-epitaxial grain sizes of UO_2 thin film grown on YSZ.

Case study: Size effects of leached spent fuel particulates to radiolysis and dissolution rates in fuel pond storage

Project Outline

The current project outline is to develop a model incorporating dissolution studies that utilize thin films. The goal is to scale up, adding complexity iteratively to build a comprehensive model for spent fuel dissolution. The model will be developed using the MOOSE framework with the MARMOT extension. Radiolysis data will be developed using FACSIMILE and incorporated into the model.

Figure 10: High-speed Atomic Force Microscopy of in-situ 0.01M H_2O_2, increasing time up to 255s At triple point of three grains.

To model size affects on radiolysis and hence H_2O_2 release rate from particle size. The rate of oxidation increases with reduced size. A predictive model on particle dissolution would be in partnership with Sellafield and NNL.

U_3O_8

Time H_2O_2 (rate)

UO_2

Particulate Size
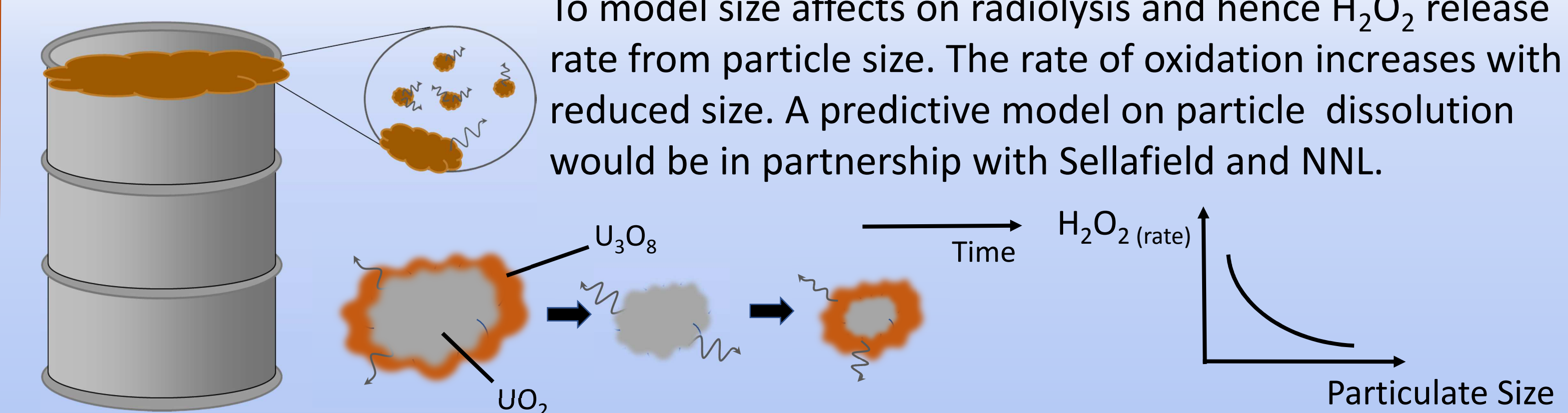
References

[1] Gov, UK. Department of Energy and Climate Change (2014)
[2] D. W. Shoesmith, Journal of Nuclear Materials 282 (2000) 1-31
[3] D. W. Shoesmith, Journal of Nuclear Materials 420 (2012) 409-423
[4] S. Rennie, Corrosion Science 145 (2018) 162-169
[5] MARMOT, MOOSE Framework, INL (2019)
[6] FACSIMILE, MCPA Software Ltd (1999)

Transformative Science and Engineering for Nuclear Decommissioning

EPSRC Engineering and Physical Sciences Research Council | UK Research and Innovation | IAC Interface Analysis Centre

transcendconsortium.org

University of BRISTOL | Energy for a Low Carbon Future

Atomistic Simulation of the ageing of PuO_2

Elanor Murray

School of Chemistry, University of Birmingham, B15 2TT

exm350@student.bham.ac.uk

Introduction

The UK has the largest civil stockpile of plutonium in the world, stored at Sellafield. However, ageing mechanisms associated with the storage of PuO_2 are poorly understood. The generation, stability and mobility of fission products in addition to the role of the surface oxide layer are key factors. Atomistic computer simulation techniques are ideally suited to provide fundamental insight into the defect chemistry of PuO_2. Interatomic potentials have been used in GULP (General Utility Lattice Program) to replicate PuO_2 accurately and to model a range of intrinsic defects. The calculated defect formation energies were compared to determine which defects are energetically favourable.
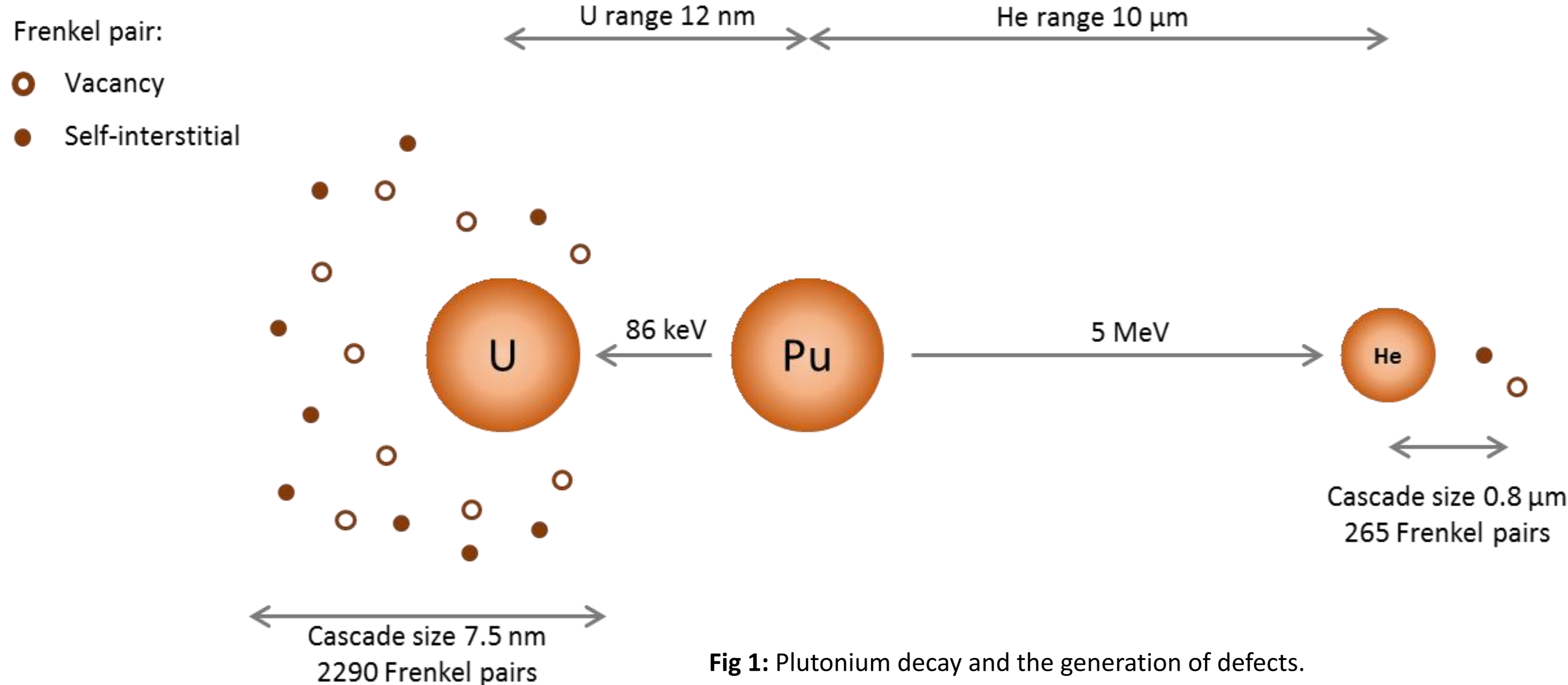
Ageing of Plutonium

Frenkel pair:
- Vacancy
- Self-interstitial

U range 12 nm   He range 10 μm

86 keV   5 MeV

Cascade size 7.5 nm
2290 Frenkel pairs

Cascade size 0.8 μm
265 Frenkel pairs

Fig 1: Plutonium decay and the generation of defects.

Plutonium is vulnerable to ageing as it is a radioactive element. Pu^{289} decays principally by α-decay. The daughter nuclei travel through the lattice initiating a collision cascade. From collisions, plutonium atoms can be displaced, creating numerous vacancies. A displaced plutonium atom may come to rest at an interstitial site, becoming a self-interstitial. Each decay event therefore creates many Frenkel pairs [1].

The Potential Model

Effective interatomic potentials, V, describe in analytical or numerical form, the variation in the energy of the molecule or solid as a function of the nuclear coordinates of the atoms present in the molecule or solid.

An appropriate form of the short range potential, ϕ, must be chosen. The Buckingham Potential is chosen to describe the predominant short-range potential for many ionic solids.

$$V(r_{ij}) = \underbrace{\frac{q_i q_j e^2}{4\pi\varepsilon_0 r_{ij}}}_{\text{Electrostatic interaction}} + \underbrace{\phi(r_{ij})}_{\text{Short-range interaction}}$$

$$\phi(r_{ij})_{Buck} = \underbrace{A_{ij}\exp\left(\frac{-r_{ij}}{\rho_{ij}}\right)}_{\text{Electron repulsion}} - \underbrace{\frac{C_{ij}}{r_{ij}^6}}_{\text{Transient dipole attraction}}$$
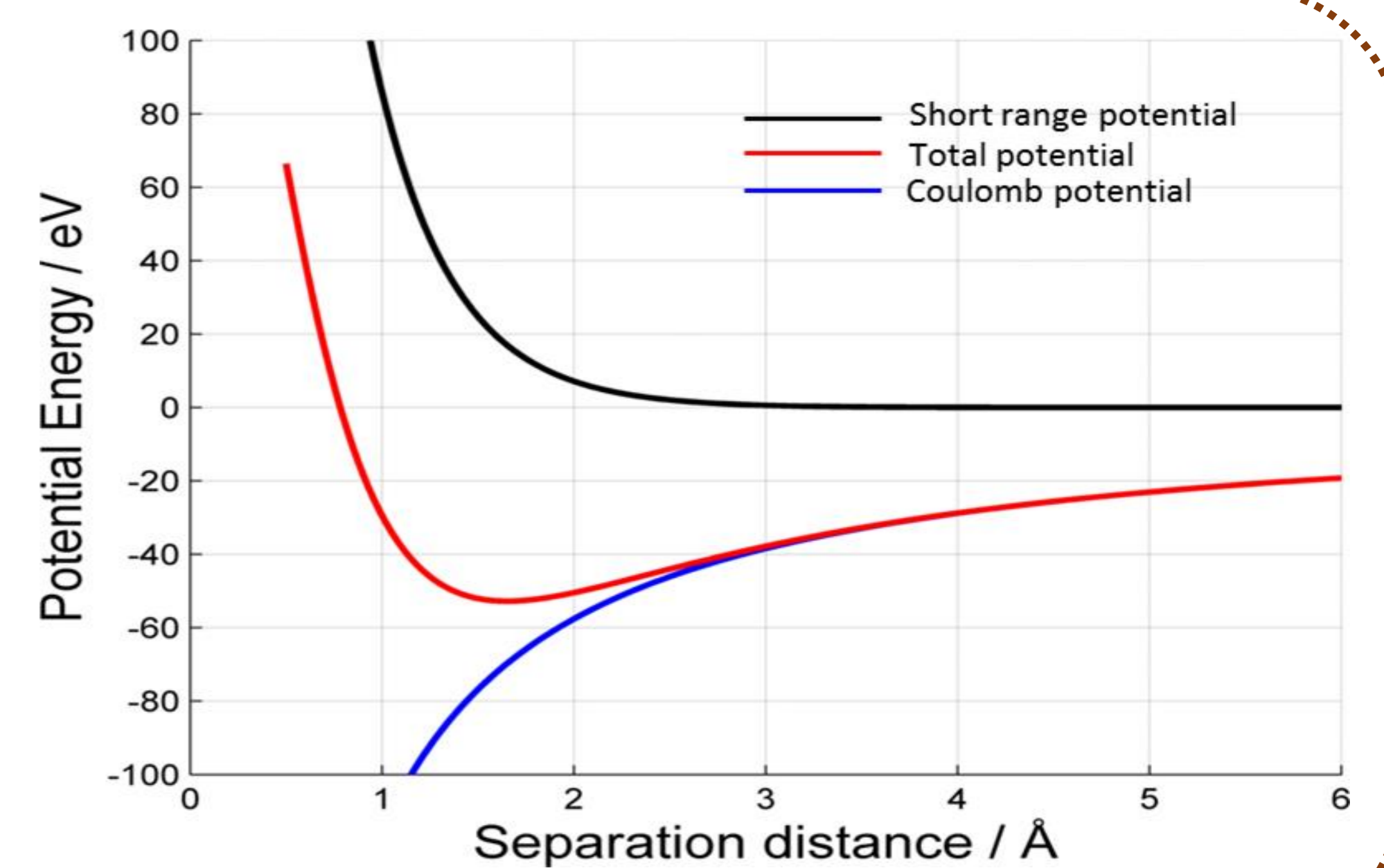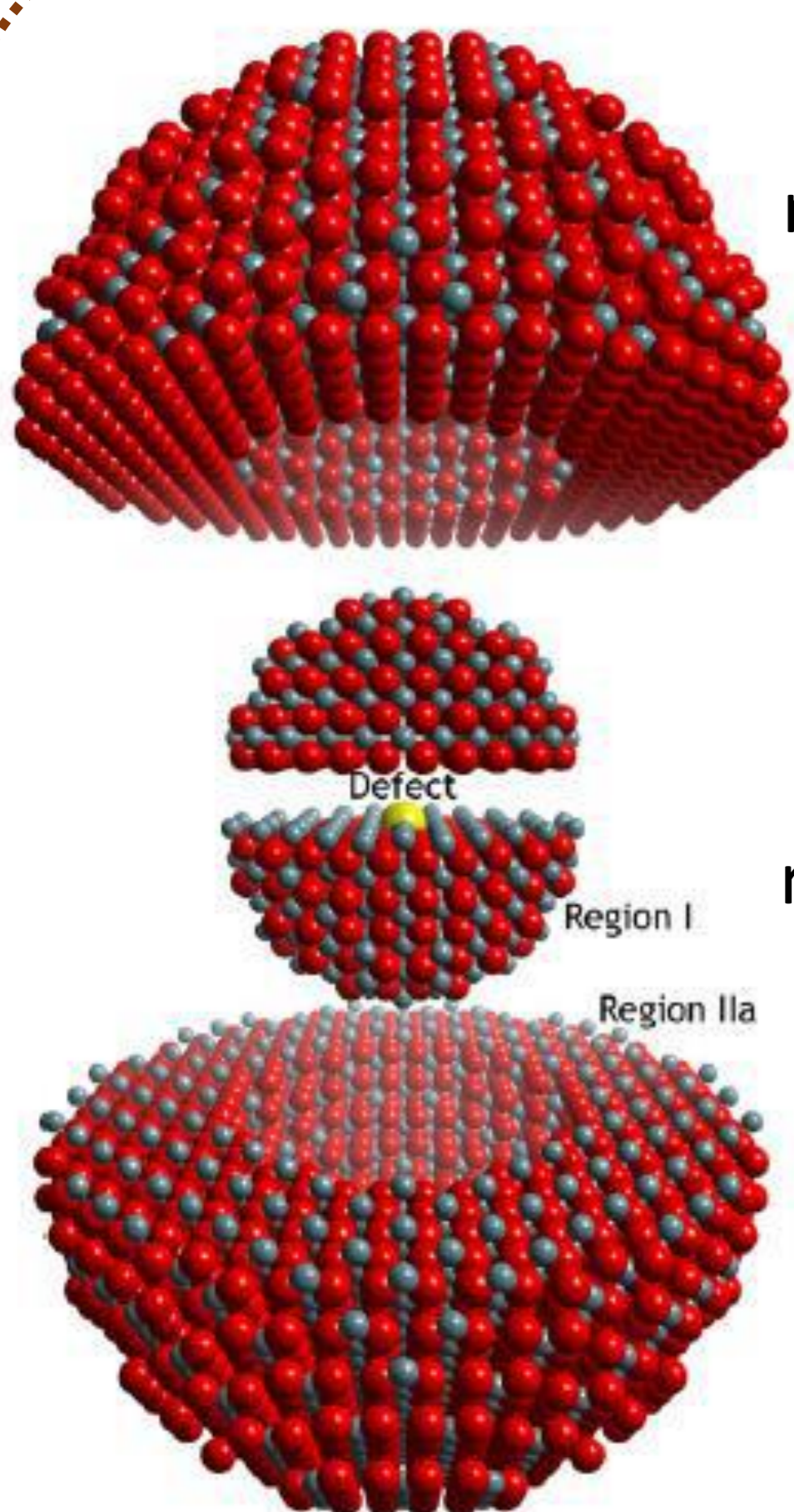

Fig 2: Potential energy, V, against interatomic distance, r.

Mott-Littleton

The Mott-Littleton methodology is used to simplify minimising the potential energy function. The defective lattice is divided into two regions: Region I and Region IIa.

Fig 3: Two region strategy for calculation of defect energy [2].

Table 1: Mott-Littleton regions

	Size	Number of Ions
Region I	14	1888
Region IIa	28	12344

Table 2: Unbound and bound Frenkel and Schottky energies (per defect).

Bound Defect	Formation reaction	Defect Formation Energy		Binding Energy (eV/Defect)
		Unbound (eV/Defect)	Bound (eV/Defect)	
Schottky Trio	$Pu_{Pu}^x + 2O_o^x \rightleftharpoons \{V_{Pu}'''' : 2V_o^{\bullet\bullet}\}^x + PuO_{2\,(surface)}$	3.545	1.929	-1.616
Oxygen Frenkel Pair	$O_o^x \rightleftharpoons \{V_o^{\bullet\bullet} : O_i''\}^x$	2.668	2.069	-0.599
Plutonium Frenkel Pair	$Pu_{Pu}^x \rightleftharpoons \{V_{Pu}'''' : Pu_i^{\bullet\bullet\bullet\bullet}\}^x$	10.029	7.868	-2.161

Conclusions and Future Work

- The most energetically favourable forms of intrinsic defects were found, by calculation, to be Schottky defects and oxygen Frenkel pairs.
- Future work includes: investigating helium migration pathways and simulating pure and defective surface structures.

References:
[1] Wolfer, W. G. Radiation effects in plutonium. *Los Alamos Sci.* **26**, 274–285 (2000)
[2] Read MSD, Jackson RA. Journal of Nuclear Materials. **406**, 293 (2010)

Transformative Science and Engineering for Nuclear Decommissioning

transcendconsortium.org

Understanding composition-structure-property-phase relations in high-Fe_2O_3 radioactive waste glasses for the US Hanford site

J. D. Eales[1], K. M. Fox[2], A. A. Kruger[3], A. Goel[4], D. P. Guillen[5], J. McCloy[6], J. D. Vienna[7], S. Aminorroaya-Yamini[1], P. A. Bingham[1]

[1]Materials and Engineering Research Institute, Sheffield Hallam University, Sheffield S1 1WB, UK | [2]Savannah River National Laboratory, Savannah River Site, Aiken, SC 29808, USA
[3]Office of River Protection, Hanford Site, Richland, WA 99354, USA | [4]Department of Materials Science and Engineering, School of Engineering, Rutgers, The State University of New Jersey, Piscataway, NJ 08854, USA
[5]Idaho National Laboratory, Idaho Falls, ID 83415, USA | [6]School of Mechanical and Materials Engineering, Washington State University, WA 99164-2920, USA
[7]Pacific Northwest National Laboratory, Richland, WA 99352, USA

The Hanford Site, Richland, WA, USA

[1]

➤ The purpose of the site was to make weapons-grade plutonium from 1943 to 1987
➤ The site is located 10km away from the Columbia river

➤ 55m US Gallons of radioactive waste are stored in steel tanks
➤ These tanks were buried in shallow trenches
➤ Some of these tanks have been found to have leaked

[2]

Proposed Clean-up Solution

The solution was detailed in 2015 by several US National Laboratories. To summarise:

➤ High-Level Waste (HLW) and Low-Activity Waste (LAW) will be processed separately
➤ Glass forming chemicals added to waste to optimise waste loading
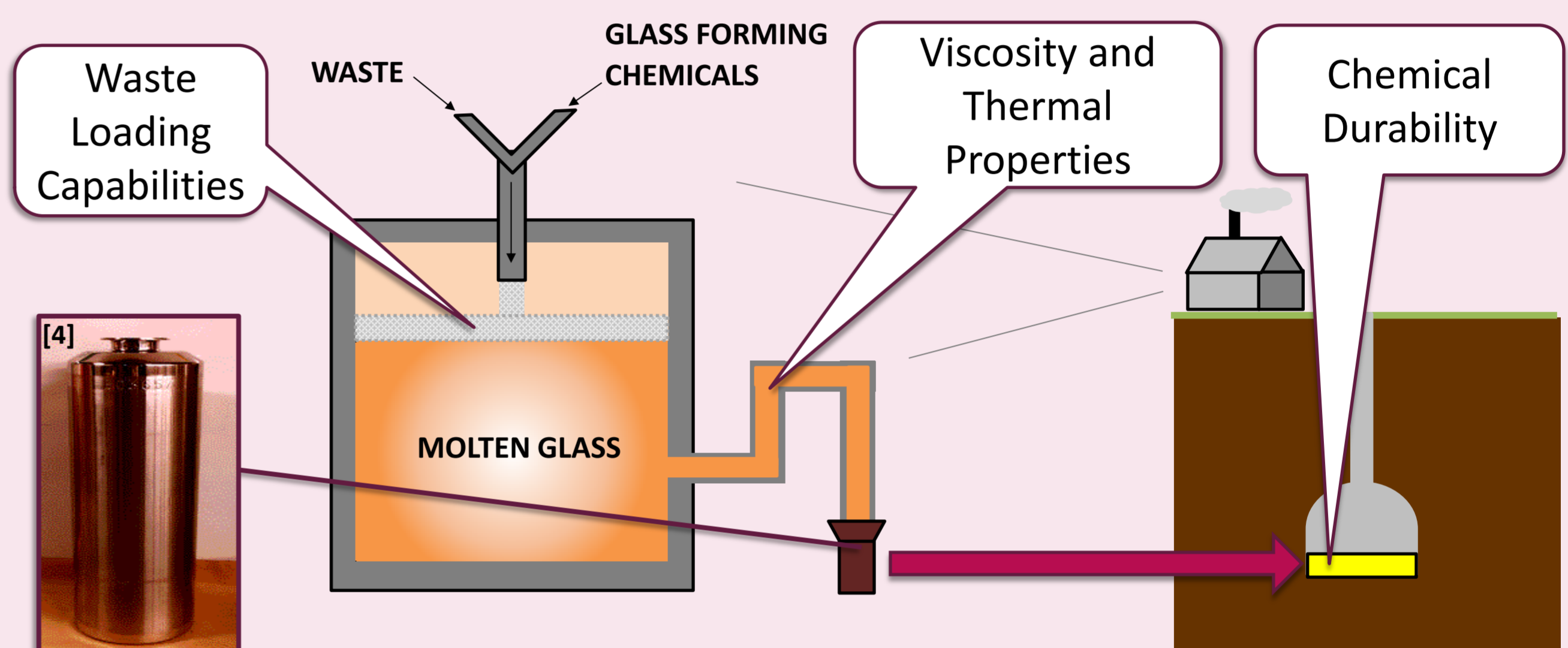➤ The waste will be vitrified into borosilicate glass

[3]
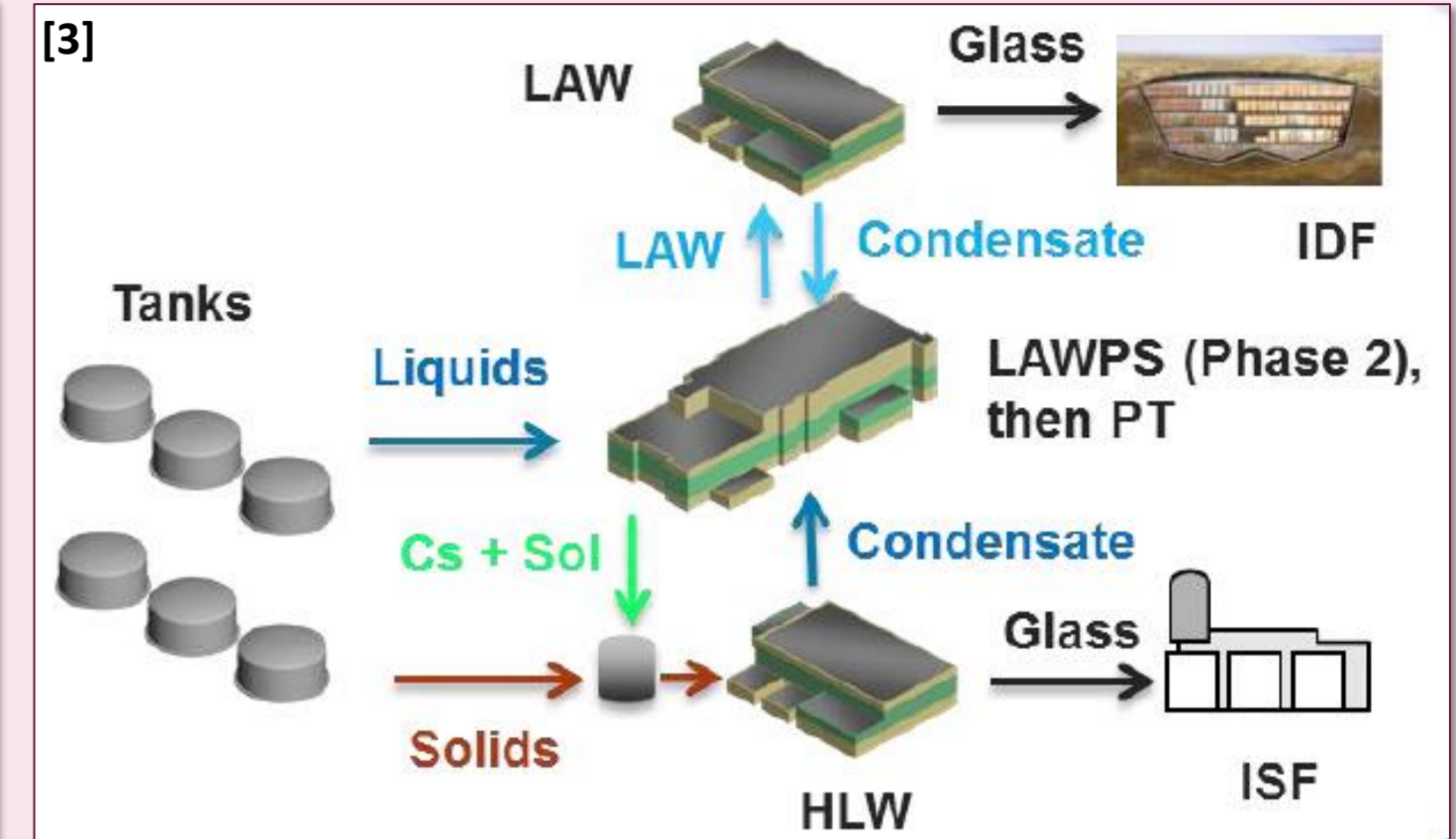
Above is a visual representation of the proposed solution, from tank to storage.

PhD Project Overview

Outline

Due to the corrosion of the steel tanks, extraction processes applied to the waste, and minimal pre-treatment applied to the waste, there will be high concentrations of iron within the waste.

To ensure the efficiency, safety, and cost effectiveness of the cleanup, this research will characterise how the high-iron content affects the glass formation, waste loading, and long-term glass wasteform performance. Below is a summary of some of the methods and techniques that will be used in this research.

WASTE • GLASS FORMING CHEMICALS

Waste Loading Capabilities

Viscosity and Thermal Properties

Chemical Durability

[4]

MOLTEN GLASS

Design
1) The waste simulant type is selected
2) The raw materials are selected
3) The mass of raw materials is calculated

Glass Making
4) The raw materials are measured out
5) They are melted to make glass at 1150°C
6) The glass is annealed at 480°C

Sample Prep
7) Samples may need milling into a powder
8) Grinding and polishing may be required
9) Suspension in chemicals (e.g. Resin)

Composition
• X-Ray Diffraction (XRD)
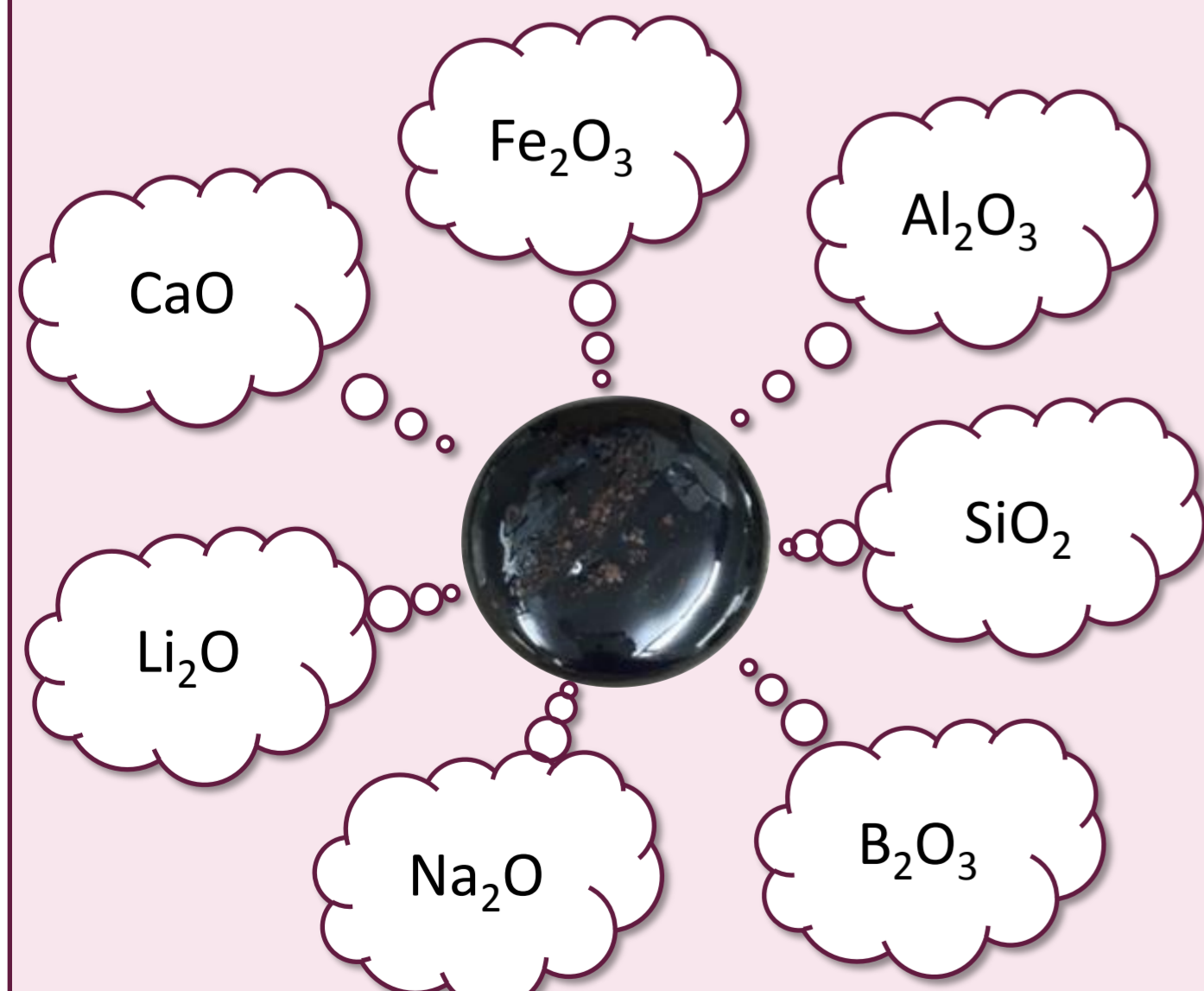• X-Ray Fluorescence (XRF)

Structure
• Raman Spectroscopy
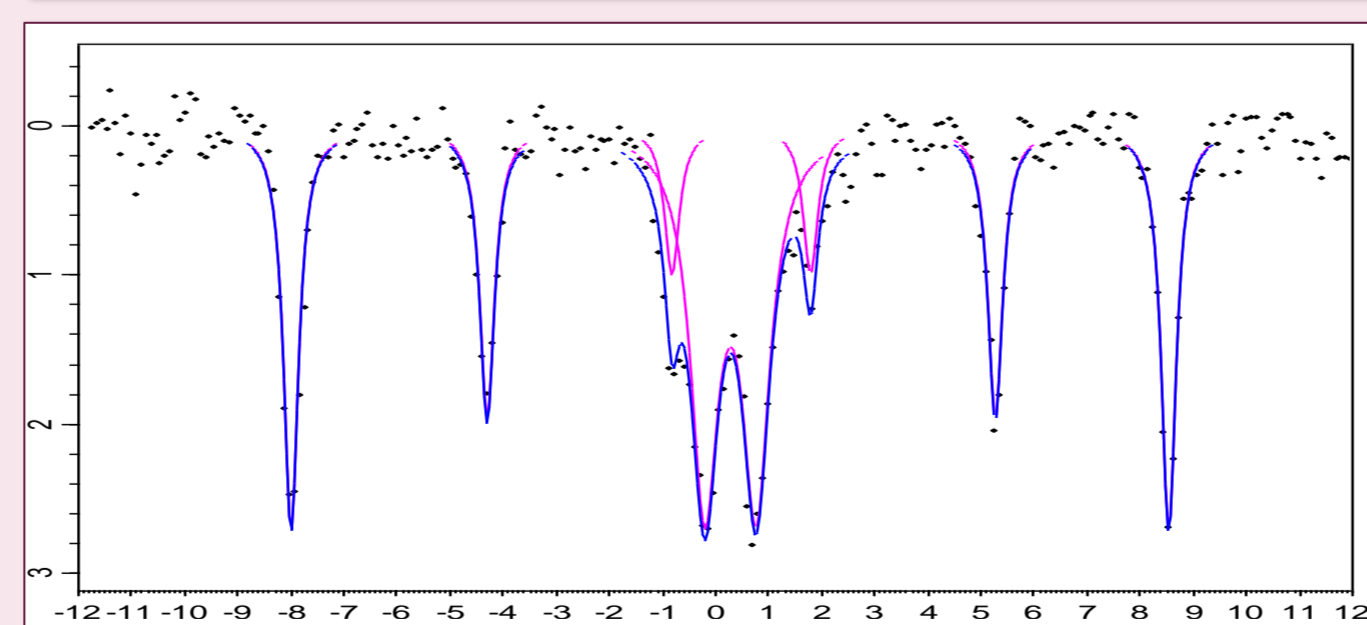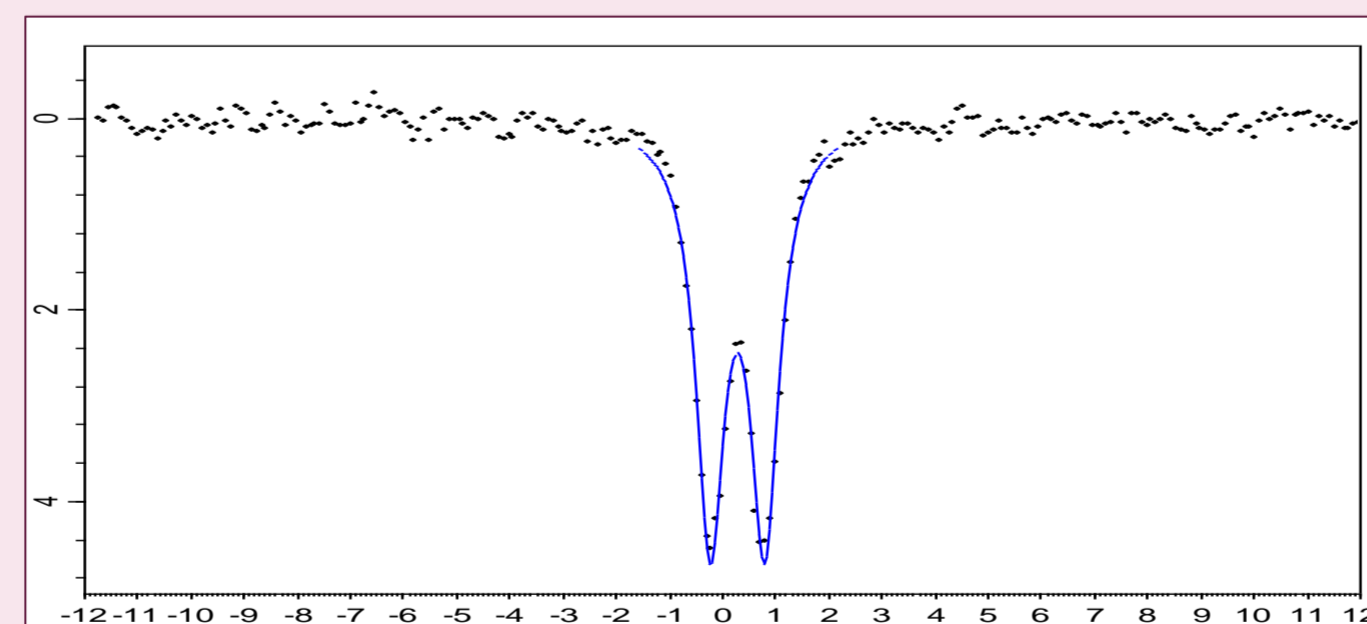• Mössbauer Spectroscopy
• X-Ray Absorption Spectroscopy (XAS)

Thermal
• Differential Thermal Analysis (DTA)
• Differential Scanning Calorimetry (DSC)

Current Work – Glass Formation Limits

Fe_2O_3 Al_2O_3 CaO SiO_2 Li_2O Na_2O B_2O_3

Constituent oxides of the current glass series

Mössbauer spectra of two HLW simulant glasses: 5.5 mol% Fe_2O_3 (Top) and 15 mol% Fe_2O_3 (Bottom)

Discussion Future Work

This work has given a good start for the research to continue from. The next steps are:

➤ To simplify the glass composition to fewer components
➤ To use the simple composition to map thermal and phase properties
➤ To add more components to understand how they affect these properties

This will be achieved by comparing phase diagrams from previous glass compositions including the International Standard Glass.

Key References

[1] US Department of Energy Office of River Protection. *Waste Treatment and Immobilisation Plant Project*. https://www.hanford.gov/page.cfm/wtp (accessed 20/02/2019).
[2] Department of Ecology, State of Washington. *Governer Inslee's Statement on Leaking Tanks at Hanford*. ecologywa.blogspot.com/2013/02/governor-inslees-statement-on-leaking.html (accessed 20/02/2019).
[3] PNNL, ORP, CUA-VSL, EnergySolutions. *ORP Grand Challenges 2015*. https://www.hanford.gov/files.cfm/Attachment_4_Grand_Challenge_Proposal_DF_HLW_FINAL.pdf (accessed 20/02/2019).
[4] World Nuclear Organisation. *Treatment and Conditioning of Nuclear Waste*. http://world-nuclear.org/uploadedImages/org/info/Nuclear_Fuel_Cycle/Nuclear_Wastes/Appendicies/vitrification.gif (accessed 20/02/2019).
McCloy J, Washton N, Gassman P, Marcial J, Weaver J, Kukkadapu R. Nepheline crystallization in the boron-rich alumino-silicate glasses as investigated by multi-nuclear NMR, Raman & Mössbauer spectroscopies. *Journal of Non-Crystalline Solids* 2015; 409

Sheffield Hallam University | Materials and Engineering Research Institute

U.S. DEPARTMENT OF ENERGY

Phosphate solubility and impacts on properties of radioactive waste glasses for the Hanford site

K.L. Love [a*], A.M.T. Bell [a], K.M. Fox [e], J.D. Vienna [b], A. Goel [c], J.S. McCloy [d], D.K. Peeler [e], D.P. Guillen [f], P.A. Bingham [a]

[a] Materials and Engineering Research Institute, Sheffield Hallam University, City Campus, Sheffield, South Yorkshire, S1 1WB, UK, [b] Pacific Northwest National Laboratory, PO BOX 999, Richland, WA 99352, USA, [c] Department of Materials Science and Engineering, School of Engineering, Rutgers University, The State university of New Jersey, 607 Taylor Road, Piscataway, NJ 08854, USA, [d] Washington State University, School of Mechanical and Materials Engineering, Washington State University, PO BOX 642920, Pullman, WA 99164 - 2920, USA, [e] Savannah River National Laboratory, Savannah River Site, Aiken, SC 29808, USA, [f] Idaho National Laboratory, 1955 N. Fremont Avenue, Idaho Falls, ID 83415, USA

1. Abstract

This research aims to understand the effects of phosphate (P_2O_5) on the properties, composition and structure of radioactive waste glasses relevant to clean-up of the Hanford site. P_2O_5 arises in the vitrified waste from the Bismuth Phosphate, REDOX and PUREX processes for plutonium extraction[1]. P_2O_5 is poorly soluble in borosilicate glasses, with concentrations >4.5 wt% potentially leading to phase separation; this can affect melt viscosity and chemical durability[2]. However, P_2O_5 has also shown positive results in terms of enhancing the solubility of other species in the glass e.g. sulphate (SO_4^{2-}) [3, 4].

Simulant waste glasses based on Hanford compositions will be prepared from dry slurry feeds and doped with P_2O_5 and co-doped with P_2O_5 and SO_4^{2-}. The glasses will be characterised using a range of synchrotron and lab-based techniques.

Most of the nuclear waste is liquid and there is approximately 53 million gallons of it [5].

There are 177 underground storage tanks filled with 200 000 m³ of nuetralised HLW, of which 70 are leaking [5, 6].

The aim is to increase waste loading of troublesome components in HLW glass and improve the processing rate [5].

Figure 6: Image of Hanford vitrification plant [13]

2. What Makes a Glass?

Glass modifiers

Glass Formers

Glass Intermediates

Figure 8: Funnel diagram [13]

1 Batching
2 Heating
3 Annealing

Hanford Simulated Waste Glass

Figure 2: Glass samples of simulated Hanford glasses with a complex composition (HLW (Left), ORP LAW (Middle), WTP LAW (Right)

Example oxides for the glass composition

Glass Former	SiO_2, B_2O_3, P_2O_5
Glass Modifier	CaO, SO_4^{2-}
Glass intermediate	Na_2O, Al_2O_3, Fe_2O_3

3. Aims and Objectives

- Understand the effects of varying the amount of P_2O_5 on the glass properties, composition and structure
- Identify & characterise phase separation in glasses, respectively
- Increasing the waste loading of current High Level Waste (HLW) & Low Activity Waste (LAW) glasses

4. Phase Separation

Phase separation or liquid (glass) - liquid (glass) immiscibility is a phenomenon that occurs in liquid systems and melts when a lower free energy is yielded from the separation of the two components [7]. Pacific Northwest National Lab (PNNL) found the upper limit of P_2O_5 in Hanford HLW and Waste Treatment Plant (WTP) LAW waste glasses, where phase separation was measureable, to be **4.5 wt%** [8].
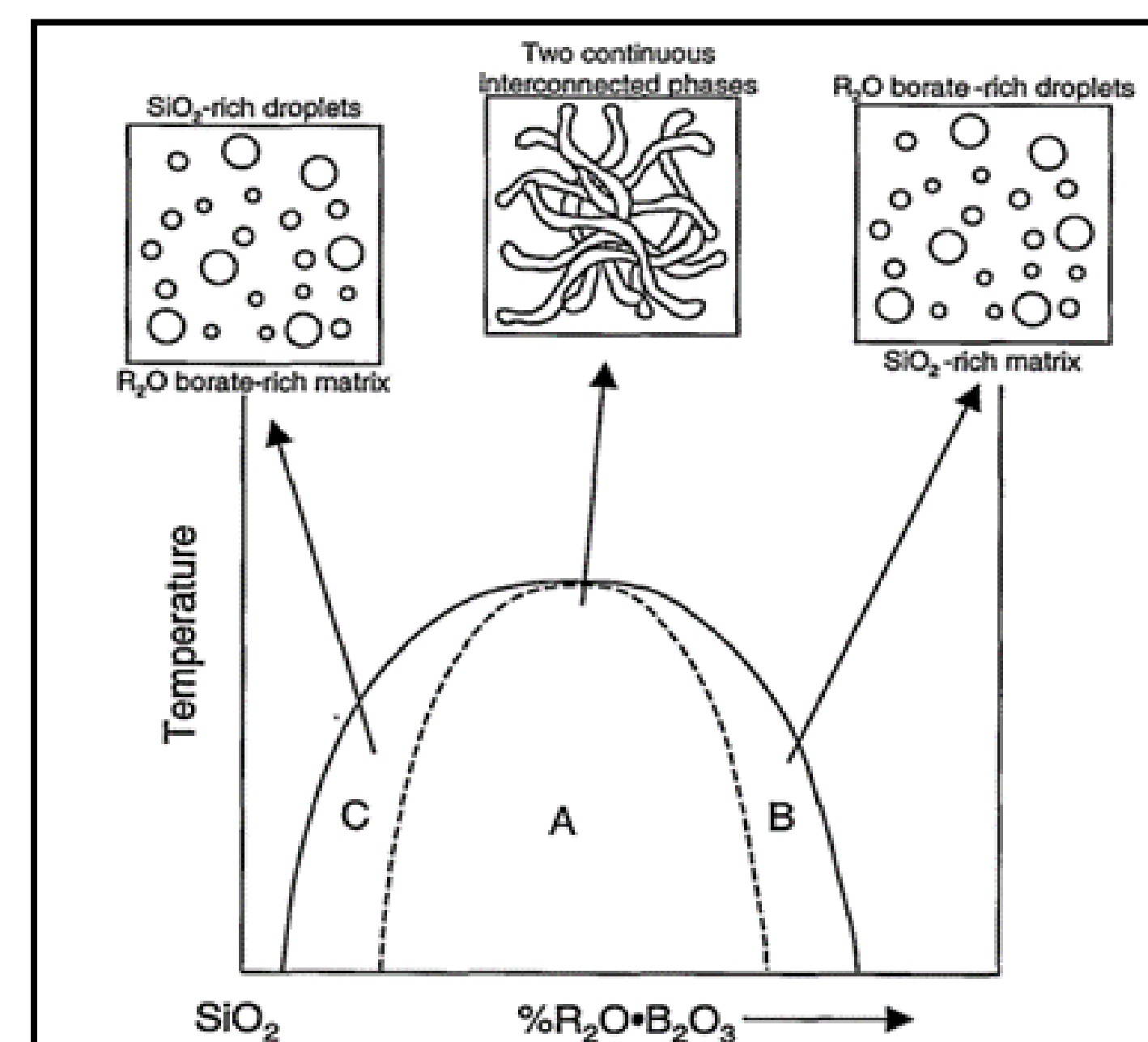
Figure 5:Crystal structure of P_2O_5 [11]
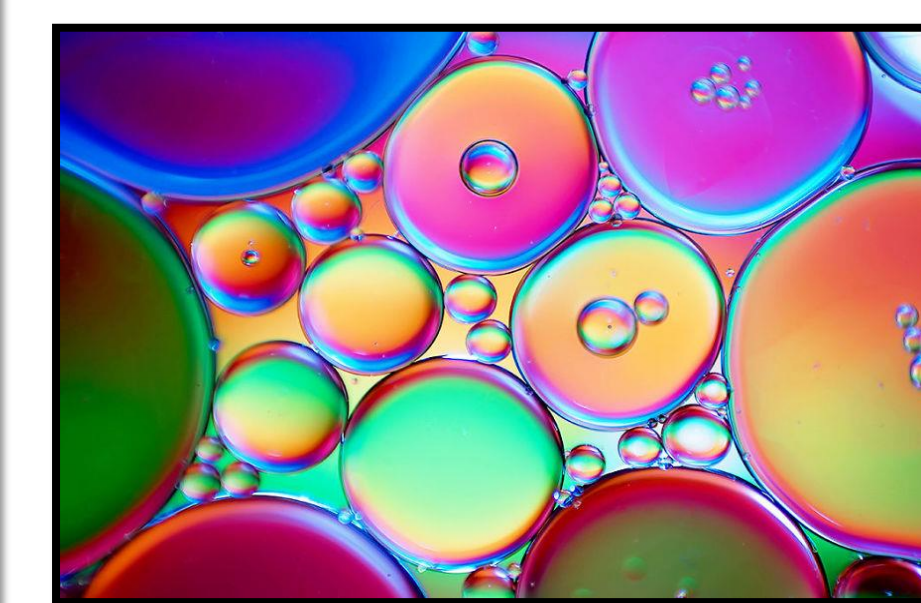
Figure 4: An example of phase separation in a liquid i.e. oil and water [10]

Figure 3: Diagram showing the different types of phase separation: spinodal decomposition (A) and nucleation & growth (B & C) [9]
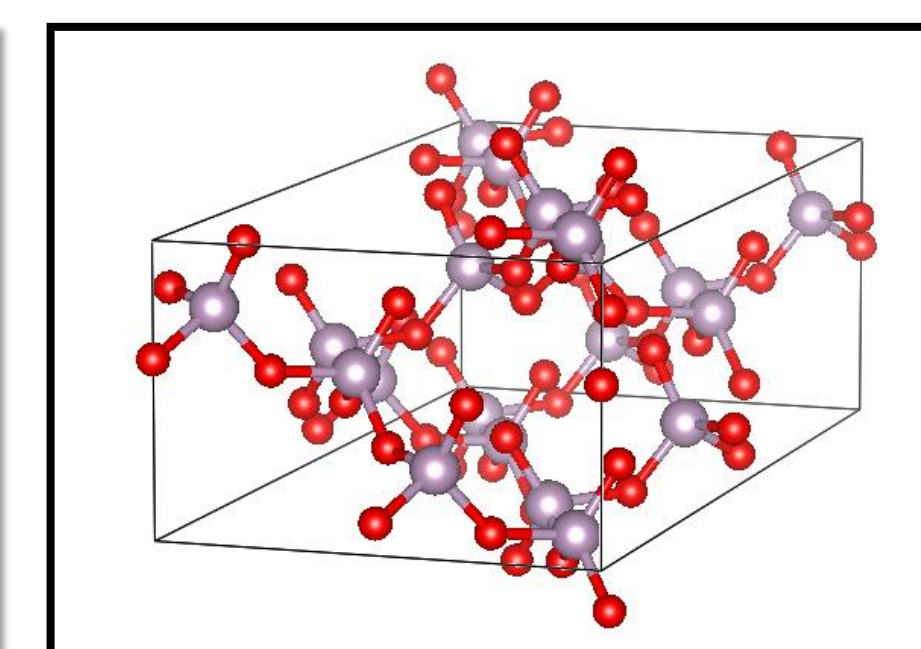
Phase separation can affect the viscosity of the glass melt; chemical durability; or cause variation in the glass structure. If there are secondary phases, they may not be measureable depending on their type; a combination of amorphous phase, liquid phase and or crystalline phase.
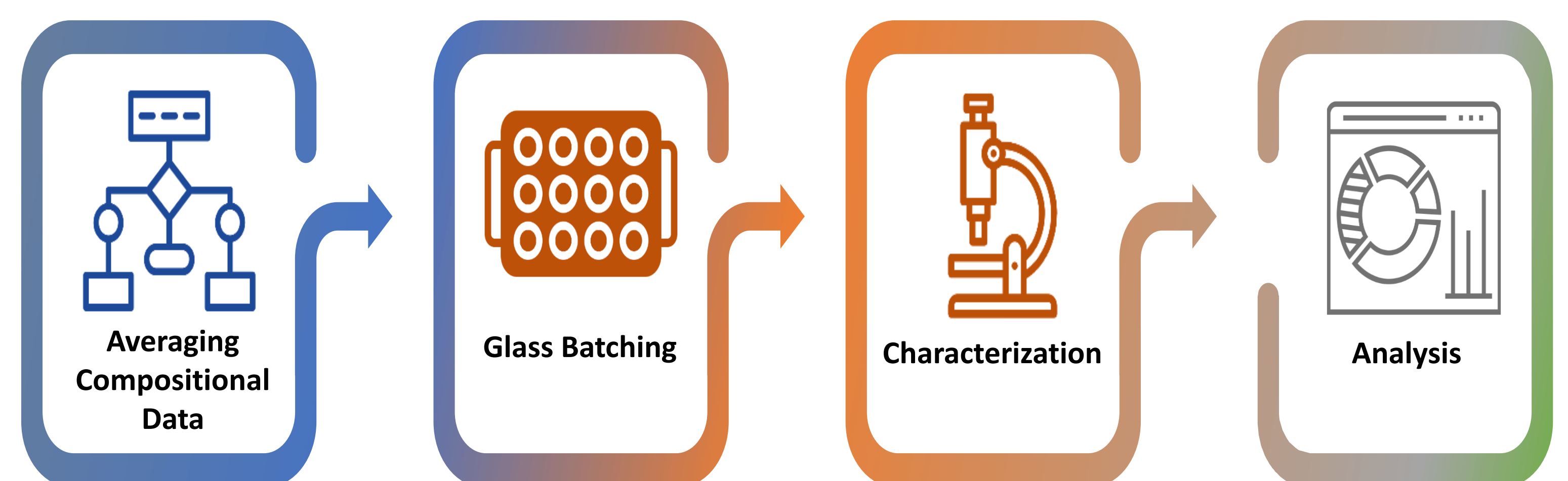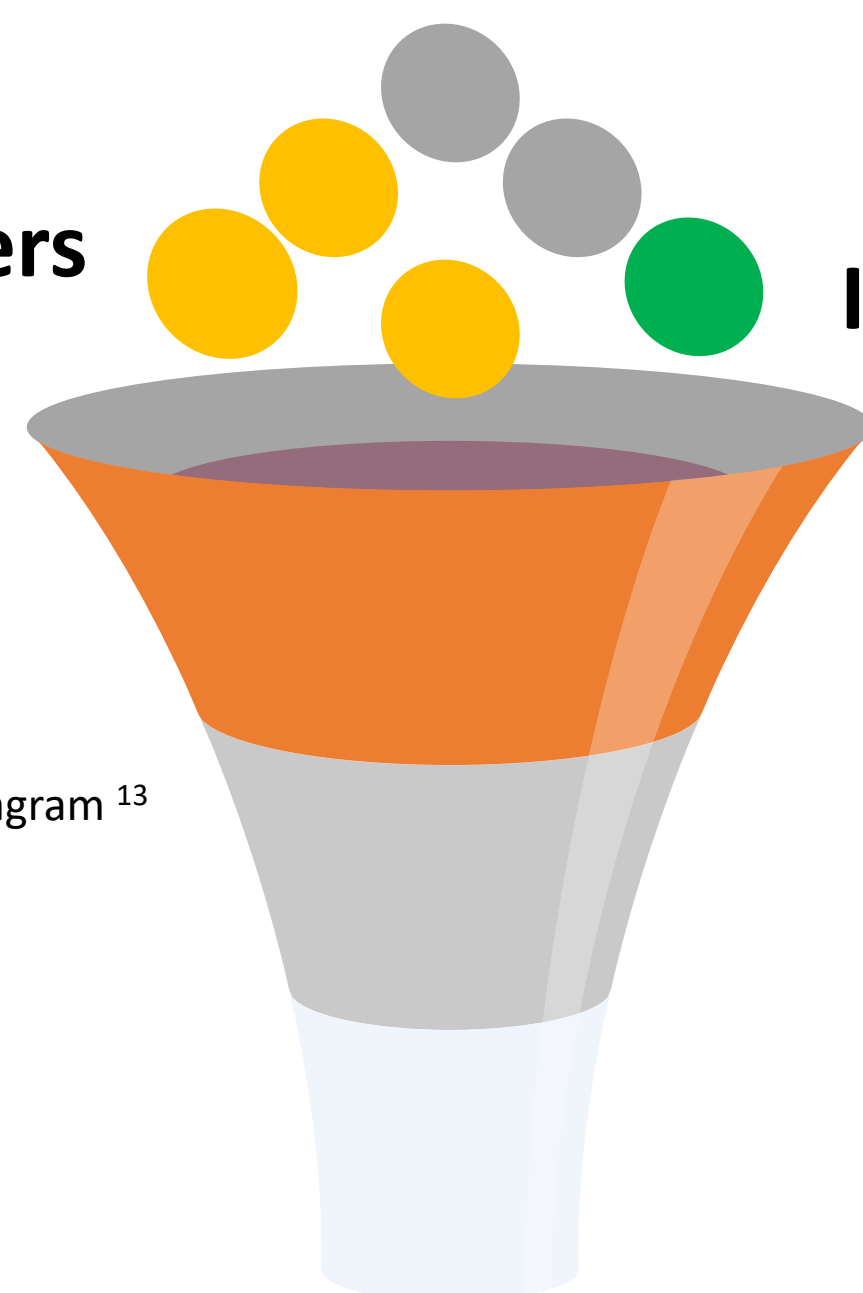
5. Methodology

Averaging Compositional Data → Glass Batching → Characterization → Analysis

Figure 7: Flow diagram of methodology [13]

6. Characterization Techniques

Structure	Properties	Composition
• Raman Spectroscopy • Scattering electron microscopy (**SEM**) • X-ray Absorption Spectroscopy (**XAS**) • X-ray Pair Distribution Function beamline (**XPDF**)	• Thermal Analysis • Liquidus Temperature (T_L) • Chemical Durability • Melt Viscosity • Density • Hardness / indentation fracture toughness	• X-ray Diffraction (**XRD**) • X-ray Fluorescence (**XRF**) • Small Angle X-ray Scattering (**SAXS**) • Energy Dispersive X-ray (**EDX**) • X-ray Pair Distribution Function beamline (**XPDF**)

Contact

Katrina Love BEng(Hons), EngTech TIMMM

Materials and Engineering Research Institute, Sheffield Hallam University

Email: b400027@my.shu.ac.uk

Website: linkedin.com/in/katrina-love-beng-hons-12bb03a9

References

1. Delegard, C. H. Jones, S. A. (2015). Chemical Disposition of Plutonium in Hanford Site Tank Wastes. doi:WTP-RPT-234 Rev. 1
2. Schuller. S. Pinet, O, Grandjean. A, Blisson, T. (2008). Phase Separation and Crystallization of Borosilicate Glass Enriched in MoO₃, P₂O₅, ZrO₂, CaO. Journal of Non-Crystalline Solids. 354. 296-300. 10.1016/j.jnoncrysol.2007.07.041.
3. Vienna, J, Kim. D-S, Muller I, Piepe. G, Kruger. A (2014). Toward Understanding the Effect of Low-Activity Waste Glass Composition on Sulfur Solubility. Journal of the American Ceramic Society. 97. 3135-3142. 10.1111/jace.13125.
4. Bingham. P.A, Vaishnav. S, Forder. S, Scrimshire. A, Jaganathan. B, Rohini. J, Marra. J.C, Fox. K.M, Pierce. E, Workman. P, Vienna, J. D (2016). Modelling the Sulfate Capacity of Simulated Radioactive Waste Borosilicate Glasses. Journal of Alloys and Compounds. 695. 10.1016/j.jallcom.2016.11.110.
5. https://www.nwcouncil.org/reports/columbia-river-history/hanford (2018)
6. https://www.hanford.gov/files.cfm/ORP-56226.pdf (2018)
7. Shelby. J.E. (2005). Introduction to Glass Science and Technology. RS.C.
8. Vienna. J.D, KIM. D-S, Skorski. D.C, M. J. PNNL-22631, Rev. 1 ORP-58289. (2013).
9. Cozzi. A.D (2018). Technical Status Report on the Effect of Phosphate and Aluminum on the Development of Amorphous Phase Separation in Sodium Borosilicate Glasses. 10.2172/9850.
10. https://static.boredpanda.com/blog/wp-content/uploads/2016/09/I-take-Abstract-Macro-pictures-using-Oil-and-Water-57e510d63efd1__880.jpg
11. Hassan. E, Arbib, Elouadi. B, Chaminade. J.P, Darriet. J. (1996). New Refinement of the Crystal Structure of o-P₂O₅.
12. https://www.hanfordvitplant.com/low-activity-waste-law-vitrification-facility (image)
13. © Copyright PresentationGO.com

Understanding REDOX Reactions in the Cold Cap for Nuclear Waste Vitrification at the Hanford Site

Sheffield Hallam University | **Materials and Engineering Research Institute**

U.S. DEPARTMENT OF ENERGY

Jessica C. Rigby[1]
b7037173@my.shu.ac.uk

Ashutosh Goel[2], John S. McCloy[3], John D. Vienna[4], Kevin M. Fox[5], David K. Peeler[5], Donna P. Guillen[6], Anthony M. T. Bell[1], Paul A. Bingham[1]

[1]Materials and Engineering Research Institute, Sheffield Hallam University, UK

[2]Rutgers University, USA; [3]Washington State University, USA; [4]Pacific Northwest National Laboratory, USA; [5]Savanah River National Laboratory, USA; [6]Idaho National Laboratory, USA

Fig 1. The Hanford Waste Vitrification Plant currently under construction[1].

Introduction

200,000m[3] of radioactive defence wastes from the Manhattan Project and the Cold War are currently stored underground in steel tanks at the Hanford site, posing an imminent risk of groundwater contamination. In one of the world's most complex and challenging clean-up operations, these wastes are to be **vitrified into stable glass wasteforms** at Hanford's Waste Treatment Plants (WTPs).

The WTPs will process both High-Level (HLW) and Low-Activity (LAW) Wastes in **Joule-Heated Ceramic Melters (JHCMs)**. The final wasteform will be stored in geological repositories until the radioactivity reaches a safe level. In the interest of safety and efficiency of this operation, a complete process control model for the JHCMs is under development to predict the behaviour of the glass melt and quality of the final product.
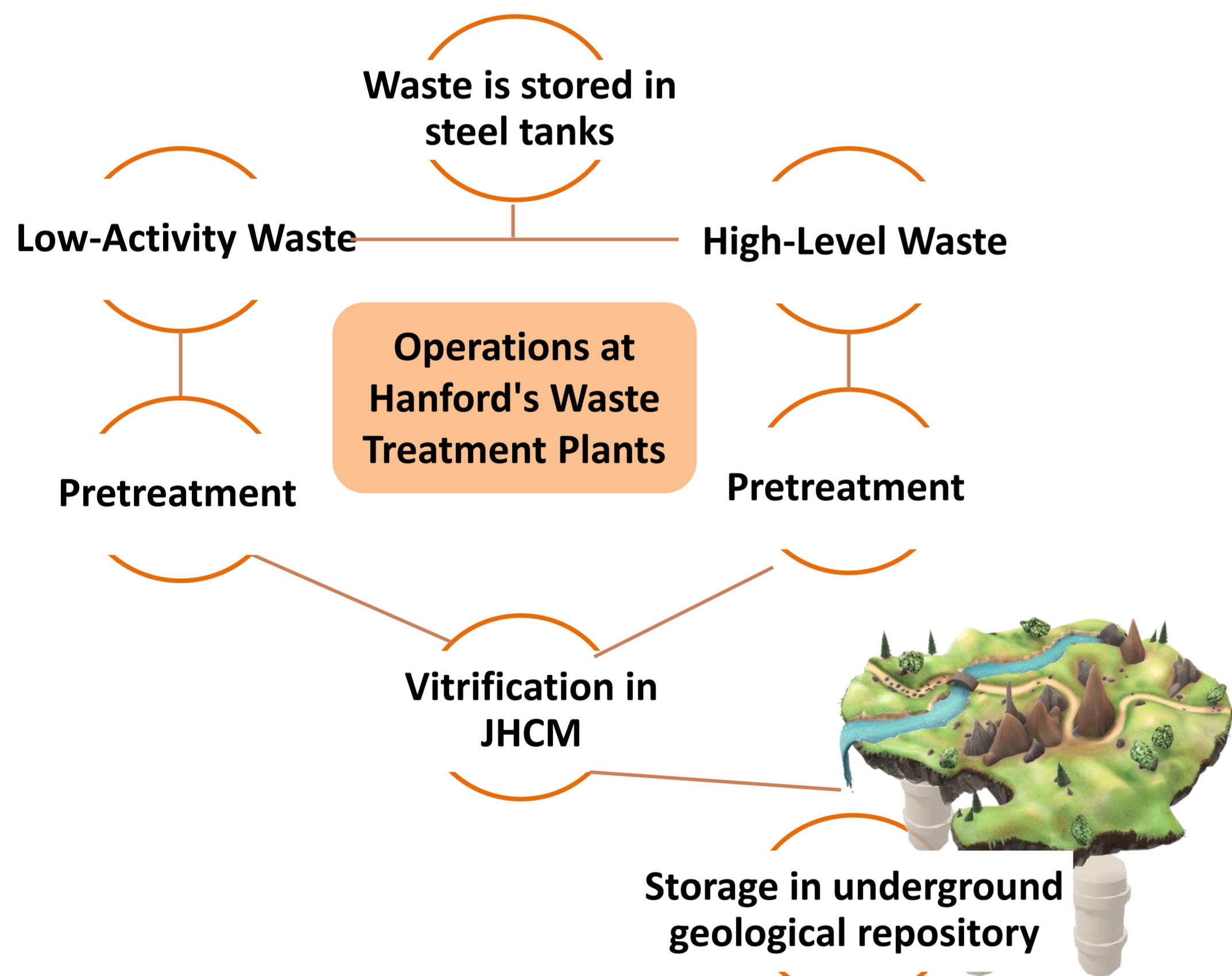

Figure 2. Operations and Hanford's WTPs for treatment of HLW and LAW

Methodology

Sample Fabrication
- Cold cap samples Laboratory Scale Melter (LSM) tests from the US
- Fast-Dried Feed Slurry (FDFS) samples from the US will simulate the cold cap behaviour
- Glass samples will be made in our laboratory by conventional melt-quenching
- Stages of melting samples prepared

Characterisation Techniques
- X-Ray fluorescence, X-ray diffraction, Scanning electron microscopy/Energy dispersive spectroscopy and Raman spectroscopy
- Advanced techniques such X-ray pair distribution function analysis will probe the local structure of the different layers

REDOX Analysis
- Various spectroscopies; Mössbauer, UV/Visible, X-ray absorption and optical absorption

Outcomes
The analysis will provide information for process and feed parameters for the WTPs to increase efficiency of the batch to glass process by exploring:
- Key melt and foam controlling reactions
- Characterisation of layers of the cold cap
- The effect of oxidation states of multivalent oxides on the cold cap behaviour
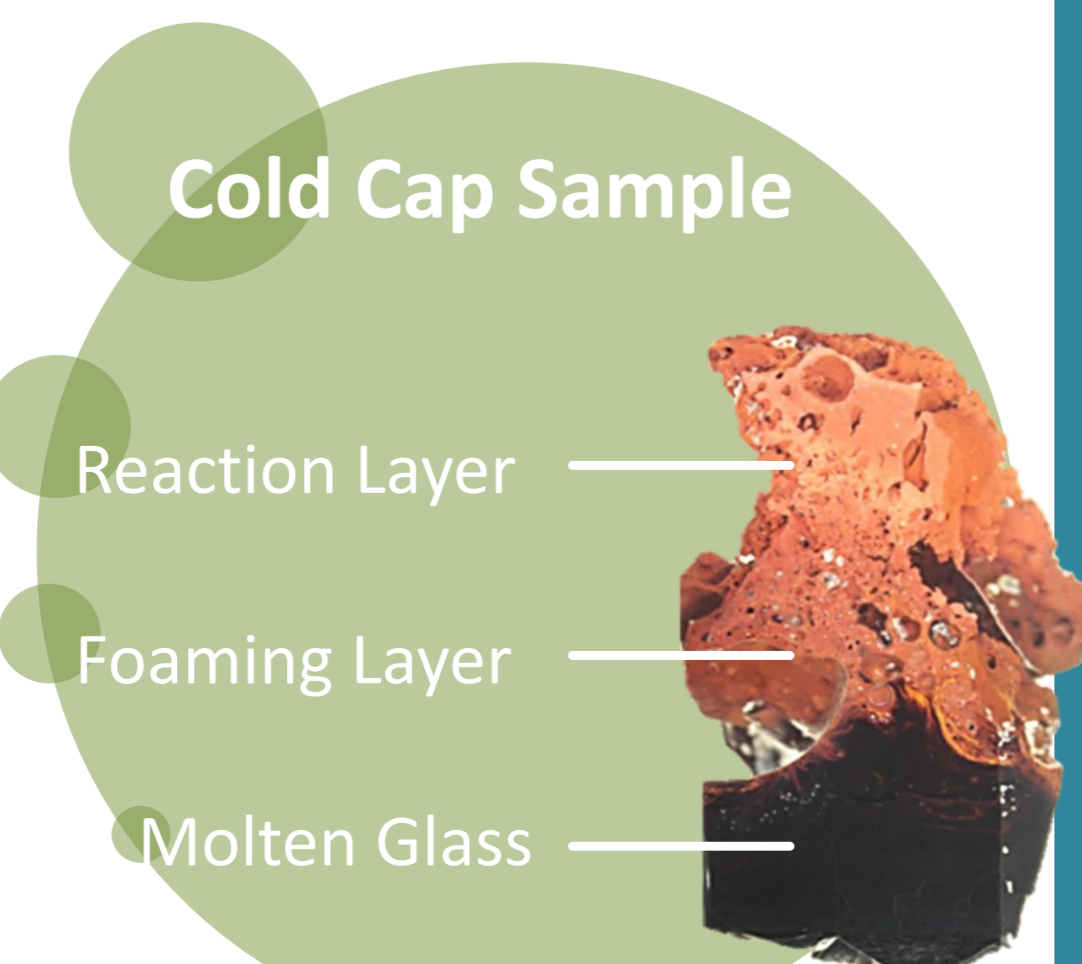- REDOX behaviour of the separate layers of the cold cap and their interfaces

Fig 3. Cold cap sample[3]

Theory

What is the cold cap?
A cold cap is formed when the incoming feed sits on top of the glass melt pool. It is the area in which batch reactions occur, turning the feed into homogenous glass. Four separate layers of the cold cap arise due to the varying temperatures and processes, they are detailed in **Fig 6**. The cold cap covers 90-95% of the melt surface.

Heat transfer in cold cap
Forced bubblers are used to generate convection currents in the glass melt, transferring heat to the bottom of the cold cap. Melting rate is improved by the use of forced bubblers.

Forced bubblers also contribute to the foaming of the glass melt; along with batch reactions and fining agents. Foaming reduces heat transfer to the cold cap reaction layer, slowing down reactions and reducing efficiency of the process.
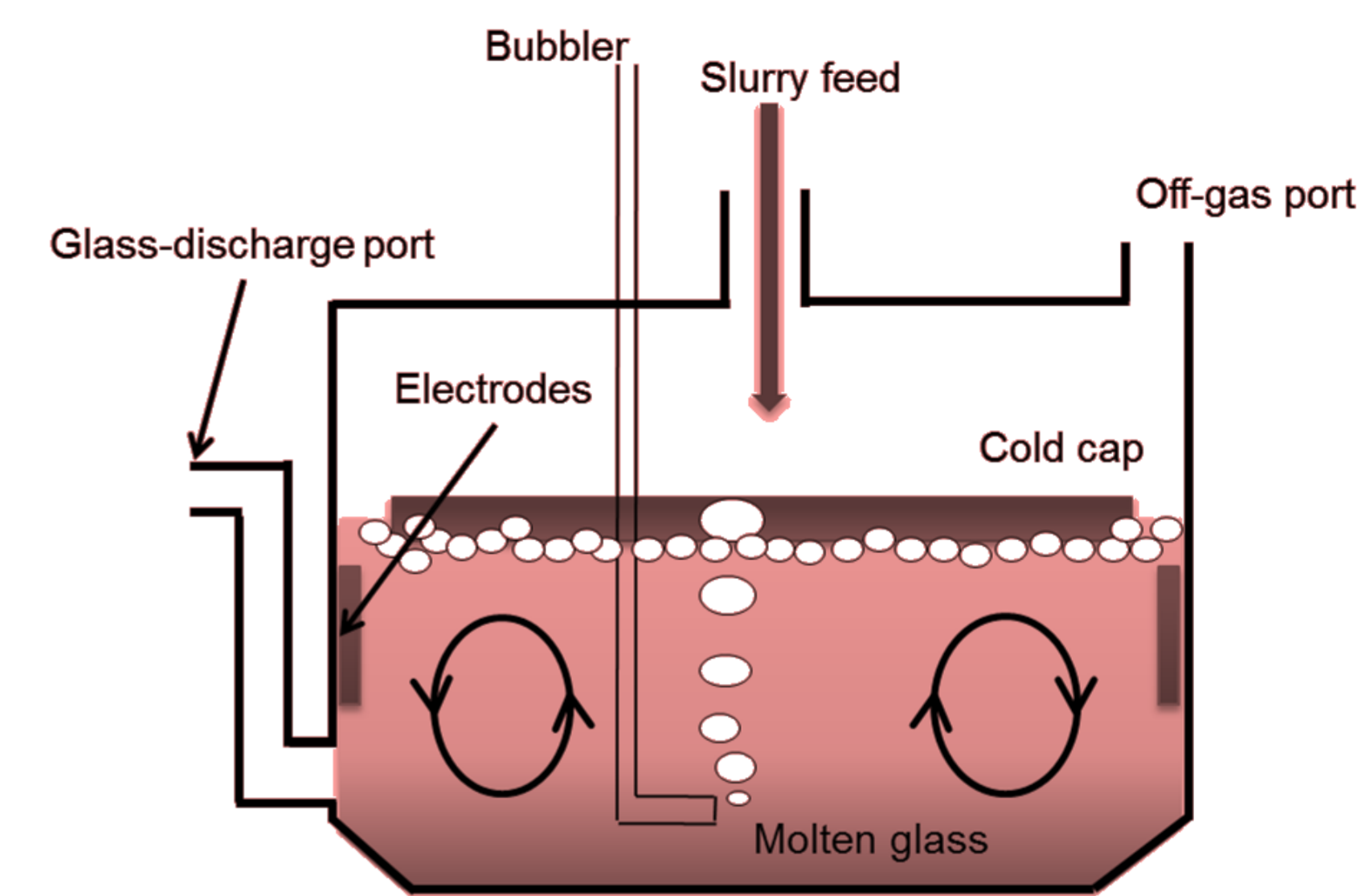

Figure 4. Cold cap profile[8]

Figure 5. Schematic of a JHCM showing the incoming feed and batch blanket[4]

REDOX Reactions
Redox reactions are critical to the amount of foaming produced.
- An oxidised melt causes more foaming
- A reduced melt causes precipitation of metallic species.

Particular multivalent species yet to be examined include: **Fe, Mn, Cr, Ni, Mo** and **Zr.** By altering the amounts of these species in the glass feed, their effect on the foaming and properties of the glass melt will be explored.
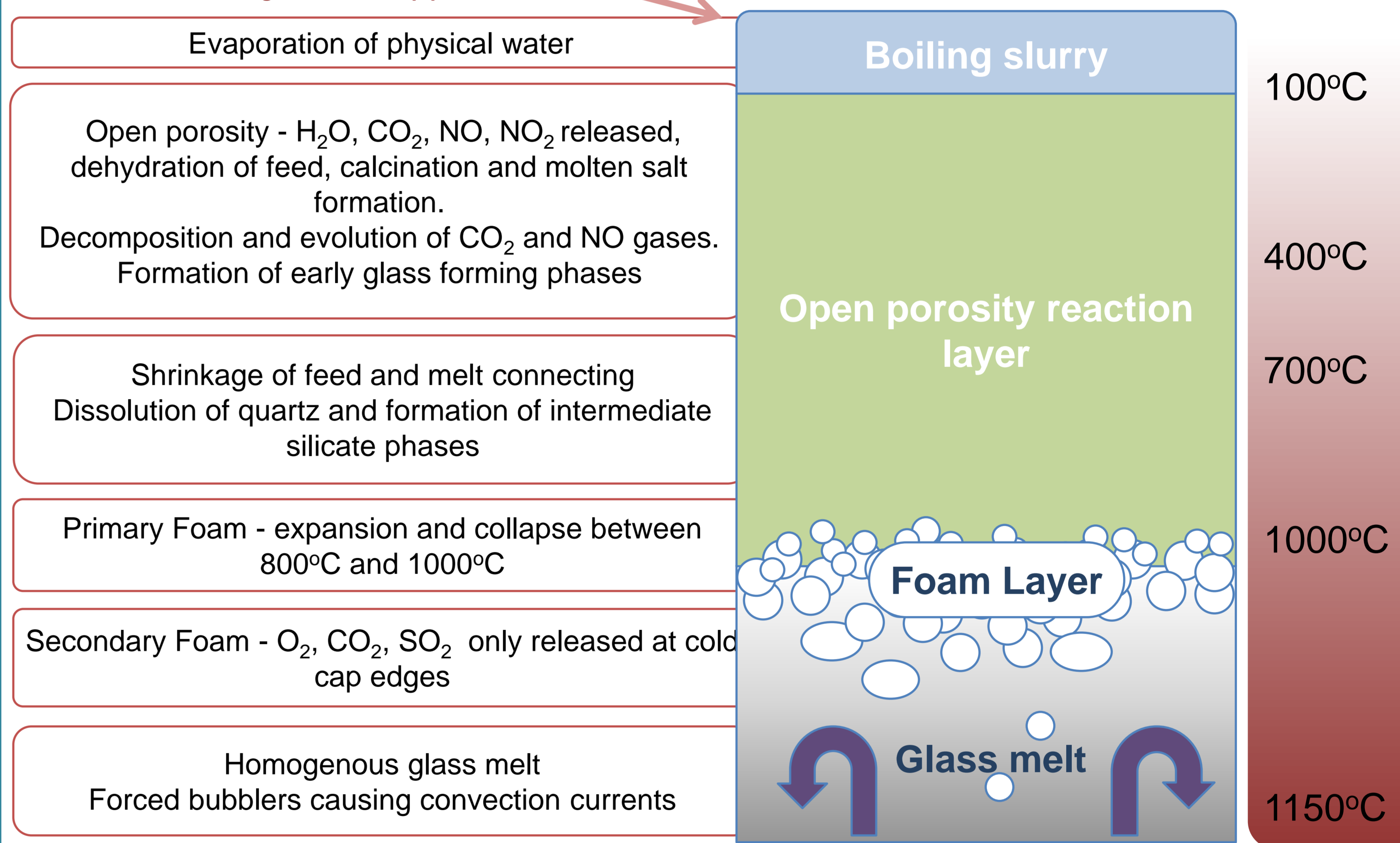
Cold cap profile	Temperature
Evaporation of physical water	100°C
Open porosity - H_2O, CO_2, NO, NO_2 released, dehydration of feed, calcination and molten salt formation. Decomposition and evolution of CO_2 and NO gases. Formation of early glass forming phases	400°C / 700°C
Shrinkage of feed and melt connecting Dissolution of quartz and formation of intermediate silicate phases	
Primary Foam - expansion and collapse between 800°C and 1000°C	1000°C
Secondary Foam - O_2, CO_2, SO_2 only released at cold cap edges	
Homogenous glass melt Forced bubblers causing convection currents	1150°C

Figure 6. Cold cap profile showing heat transfer and layers.[7]

Boiling slurry
Open porosity reaction layer
Foam Layer
Glass melt

Further Work

Stage 1
- Design a study to explore the effect of REDOX conditions on the behaviour of the cold cap
- Characterise cold cap samples (XRD, SEM/EDX, XRF, Raman spectroscopy)

Stage 2
- Explore the oxidation states of key elements, particularly; **Fe, Cr, Mn, Ni, Mo,** and **Zr**
- Analyse the effect of different oxidation states on cold cap behaviour and foaming

Stage 3
- Expand upon the current model of the JHCM to include the effect of REDOX reactions
- Inform process parameters for Hanford's HLW and LAW processing to increase operational safety and efficiency

References

[1] https://www.hanfordvitplant.com/hanford-vit-plant-facilities-overview
[2] https://www.hanfordvitplant.com/high-level-waste-hlw-vitrification-facility
[3] Hujová, M., Pokorný, R. & Kloužek, J. Vitrification of nuclear waste : Exploring the cold cap. 195–201 (2018).
[4] Pokorny, R., & Hrma, P. R. (2014). Model for the conversion of nuclear waste melter feed to glass. *Journal of Nuclear Materials, 445*(1–3), 190–199. https://doi.org/10.1016/j.jnucmat.2013.11.009
[5] McCarthy, B. P. *et al.* Rheology of simulated radioactive waste slurry and cold cap during vitrification. *J. Am. Ceram. Soc.* **101,** 5020–5029 (2018).
[6] http://library.open.oregonstate.edu/microbiology/chapter/energetics-redox-reactions/
[7] Lee, S. M. *et al.* Effect of melter feed foaming on heat flux to the cold cap. *J. Nucl. Mater.* **496,** 54–65 (2017).
[8] Hrma, P. R. & Pokorny, R. The Office of River Protection Cold Cap and Melt Dynamics Technology Development and Research Plan. (2016).
[9] Perez, J. M. *et al. High-Level Waste Melter Study Report. PNNL - 13582* (2001).
[10] Guillen, D. P. *et al.* Development of a Validation Approach for an Integrated Waste Glass Melter Model Development of a Validation Approach for an
[11] Integrated Waste Glass Melter Model. *Nucl. Technol.* **203,** 244–260 (2018).
[12] Pokorny, R. & Hrma, P. R. *Mathematical Model of Cold Cap — Preliminary One-Dimensional Model Development.* (2011).
[13] Dixon, D. R. *et al.* Cold-Cap Temperature Profile Comparison between the Laboratory and Mathematical Model – 15591. in *WM 2015 Conference* 1–9 (2015).
[13] Matlack, K. S. *et al. Improving Technetium Retention in Hanford LAW Glass - Phase 2.* (2011).

Modelling the Thermal Desorption of HCl from PuO$_2$ Surfaces

Jonathan Collard[a], Helen Steele[b], and Nikolas Kaltsoyannis[c]

a, c Centre for Radiochemistry Research, School of Chemistry , The University of Manchester, Oxford Road, Manchester, M13 9PL, UK

b Sellafield Ltd., Sellafield, Cumbria, CA20 1PG, UK

a jonathan.collard@postgrad.manchester.ac.uk

b helen.steele@sellafieldsites.com

c nikolas.kaltsoyannis@manchester.ac.uk

1. Introduction

- Over the last few decades the UK has accumulated the largest stockpile of civil plutonium in the world.

- Early Magnox PuO$_2$ is currently stored at Sellafield in nested, non-welded stainless steel canisters as seen in Figure 1.

- Around the inner canister is a PVC bagging layer.

- It is suspected that the thermal and radiolytic degradation of this PVC has lead to the production of chlorine-based contaminants, in particular HCl.

- Due to the inherent risks associated with handling physical plutonium, this project aims to explore the interactions of various species with PuO$_2$ surfaces computationally.
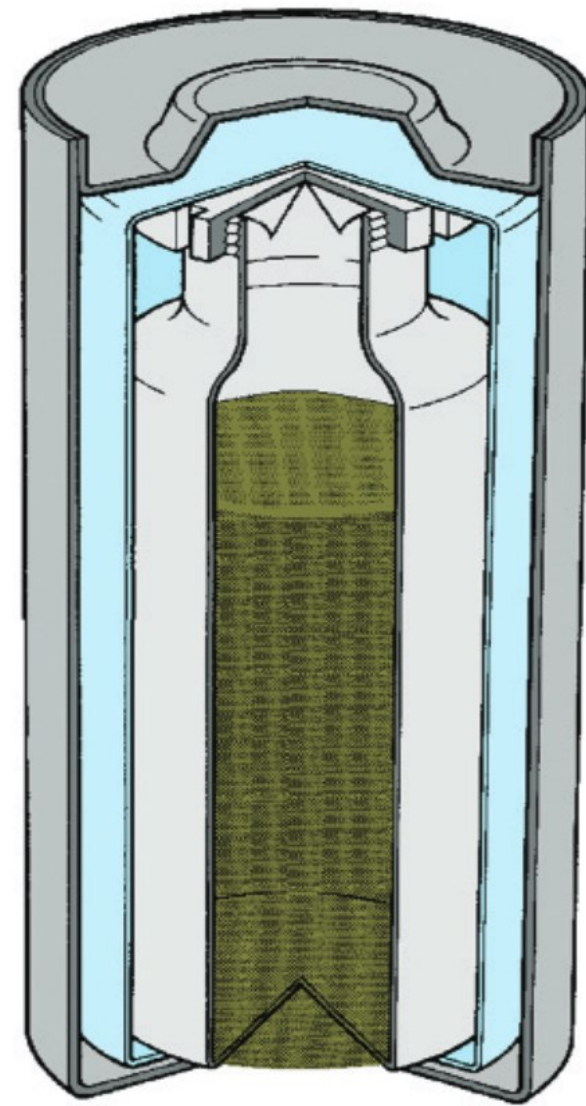
Figure 1. Cutaway diagram of the assembled Magnox PuO$_2$ package (light blue = PVC).

2. Computational Details

- The calculations for this study have been carried out using hybrid density functional theory, within the Periodic Electrostatic Embedded Cluster Method.
  - Software: TURBOMOLE 7.2[1]
  - Functional: PBE0[2] (Hybrid-GGA with 25% Hartree-Fock exchange)
- The {111}, {110} and {100} surfaces have been chosen as representative examples of low index surfaces which span a range of surface morphologies and stabilities.
- The counterpoise correction was applied to account for basis set superposition error.
- Grimme's D3[3] dispersion correction was used to account for dispersive effects.

3. Electronic Structure of Defect Surfaces

- Due to the intense heat and radiation within the storage canisters, it is unlikely that surfaces displayed by the PuO$_2$ surfaces will be pristine. Hence, as with previous work[4], we are also studying interactions with surfaces containing single neutral oxygen vacancy defects.

- When such a defect is introduced, two unpaired electrons are left behind - the localisation behaviour of which will have an impact on any chemical interactions.

- Figure 2 shows the projected density of states (PDOS) and spin density isosurface plots for pristine and defect PuO$_2$ surfaces, and compares them to equivalent UO$_2$ systems.
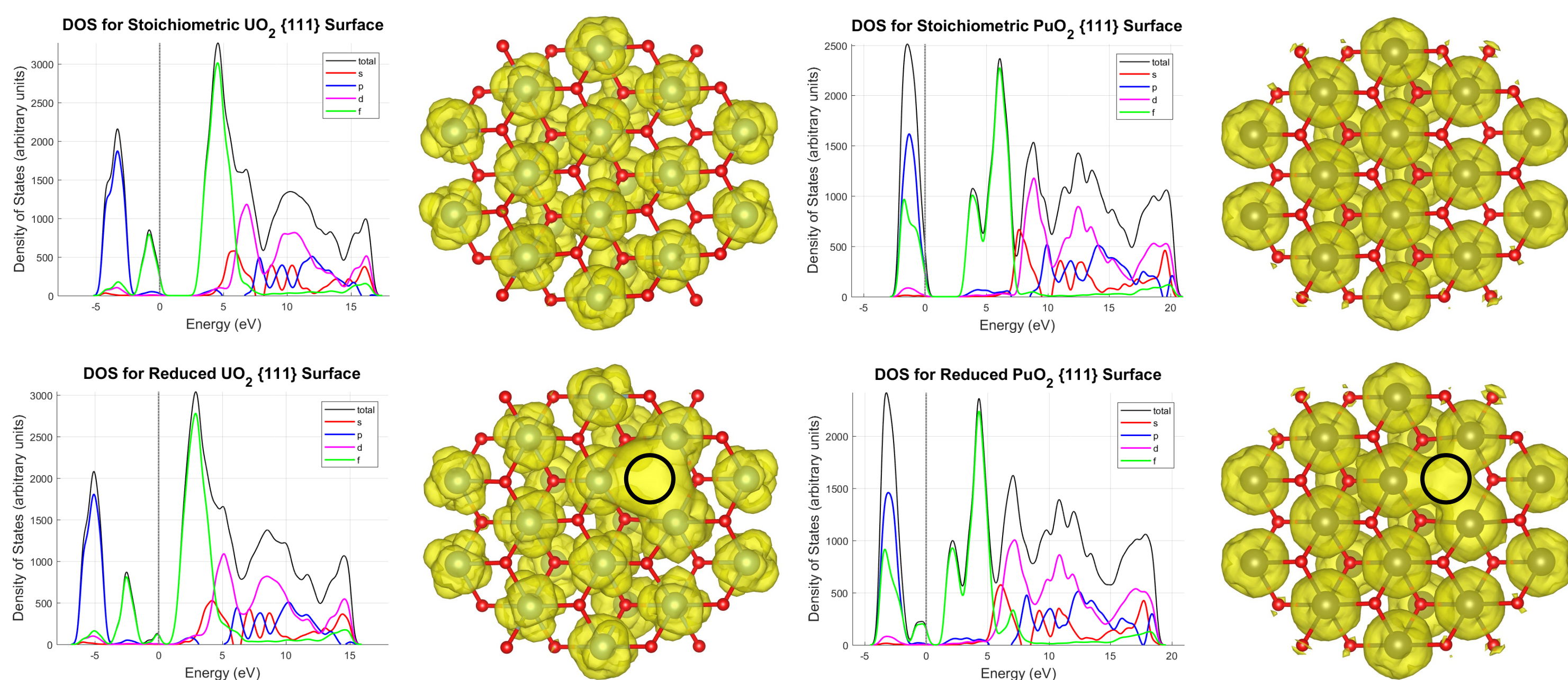

Figure 2. PDOS and spin density isosurface plots for the pristine (top) and defect (bottom) {111} surface of UO$_2$ (left) and PuO$_2$ (right). The unpaired electrons left in the defect site delocalise more in the case of UO$_2$, creating new f-states and decreasing the size of the band gap. The location of the oxygen vacancy is denoted by a circle.

4. HCl Adsorptions on PuO$_2$ Surfaces

- When placing molecular HCl on the PuO$_2$ surface, in all cases except the pristine {100} the HCl molecule spontaneously breaks apart (dissociates) upon optimisation.

- Even after dissociation, some electrostatic attraction was observed between the H and Cl atoms. Although this interaction stabilises the H and Cl atoms individually, the same was not necessarily true for the overall surface (although it was for the {111} surface).

- The "Defect (Healing)" configurations correspond to those where, as in Figure 3, the Cl atom attempts to "heal" the gap left by the vacancy, bonding with the reduced Pu(III).

- The "Defect (Non-healing)" configurations correspond to those where the Cl does not directly interact with the vacancy, instead forming geometries comparable to the pristine case.

- The results of this study indicate that HCl interacts very strongly with oxygen vacancy defect sites in PuO$_2$, compared to the pristine case. However, the presence of a vacancy has minimal indirect effect on adsorptions if the Cl atom does not interact with Pu(III).

Table 1. Adsorption energies, in eV, of the different adsorption configurations calculated for HCl on the PuO$_2$ {111} surface. In all cases the HCl molecule spontaneously dissociated onto the surface upon optimisation.

	Pristine Surface	Defect (Non-healing)	Defect (Healing)
Small Separation	-1.51	-1.41	-3.41
Large Separation	-0.76	-0.74	-2.93

Figure 3. Side-on (left) and top-down (right) images of the "vacancy healing" geometry for HCl adsorbing onto the PuO$_2$ {111} defect surface. The location of the oxygen vacancy in the surface is denoted by a circle.

5. Molecular Thermodynamics

- In order to convert zero-Kelvin DFT adsorption energies into more physically relatable data, a set of desorption temperatures for each configuration was calculated.

- From thermodynamics, the adsorbed surface energy (as a function of temperature T and partial pressure p) is given by:

$$\gamma_{s,HCl}(T,p) = \gamma_{s,clean} + C\left[E_{ads}(T) - RT\ln\left(\frac{p}{p_0}\right)\right]$$

- However, since desorption occurs at the point at which the adsorbed surface energy becomes more energetic than the clean surface, this can be simplified:

$$\ln\left(\frac{p}{p_0}\right) \leq \frac{E_{ads}(T)}{RT}$$

- To obtain temperature-dependent adsorption energy the molar entropy of HCl must be considered, which was interpolated using a power law from NIST-JANAF thermochemical data (see Figure 4)

$$E_{ads}(T) = E_{ads}^{DFT} + TS_{HCl}^0(T)$$

- Substituting this into the inequality yields an expression for HCl partial pressure solely in terms of temperature and the zero-Kelvin DFT adsorption energy which, when satisfied, indicates that thermal desorption will occur.
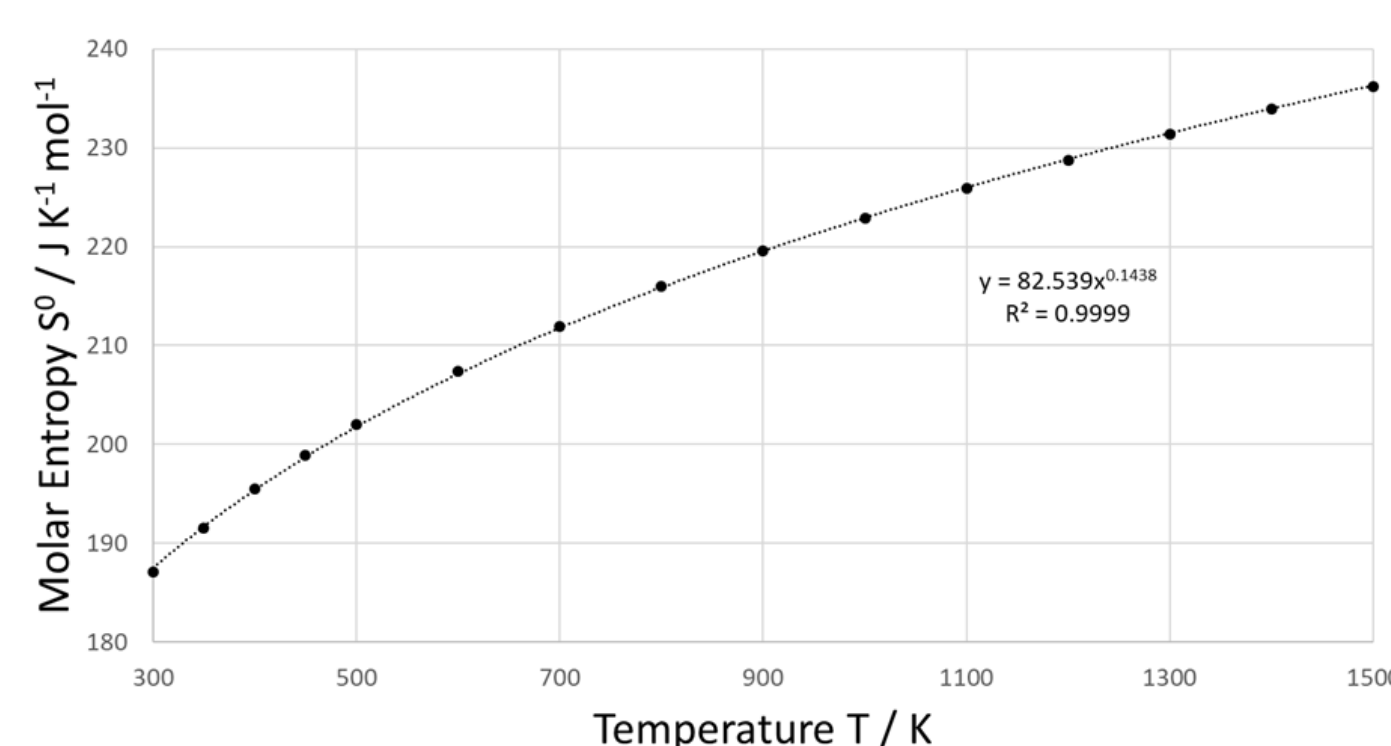

Figure 4. Interpolation of NIST-JANAF entropy data for HCl. Data points denote actual values, whereas the dotted line represents the fit S^0 = 82.539T$^{0.1438}$.
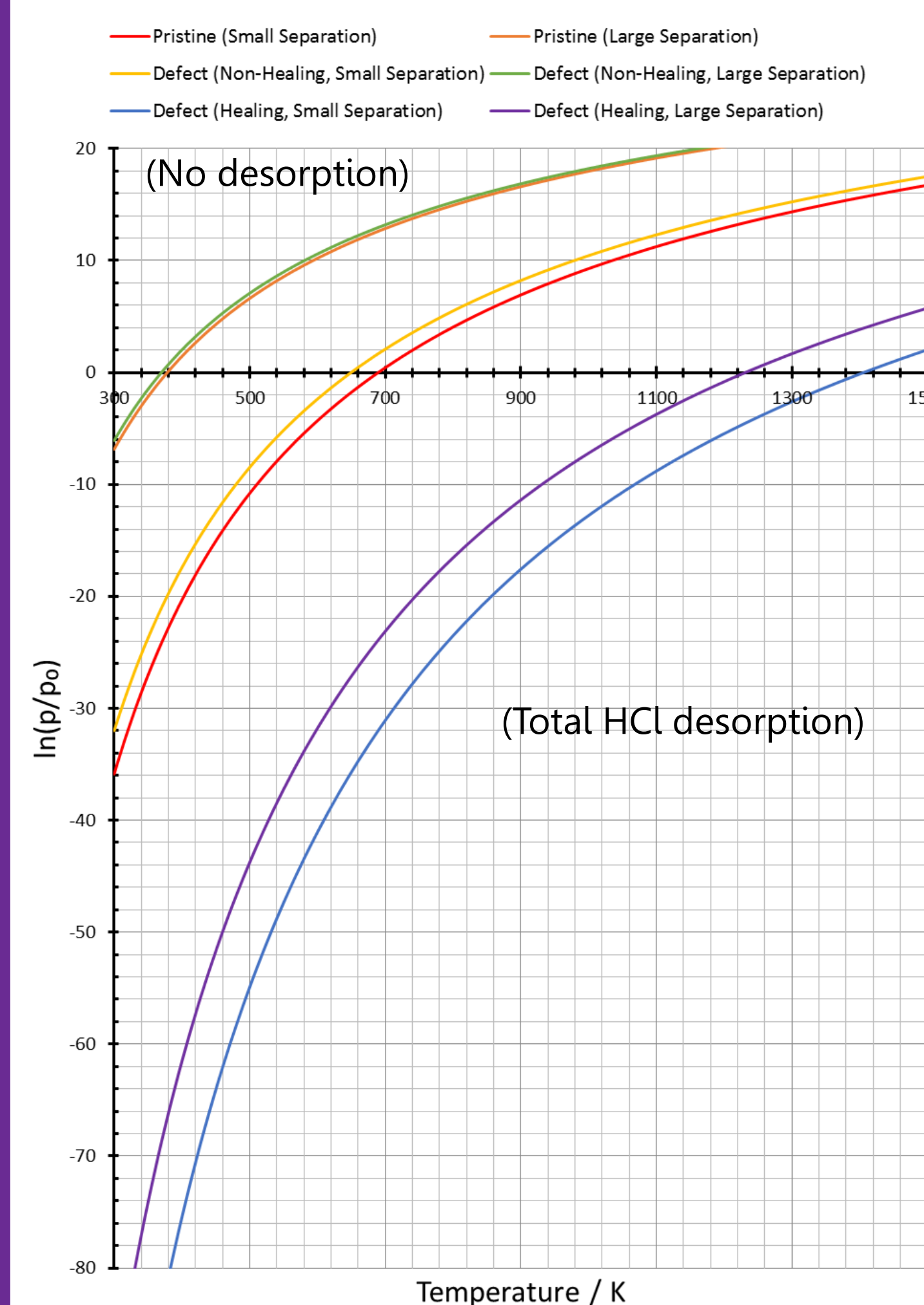
6. Thermal Desorption of HCl from PuO$_2$

- By inserting the zero-Kelvin adsorption energies calculated in Table 1 into the desorption inequality, a set of desorption temperature curves were produced.

- The temperature range was restricted to 300 < T < 1500 K and a wide range of partial pressures were sampled, owing to the uncertainty as to what values for p would be expected in such storage canisters.

- From Figure 5, it is clear that chlorine in a "vacancy-healing" configuration is very strongly bound, requiring very high temperatures to remove even at relatively low partial pressures.

- This is a simplification however, as of course in reality many species would be simultaneously interacting rather than just single independent HCl molecules.

Figure 5. Desorption curves for each configuration calculated on the {111} surface.

References

[1] Ahlrichs, R.; Bär, M.; Häser, M.; Horn, H.; Kölmel, C., *Chem. Phys. Lett.* **162**, 165 (1989)

[2] Perdew, J.P.; Ernzerhof, M.; Burke, K., *J. Chem. Phys.* **105**, 9982 (1996)

[3] Grimme, S.; Antony, J.; Ehrlich, S.; Krieg, H., *J. Chem. Phys.* **132**, 154104 (2010)

[4] Wellington, J.P.W.; Tegner, B.E.; Collard, J.; Kerridge, A.; Kaltsoyannis, N., *J. Phys. Chem. C.* **122**, 7149 (2018)

Future Work & Acknowledgements

- Future work will focus on investigating the simultaneous adsorption of H$_2$O and HCl.

- Thanks go out to the University of Manchester and Sellafield Ltd., for funding this PhD project, and Manchester's Computational Shared Facility (CSF) for compute resources.

Computational Studies of Incorporation of Pu and Ce into Ceramic Matrices Such as Zirconolite

Jonathan Tanti, Nikolas Kaltsoyannis

Email:jonathan.tanti@postgrad.manchester.ac.uk

School of Chemistry, The University of Manchester, Oxford Road, Manchester, M13 9PL

Background

A potential long-term solution to the build-up of nuclear waste is to immobilise and safely sequester it, through underground containment/disposal, from the biosphere.

Immobilisation requires the atomistic replacement of constituents of the proposed waste form by nuclear waste materials, such as Pu.

The ceramic zirconolite ($CaZrTi_2O_7$) has been identified as a candidate waste form for plutonium.

Zirconolite is able to accommodate actinides on its Zr and Ca sites, with cations such as Fe^{3+} able to occupy the Ti-site for charge balancing.

Through use of the Periodic Electrostatic Embedded Cluster Method (PEECM) and hybrid DFT, analysis of energetic and structural properties can be performed.
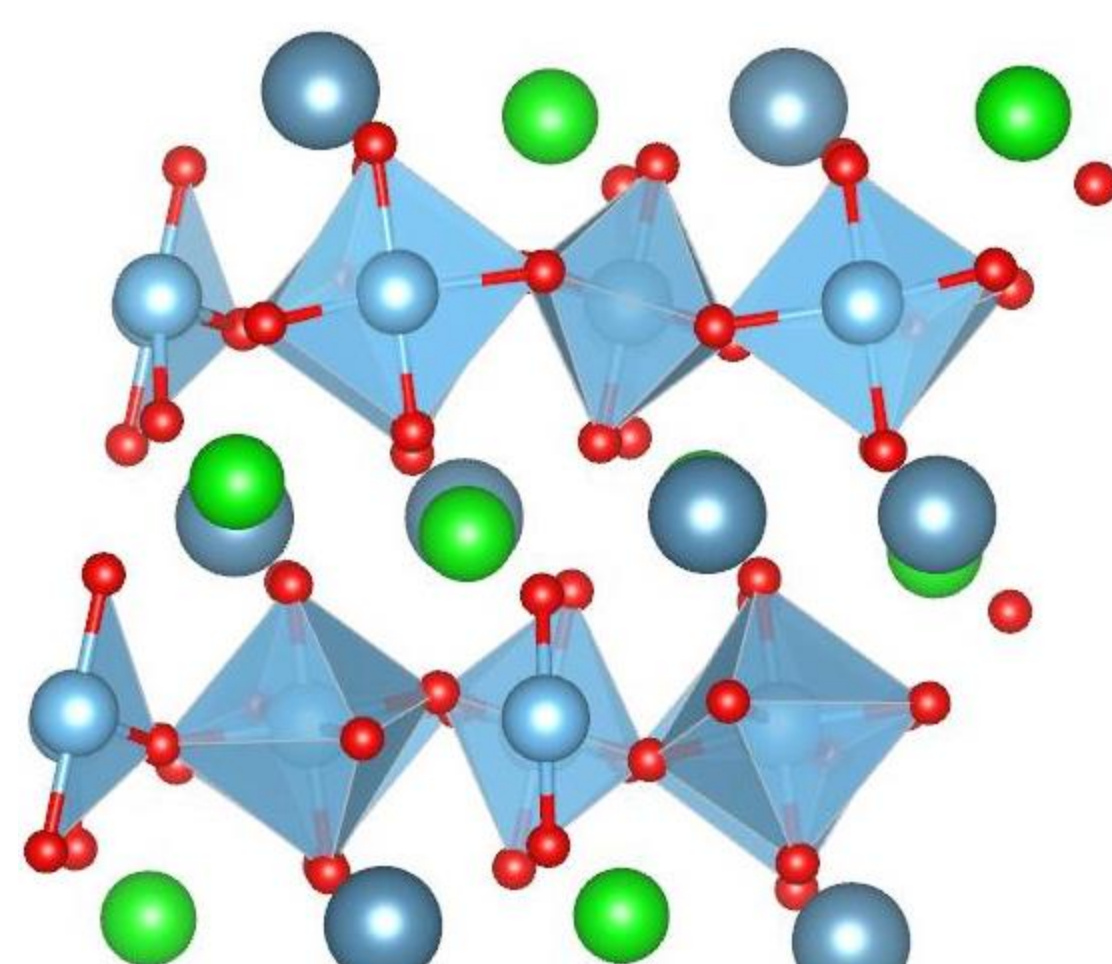
Fig 1. The 88-atom unit cell of zirconolite.
Colour key: dark blue - Ca, green - Zr, light blue - Ti and red - O.

PEECM

In the PEECM, the zirconolite lattice is separated into 3 distinct regions. These regions are the quantum mechanically treated local cluster, the intermediate region and an infinite periodic region of point charges. The use of PEECM allows the use of hybrid functionals which better describe insulators compared to GGA functionals such as PBE.

The local cluster is made up of 110 atoms (10 Ca, 70 O, 20 Ti, and 10 Zr). Within this region, 17 atoms (2 Ca, 9 O, 4 Ti and 2 Zr) are free to move during geometry optimisations.

a)

The intermediate region surrounds the local cluster and is used to prevent over-polarisation of the local cluster.
It contains effective core potentials on the cations (Ca^{2+}, Zr^{4+} and Ti^{4+}) and (2-) point charges (not shown in Fig 2b.) in place of the oxygen atoms.

b)

Both the cluster and the intermediate region are embedded into an infinite, periodic region of point charges. This region recreates the properties of the system's bulk and its interaction with the local cluster.

c)

Figs 2a-c. The local cluster, intermediate region and the point charge region of the zirconolite structure. Large spheres represent QM treated atoms, medium spheres represent full-electron ECPs and small spheres represent point charges.

Computational Details

- Program used: TURBOMOLE 7.2

- Functionals used: PBE & PBE0

- Basis sets: def2-SVP basis sets on all atoms smaller than Th (inclusive), def-SV(P) for atoms larger than Th. Default small-core ECPs (def2-ecp or def-ecp) have been used for Zr and all larger atoms.

Density Of States

The Projected Density of States (PDOS) show that PBE underestimates the HOMO-LUMO gap of zirconolite (analogous to the band gap) as 2.02 eV while PBE0 calculated a more realistic gap of 4.40 eV compared to the experimental value of 3.60 eV[1].

Analysis of the PDOS shows a similar orbital make-up around the valence (mainly O 2p) and conduction band (mainly Ti 3d orbitals) edges compared to previous computational research from Mulroue et al[2].

Upon substitution of an f element (e.g. Np, fig 3), there is little change in the orbital make up of the valence and conduction bands, but f-states appear. These energies stabilise across the actinides and lowers the band gap.
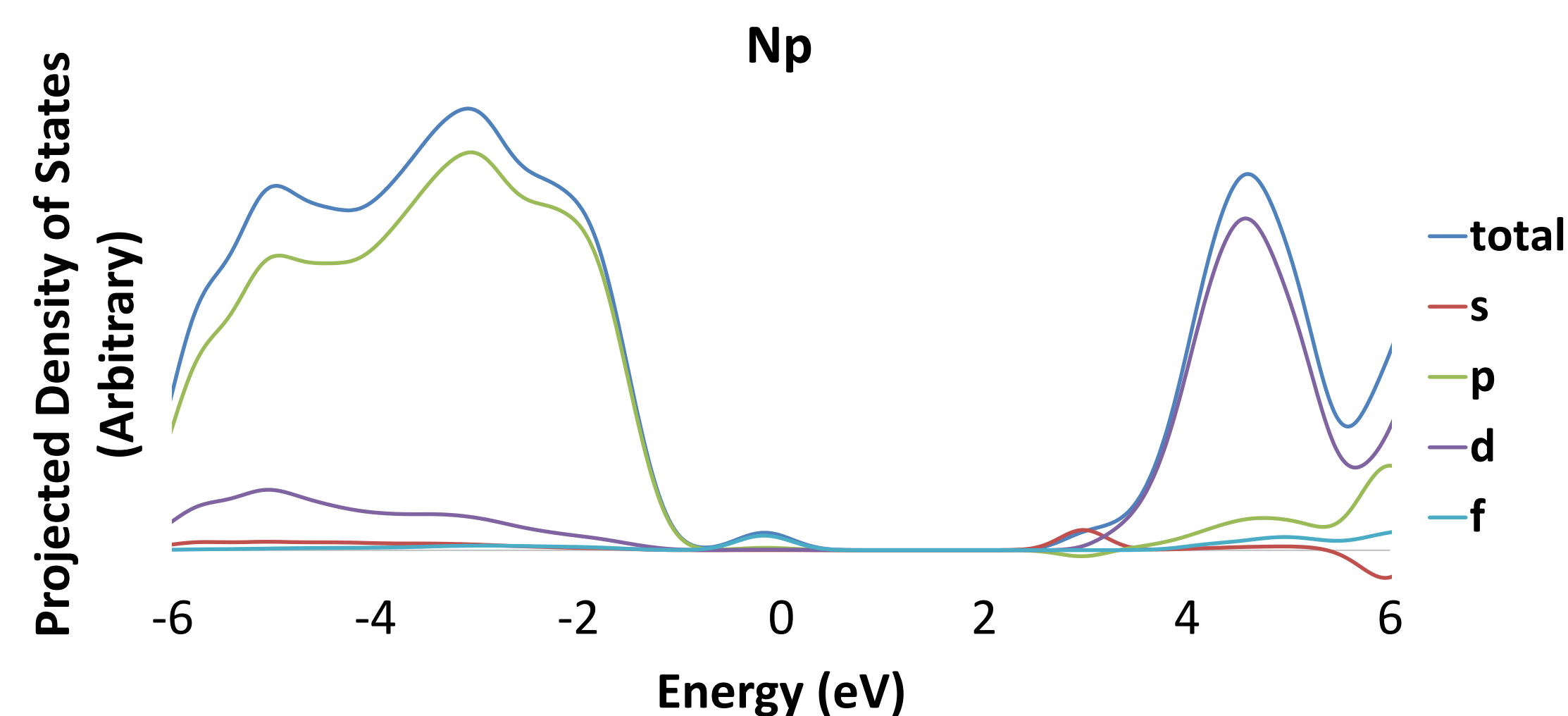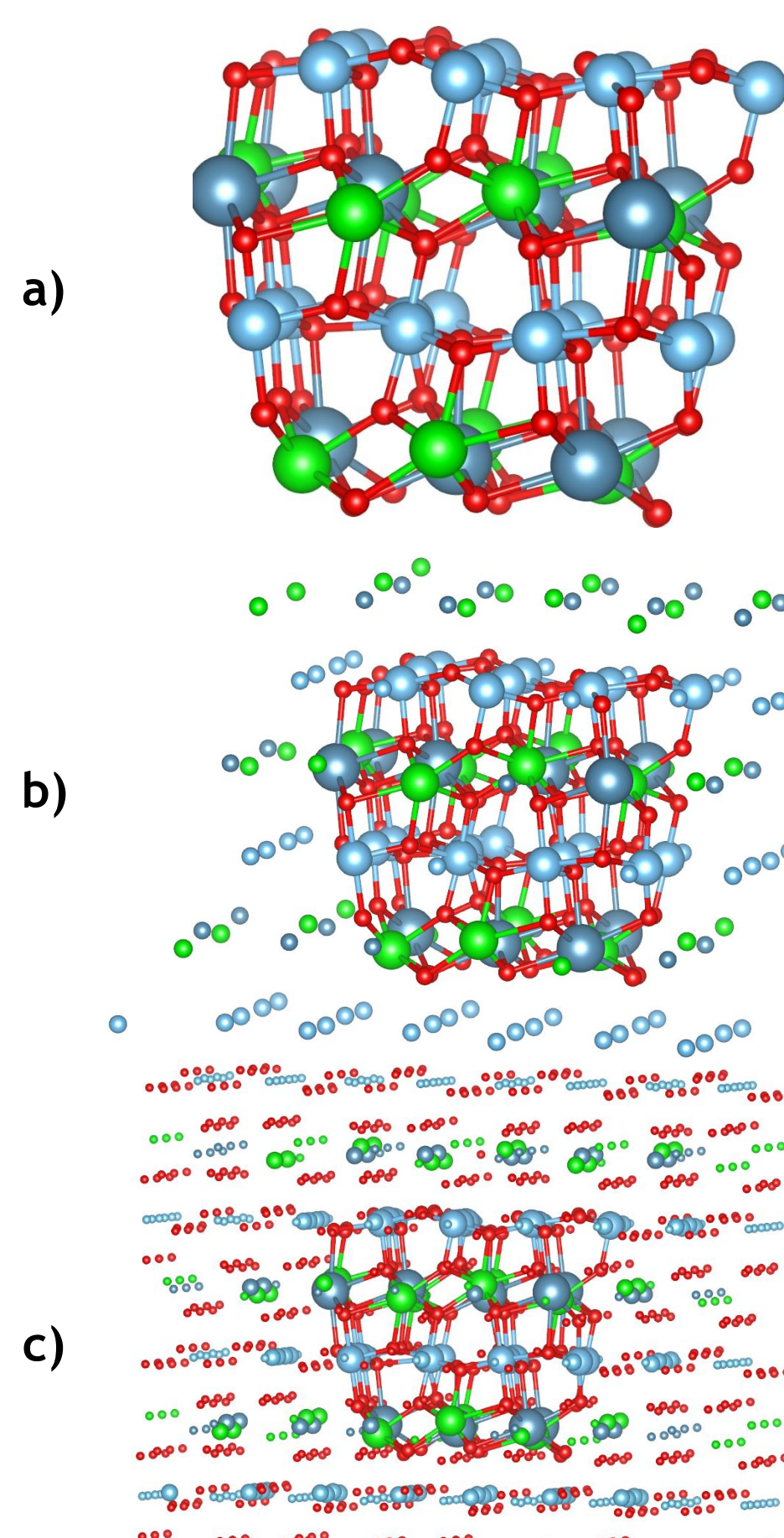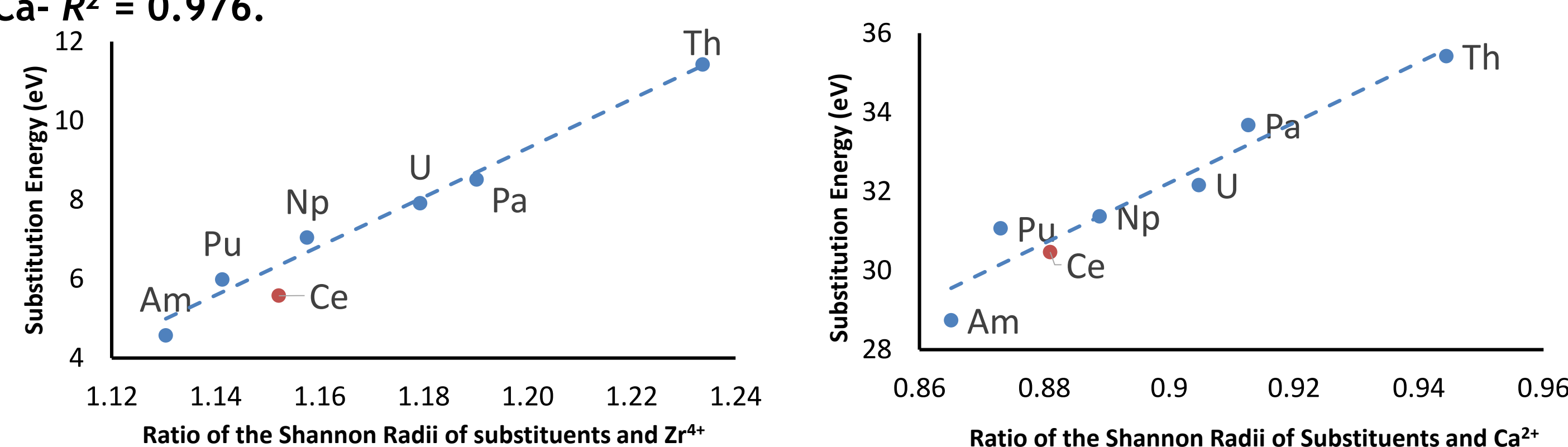
Fig 3. PDOS of Np^X_{Zr}-substituted zirconolite, showing the presence of f-states within the bandgap.

Substitution Energies

Substitution energies are calculated as:
$$E_{sub} = E_{Products} - E_{Reactants} = E_{An^X_{Zr}} + E_{Zr^{4+}} - (E_{Zirconolite} + E_{An^{4+}})$$
where $E_{An^X_{Zr}}$ is the energy of the substituted cluster within the PEECM, E_X is the energy of cation X, and $E_{Zirconolite}$ is the energy of the unsubstituted zirconolite cluster.

Strong correlations have been found between the substitution energy of actinides (and Fe^{3+}, for charge balancing) into the zirconolite lattice and the ratio of the substituent and the substituted atom for both Zr- and Ca-substituted systems. Across the actinide series, the substitution energy is positive and decreases with a reduction of the radius ratio.

Pu^{4+} and Ce^{4+} substitution energies are similar, justifying the use of Ce as a non-radioactive surrogate for Pu in isovalent substitutions. Double substitutions were also calculated, with similarly strong correlations found. 2x Zr-substitutions R^2 = 0.974, 2x Ca- R^2 = 0.976.

Figs 4a and 4b. Correlations between substitution energy and substituent-substituted Shannon ionic radii for the Zr-substituted (R^2 = 0.983) and Ca-Substituted (R^2 = 0.927) systems respectively.

Conclusions and Next Steps

Small differences are seen in the electronic structure of zirconolite following the introduction of f-element defects. This difference is larger for Ca-substituted systems, presumably due to the additional substitution of Fe^{3+} for charge balancing. Introduced f-orbital states decrease in energy across the actinides.

A correlation between the radius of the substituent atom and the substitution energy is seen across the actinides. Further investigation will examine the changes in oxidation state seen for some actinides following substitution into the lattice.

[1]Y. Miseki, K. Saito and A. Kudo, Chem. Lett., 2009, 38, 180-181.
[2]J. Mulroue, A. J. Morris and D. M. Duffy, Phys. Rev. B, 2011, 84, 094118

James Kennedy
CINDe PhD Researcher
j.kennedy2@Lancaster.ac.uk

Decontamination Of Plutonium Contaminated Brick Surfaces

Supervisors: **Professor Colin Boxall** — Engineering Department, Lancaster University, Lancaster UK   **Professor Anthony Banford** — Chief Technologist, National Nuclear Laboratory

Introduction

Aims and Objectives:

To develop an understanding of the materials and mineralogical properties of relevant brick formulations – especially key constituent phases, surface pH, surface charge, permeability and cation exchange capacity.

Based on this and a knowledge of Plutonium chemistry, we will develop an understanding of the mechanisms by which Plutonium and other key contaminants contaminate relevant brick formulations. Especially Whitehaven brick in this study.

Using this, we will develop a representative non-active simulant system for Pu-contaminated bricks.

Finally, employing this simulant system, we will determine the efficiency of brick decontamination using a range of chemically based decontamination methods including those based on aqueous and non-aqueous solvents, redox reagents, chelates, acid/ base treatments, gels and foams.

http://www.wmsym.org/archives/1998/html/sess31/31-03/31-03.htm
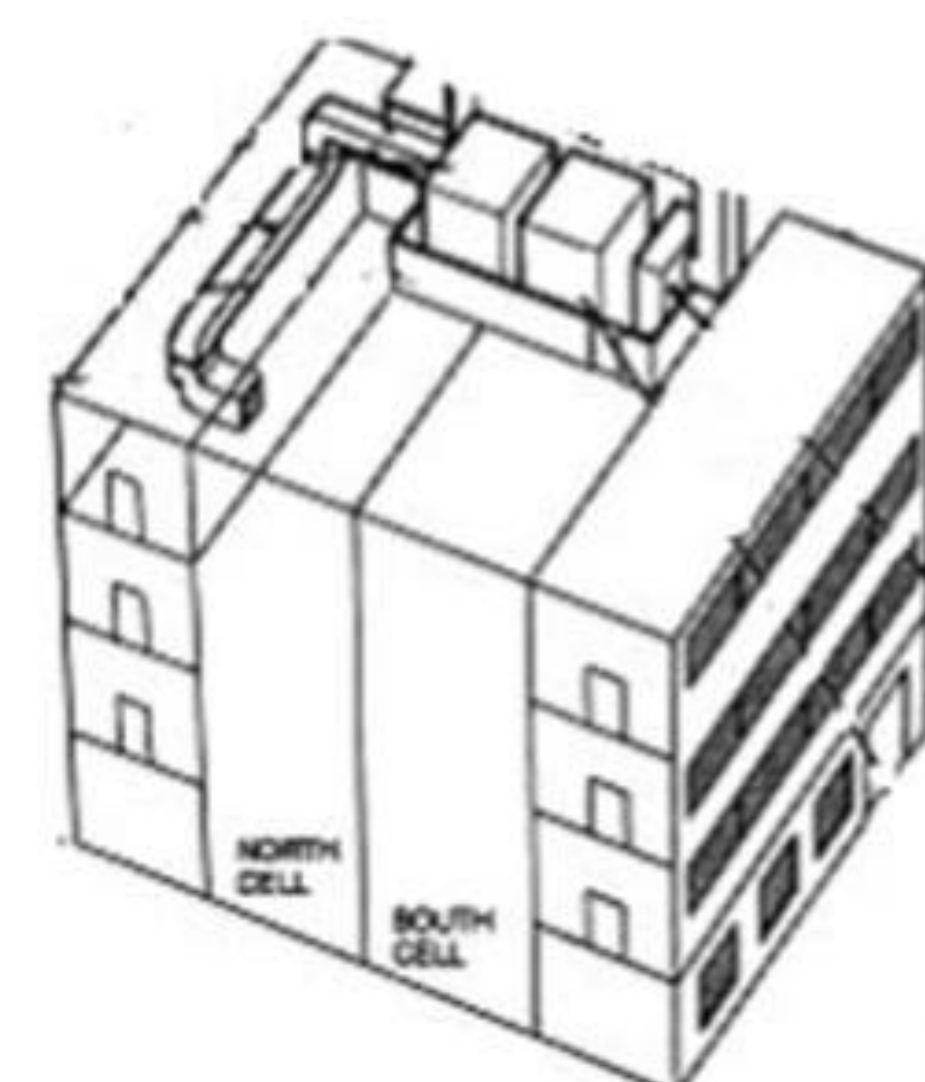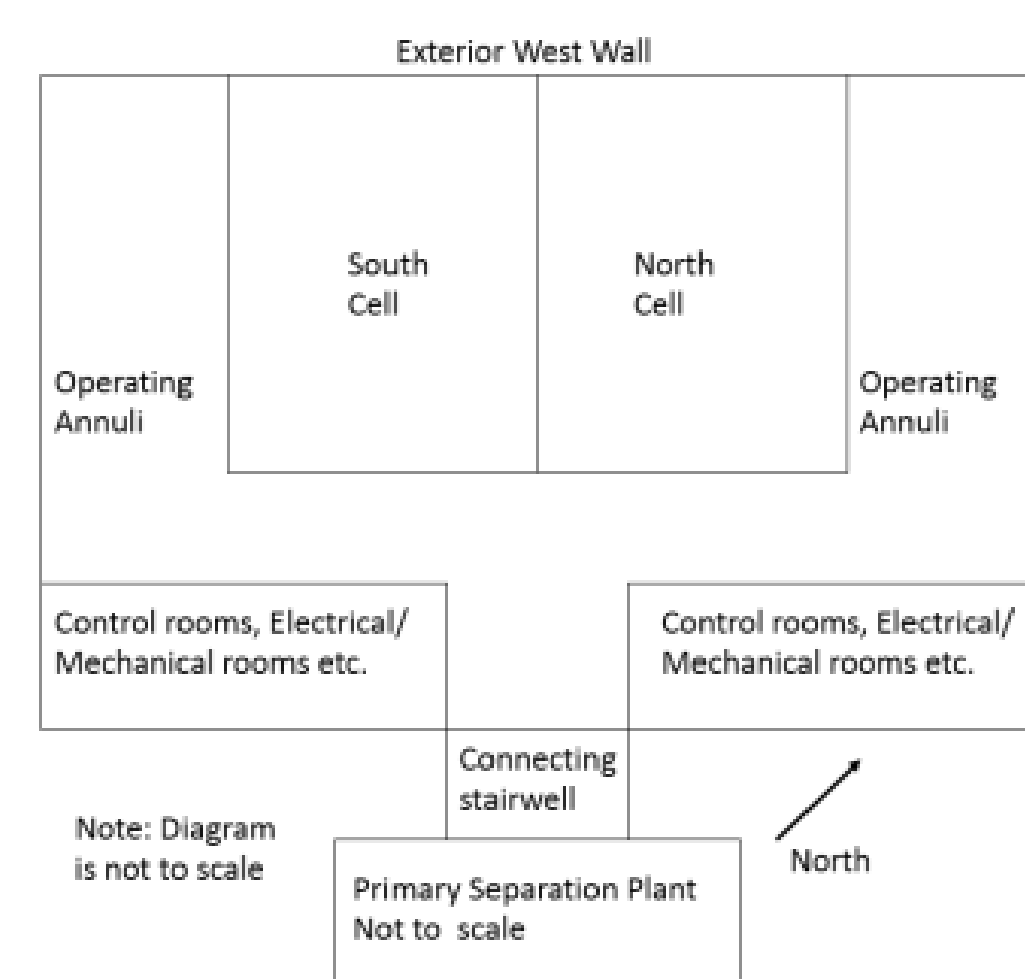
Background:

The main building that will be looked at in this study is the former Plutonium Purification Plant at Sellafield. Constructed in the early to mid 1950's for the processing of Plutonium from the Windscale Piles and later MAGNOX, it is connected to the First Generation Primary Separation Plant. The plant ceased processing of Plutonium in the mid 60's when the MAGNOX processing plant was commissioned. The Plant consists of a 4 storey building containing two identical and adjoining, brick cells, surrounded on 3 sides by an operating annulus. During the plants 10 year operation the BUTEX process was used for primary separation and purification.

BUTEX:

The BUTEX process is a prototype of the currently used PUREX process for the processing of spent nuclear fuel. The process was originally developed at Chalk River in Ontario Canada. The process involved the use of Nitric acid, TPB, OK (odourless kerosene) and the BUTEX solvent 1-[2-(2-butoxyethoxy) ethoxy] butane. A simplified diagram of the BUTEX process is shown on the right.

The Purification Plant at the Sellafield site is a copy of the pilot plant a Chalk River, Canada.

From a study of the plant's blueprints, the purification stage (highlighted in the diagram) was a two stage process with only the second stage occurring within the Purification Plant, the first stage having taken place in the Primary Separation Building.
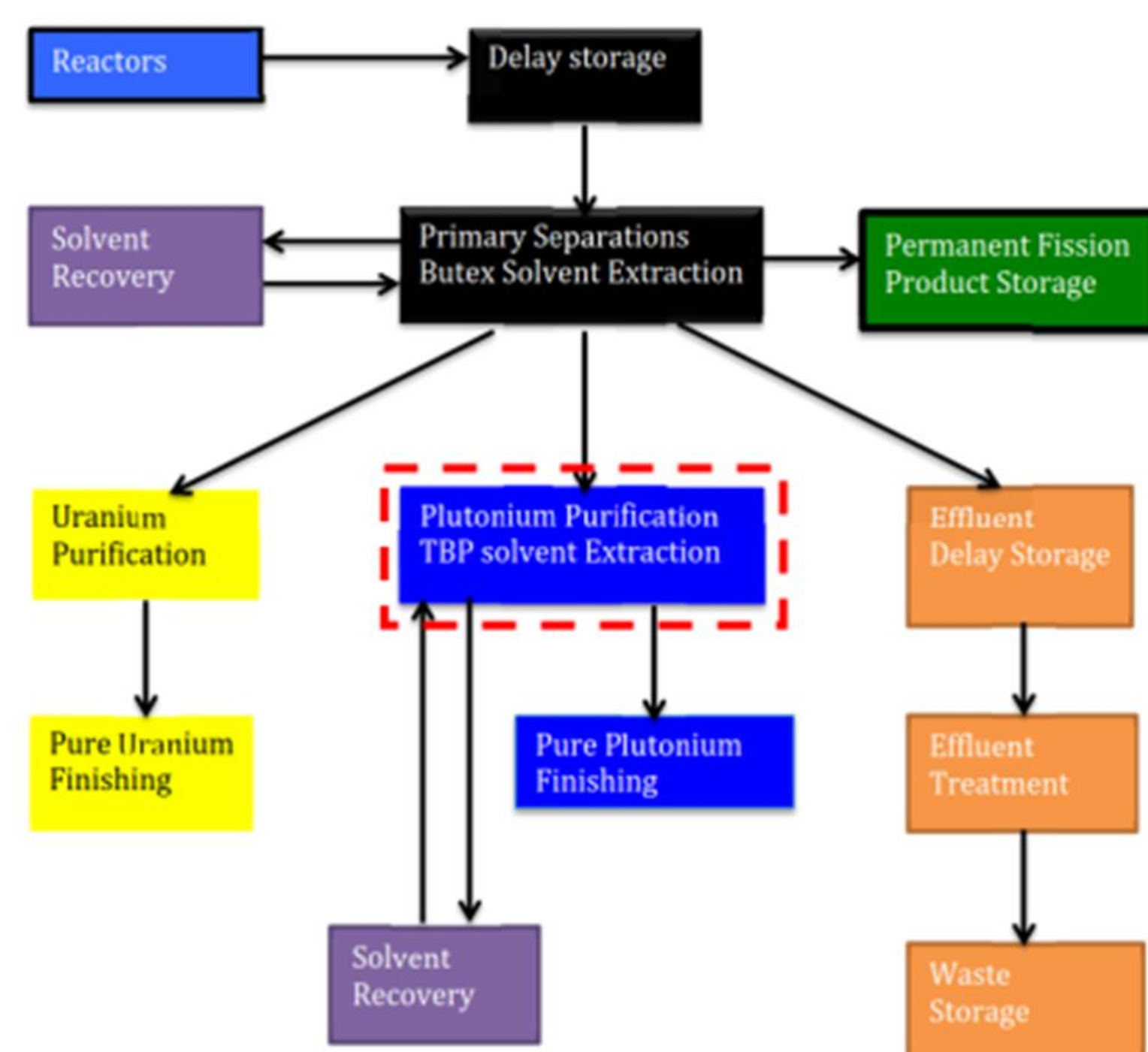
L.W. Gray, K.S. Holliday, A. Murray, M. Thompson, D.T. Thorp, S. Yarbro, T.J. Venetz, Separation of Plutonium from Irradiated Fuels and Targets, Lawrence Livermore National Laboratory, 2015, Report for U.S. D.O.E.
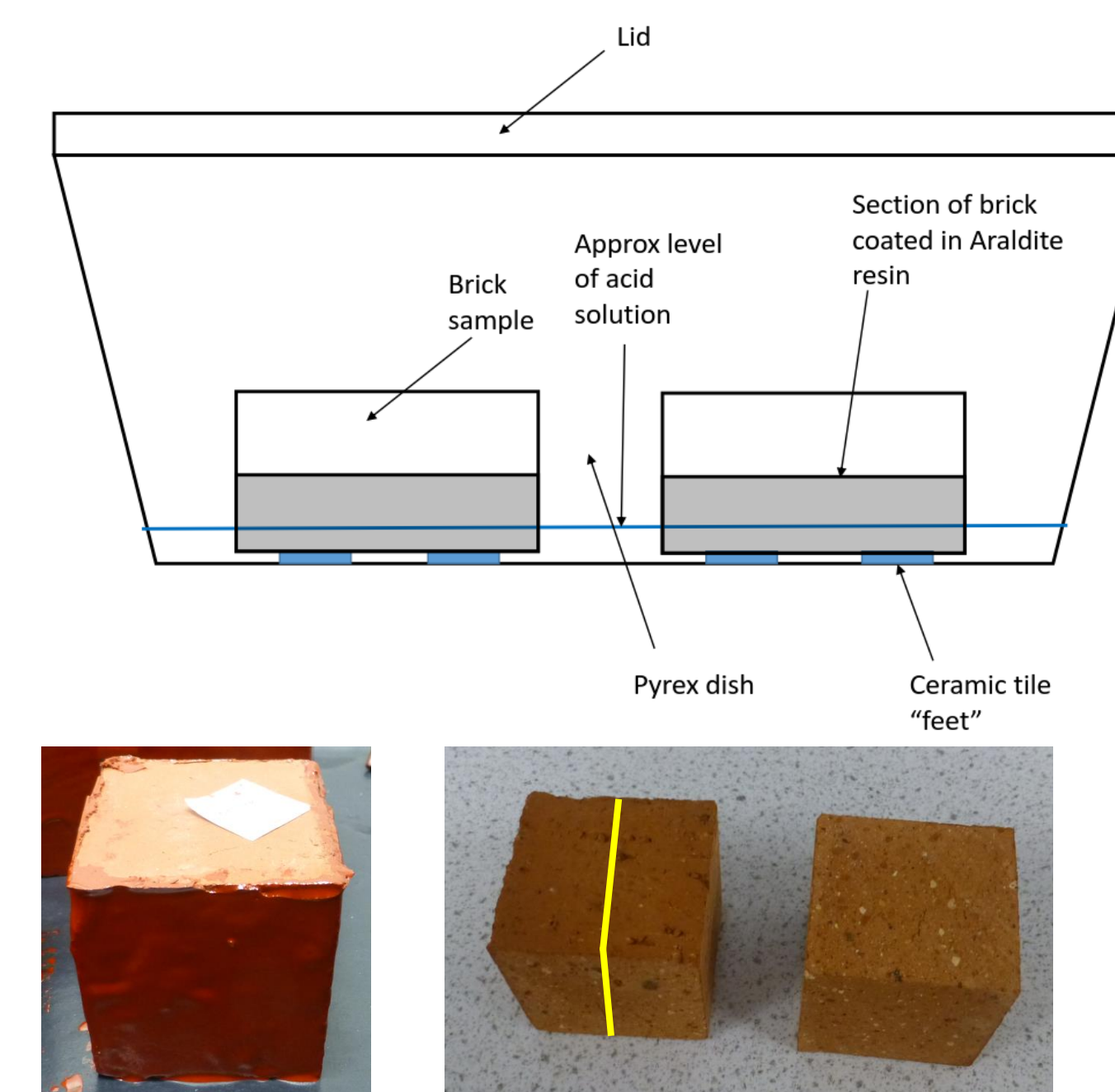
Results

Experimental:

Modern Engineering bricks have been cut into 50mm cubes an coated with chemical resistant paint as shown in the diagram on the left.

The brick samples were then soaked in three different solutions: two simulant contaminate solutions of 10 mmol of Cerium (III) and Cerium (IV) respective dissolved in 8 M Nitric Acid and a solution of pure 8 M Nitric Acid.

The samples were left in the solutions for varying length of time, ranging from 1 day to 6 weeks. This is in order to test the effects of the simulant contaminate on the brick samples as well as to determine the rate of contaminate penetration.

Once soaked the brick samples will be cut in half and analysed using SEM and XRF to establish the depth of simulant penetration and asses any deterioration to the brick.

Results:

Samples of Whitehaven brick were analysed using SEM and EDS, to determine the elemental composition of the brick. As can be seen in the graph.

One of the samples was also soaked in 8M Nitric acid for 1 week to establish the effect of acid on the brick composition. The results can be seen on the right.

The two SEM images show: Top, pre acid and Bottom, post acid, brick samples.
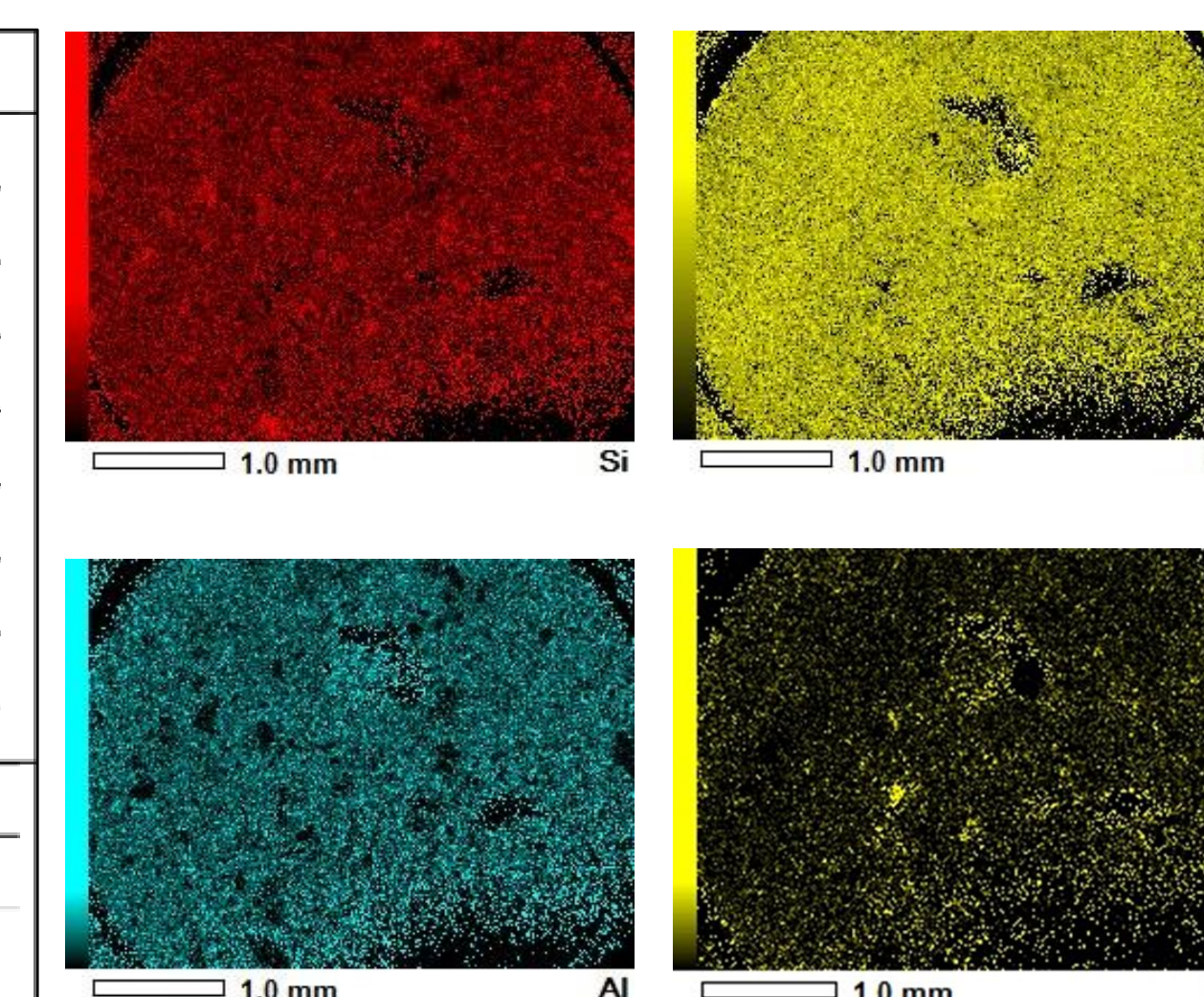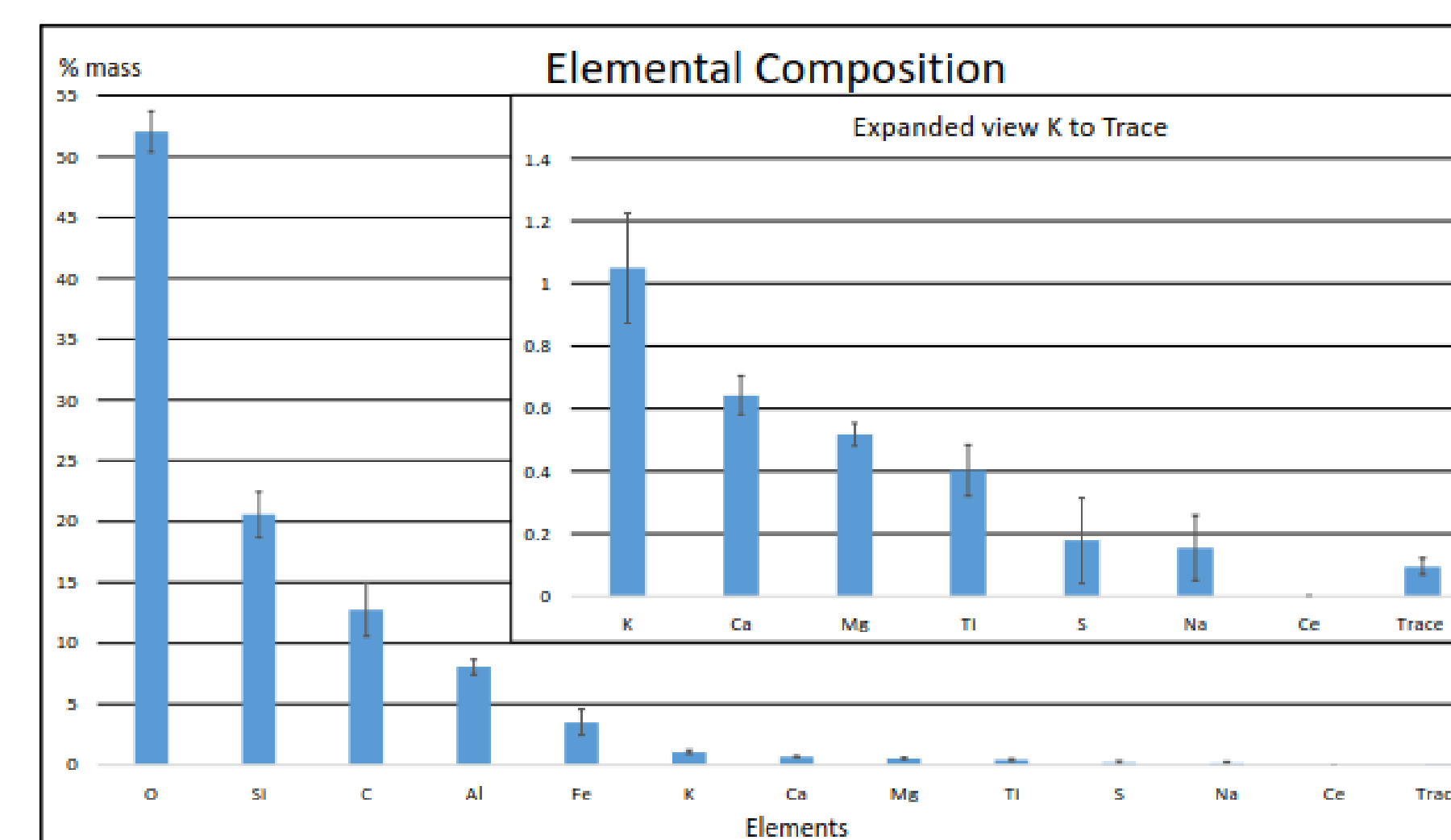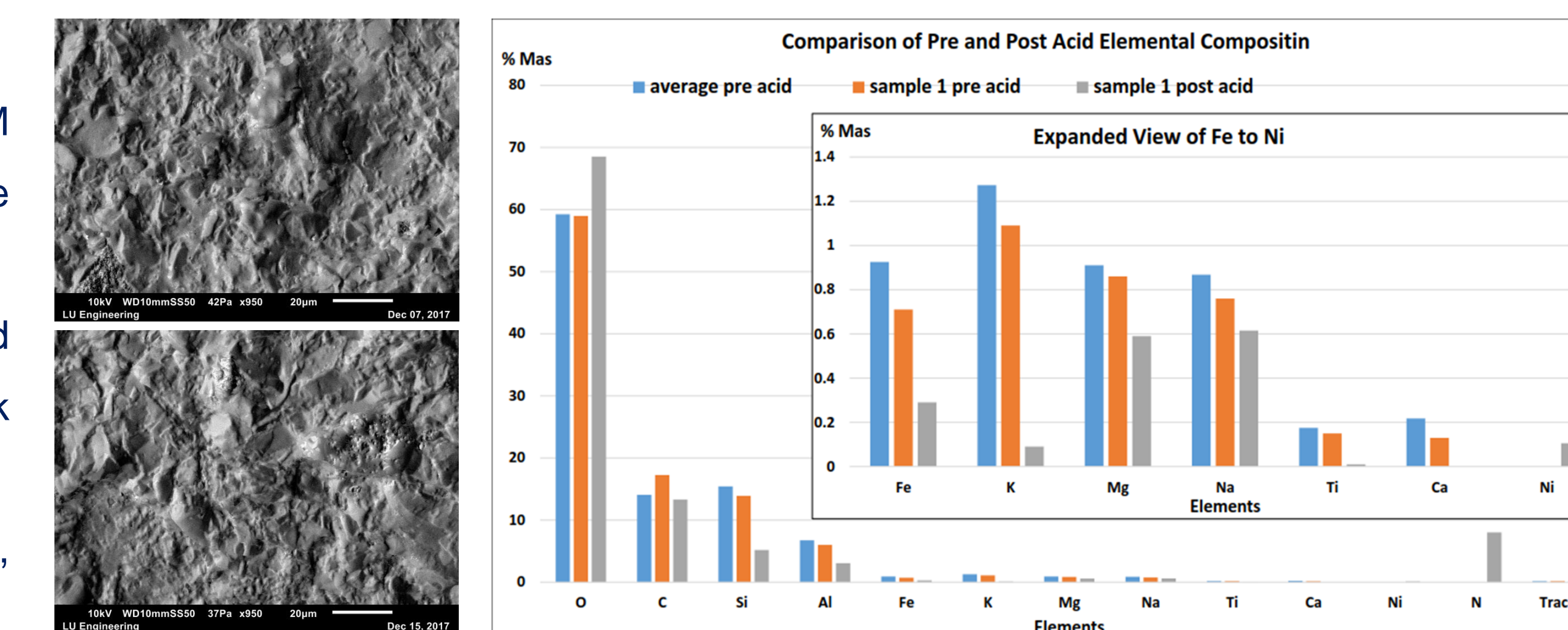
Analysis using SEM and EDS was also carried out on the modern engineering bricks used. A graph of the averaged elemental composition is shown on the right. In addition EDS element mapping for the major elements has also been provided showing their distribution within the samples.

Future Experimentation

Future Studies for this project will involve:

- Determine binding characteristics of contaminant simulant using varying techniques.
- Additional testing on brick porosity/ permeability using Mercury porosimetry
- Application for beam time at DIAMOND to further investigate contaminant simulant binding using XANES and XPS.

- Begin bench scale testing of a range of decontamination agents.
  - RAD-release, DeconGel, TBP, etc.
- Start larger scale test with best 3 or 4 solutions

Collaborating with, and co-funded by: